



D.U.S.T.I.N.

Dust Understanding and Storm Tracking INvestigator on Mars

Team 2

P. Code	Surname	Name
10882032	Aranda Romero	Fernando
10885603	Grover	Kotish
10643558	Moscotti	Mattia
10607120	Pecoraro	Gaetano
10460186	Prudenzi	Luca
10940353	Stabile	Remo

Payload Design

Prof: Mauro Massari

M.Sc Space Engineering

Academic Year 2023-2024



POLITECNICO
MILANO 1863

This work is licensed under a Creative Commons “Attribution-NonCommercial-ShareAlike 4.0 International” license.



Abstract

This report presents the preliminary design of an infrared payload aimed at studying and mapping the formation of dust storms on Mars. The primary mission objective focuses on mapping dust storms within the latitudinal range of $\pm 70^\circ$, satisfying the requirements about achieving high temporal resolution, aiming to provide fundamental information into the mechanisms underlying dust storm formation, including the early phases of their development, leading significant improvement in the martian atmosphere model.

Starting with an assessment of the physical phenomenon to be described and the legacy of previous missions, this report aims to identify the most effective solution to deal with each challenge. High-level requirements are systematically derived to guide through the design process, from the selection of optimal optical architecture to the acquisition strategy, bus configuration, structural and thermal analysis.

By employing comparative analysis methodologies, the final goal is to determine the best-suited solution at each stage of development, ensuring the fulfillment of the mission objectives and guarantee technical feasibility.

By learning from past missions, this report sets the foundation for the design of a robust infrared payload to address the different aspects of the dust storm dynamics on Mars.

Contents

1	Introduction	1
1.1	Dust storms on Mars	1
1.2	Regions of interest for future human missions on Mars	2
1.3	Introduction to dust opacity observation	2
2	Concept definition	5
2.1	Mission Statement	5
2.2	High Level Requirements	5
2.3	Drivers	6
2.4	Mission Phases	6
2.5	Payload Modes & ConOps	8
3	Mission Analysis	10
3.1	Potential Launch Window	10
3.2	Launcher Selection	11
3.3	Nominal Orbit Trade-Off	12
3.3.1	Areostationary Orbit	13
3.4	Environmental Analysis	15
3.4.1	Main Assumptions	15
3.4.2	Interplanetary Transfer	16
3.4.3	Areostationary Orbit	16
3.4.4	Areostationary Orbit Thermal Environment	18
3.5	Eclipse Analysis	18
3.6	Visibility Windows Analysis	19
3.7	Orbital Technical Requirements	20
4	Optics and Detector	21
4.1	Architecture Selection	21
4.2	Interferometric System Trade-Off	21
4.3	Pin-Hole Model	22
4.4	Optical Model	23
4.5	Materials	24
4.6	Mass Budget	25
4.7	Additional Components	25
4.7.1	Laser Diode	25
4.7.2	Gimbal Mirror	25
4.7.3	Paraxial Mirror	26
4.7.4	Bandpass filter	26
4.8	Detectors trade-off	26
4.9	Radiometric Analysis	28
4.10	Observation Strategy	29
4.10.1	Calibration Strategy	29
4.10.2	Raster scan	31
4.11	Optics Technical Requirements	32
5	Subsystem Configuration	34
5.1	Configuration Description	34
5.2	Architecture Description	35
6	On-Board Data Handling	37
6.1	Estimation-By-Similarity Considerations	37
6.2	OBDH Functionalities	37
6.3	Sizing	38

6.3.1	Telemetry Data	38
6.3.2	EPS and TCS Control	38
6.3.3	Interface and Autonomy	39
6.3.4	Optics and Interferometer Control	39
6.3.5	Operating System	40
6.3.6	Sizing per Mode	40
6.4	Heritage Solutions	41
6.5	OBDH Solution	41
6.6	Data Rate Analysis	42
6.7	Science Data Acquisition Strategy	44
6.8	OBDH Technical Requirements	44
7	Electric Power Subsystem	47
7.1	Architecture	47
7.2	Technical requirements	48
8	Thermal Control System	50
8.1	Temperature Limits	50
8.1.1	Internal heat sources	50
8.1.2	TCS Architecture	50
8.2	Thermal Simulation	51
8.2.1	Hot Case Scenario	52
8.2.2	Cold case scenario	52
8.3	TCS technical requirements	52
9	Structure	54
9.1	Structural Analysis	54
9.1.1	FEM Description	55
9.2	Results	55
9.2.1	Modal Analysis	55
9.2.2	Static Analysis	56
9.2.3	Random Analysis	59
9.2.4	Lateral Acceleration (X Direction)	60
9.2.5	Lateral Acceleration (Z Direction)	61
9.3	Mass Budget	61
9.4	Structural technical requirements	62
10	Conclusion	64
A	Requirements	68
A.1	High Level Requirements	68
A.2	Technical Requirements	70
A.2.1	Orbit Requirements	70
A.2.2	Optics Requirements	71
A.2.3	OBDH Requirements	74
A.2.4	EPS Requirements	78
A.2.5	TCS Requirements	80
A.2.6	STR Requirements	81

List of Figures

1.1	Distribution of directly confirmed and dubious global dust storms from 11 th April 1955 (MY 1) to 18 th June 2015 (end of MY 32). The event in Martian year 15 dust storm. Between the end of Viking mission and the beginning of Mars Global Surveyor (1983-1999) information is fragmented and only acquired from Earth observations	1
1.2	Selected landing sites for future Starship missions	2
1.3	Contributing functions for the wavenumbers used in the temperature retrievals. These contributions can be obtained with a spectral resolution of 10 cm^{-1} around the $15\text{ }\mu\text{m}$ band	3
1.4	Spectral dependence of dust, water ice, CO_2 optical depth and of surface emissivity. Data in the region $500\text{-}800\text{ cm}^{-1}$ are not shown for the strong absorption by $15\mu\text{m}$ CO_2 band	4
1.5	Spectra of Martian atmosphere for observation performed at local noon with clear sky, during a diurnal dust storm, during passage of thick water ice clouds and at local midnight	4
3.1	Solar cycle prediction	10
3.2	Possible Mars launch windows	10
3.3	SpaceX's Falcon Heavy launcher	11
3.4	Annual Δv for longitudinal station keeping manoeuvres for areostationary and geostationary orbits	14
3.5	Mars surface coverage from a four-platform areostationary constellation	15
3.6	Mars observed from a constellation of 4 satellites from an areostationary orbit	15
3.7	Total Ionizing Dose as function of shield thickness for the Interplanetary Segment	16
3.8	TID received by D.U.S.T.I.N. in its 12 year operations	17
3.9	LET integral and differential fluxes for the areostationary orbit	18
3.10	Total eclipse time per day and number of eclipses per day over the whole mission span	19
3.11	Visibility windows analysis	20
4.1	Different interferometric solutions	22
4.2	Optic design	23
4.3	Different coatings for IR mirrors by ThorLabs, Inc.	24
4.4	Paraxial mirror	26
4.5	Detectors trade off	27
4.6	Typical relative responsivity, D^* and NEP for detector series 99 by Leonardo company	28
4.7	GUI of the NASA Planetary Spectrum Generator	28
4.8	Radiometric analysis results from PSG	29
4.9	Conceptual scheme followed to perform the calibration of the instruments and to retrieve the desired output, the radiance of the scene R_{scene}	30
4.10	Acquisition strategy	31
5.1	D.U.S.T.I.N. external view.	34
5.2	Semi-transparent representation of the system, the bottom plate is reported in yellow. It is possible to appreciate the interferometer external casing and the elements of the primary and secondary structure	34
5.3	On the left: Cassegrain and interferometer assembly. On the right: components of the optical chain including the black body for calibration	35

5.4	Isometric view of the main components of D.U.S.T.I.N.	35
5.5	D.U.S.T.I.N. architecture	36
6.1	Data Rates Diagram	44
8.1	Thermal net developed, the thermal connections between nodes are highlighted	51
9.1	Static loads envelope as prescribed by the laucher user manual	54
9.2	Sine test load histories (axial and lateral)	54
9.3	Cut view and external view of D.U.S.T.I.N. FEM model, the rigid elements that model the lenses have been highlighted)	55
9.4	From left to right, from top to bottom: mode 1 (section), mode 5 (section), mode 5 (external view), mode 6 (section), mode 7 (section)	56
9.5	Displacements (mm) for load case 1	57
9.6	Stresses (MPa) evaluated for load case 1	57
9.7	Displacements (mm) for load case 2	57
9.8	Stresses (MPa) evaluated for load case 2	58
9.9	Displacements (mm) for load case 3	58
9.10	Stresses (MPa) evaluated for load case 3	58
9.11	Displacements (mm) for load case 4	59
9.12	Stresses (MPa) evaluated for load case 4	59
9.13	From left to right, computed accelerations [mm/s ²] at 20 Hz, 60 Hz and 100 Hz	60
9.14	From left to right, computed stresses [MPa] at 20 Hz, 60 Hz and 100 Hz	60
9.15	From left to right, computed accelerations [mm/s ²] at 20 Hz, 60 Hz and 100 Hz	60
9.16	From left to right, computed stresses [MPa] at 20 Hz, 60 Hz and 100 Hz	60
9.17	From left to right, computed accelerations [mm/s ²] at 20 Hz, 60 Hz and 100 Hz	61
9.18	From left to right, computed stresses [MPa] at 20 Hz, 60 Hz and 100 Hz	61

List of Tables

2.1	High level requirements	5
2.2	D.U.S.T.I.N. design drivers	6
2.3	D.U.S.T.I.N. Operational Mission Phases	7
2.4	D.U.S.T.I.N. Operational Modes	8
2.5	Possible modes for each mission phases	9
3.1	Transfer characterisation	11
3.2	Polar orbit analysis	12
3.3	Areostationary orbit analysis	13
3.4	High elliptical orbit analysis	13
3.5	Orbital parameters	14
3.6	Segmentation of the transfer orbit for environmental analysis	16
3.7	Expected short-term SEU rates for high energetic protons flux	17
3.8	Total mission SEU due to GCR	17
3.9	DSN ground stations	19
3.10	Orbital technical requirements	20
4.1	Trade-off for optical architecture	21
4.2	Pin Hole model	22
4.3	Optical model	24
4.4	Mass budget of the optical system	25
4.5	Detector's properties	27
4.6	Optics technical requirements	32
6.1	Science and housekeeping OBDH analysis	38
6.2	Science and housekeeping data generation	39
6.3	EPS and TCS subsystems OBDH analysis	39
6.4	Interface and autonomy OBDH analysis	39
6.5	Optics and interferometer control OBDH analysis	40
6.6	Operating System OBDH analysis	40
6.7	OBDH Sizing per Mode	41
6.8	Heritage OBDH Solutions	41
6.9	Specifications of OBDH Components for D.U.S.T.I.N.	42
6.10	D.U.S.T.I.N. Data rates	43
6.11	Specifications for potential data buses	43
6.12	On-board data handling technical requirements	45
7.1	EPS power budget - Acquisition/Calibration/Software Update mode	47
7.2	EPS power budget - Sleep/Boot mode [75% OBDH, 25% Motors, Interferometer off]	47
7.3	EPS power budget - Safe Mode [25% OBDH, 25% Motors, Interferometer assembly off]	47
7.4	EPS DC/DC converters	48
7.5	EPS technical requirements	48
8.1	Temperature thresholds for the payload components	50
8.2	Thermal net characterization	51
8.3	Steady state temperatures reached in hot case scenario	52

8.4	Steady state temperatures reached in cold case scenario	52
8.5	TCS technical requirements	53
9.1	Al-7075 properties	55
9.2	Honeycomb panel properties	55
9.3	First 10 modes of the payload	55
9.4	Mass budget, computed and margined values, for D.U.S.T.I.N.	61
9.5	Structural technical requirements	62

List of Symbols

Variable	Description	Unit	Variable	Description	Unit
A_x	Variation of the opacity od element x	km	N	Number of components	-
a	Semi-major axis	km	n	Refractive index	-
al	Albedo	-	NEP	Noise Equivalent Power	W
B	Plank function	-	Q_{abs}	Dust absorption parameter	m^2/kg
bpw	Bits Per Word	b	q_{Albedo}	Albedo flux	W/m^2
D^*	Detectivity	$cm/\sqrt{Hz}/W$	q_{Sun}	Solar flux	W/m^2
d_{eq}	Equivalent aperture	mm	q_{IR}	Thermal IR flux	W/m^2
d_{int}	Diameter interferometer mirror	mm	R	Reflectivity	-
d_{pm}	Diameter primary mirror	mm	r_{eff}	Effective radius of dust	μm
d_{pn}	Diameter pointing mirror	mm	R_{Mars}	Mars radius	km
d_{sm}	Diameter secondary mirror	mm	R_p	Responsivity	V/W
E	Young's modulus	Mpa	r_{pn}	External radius of the pointing mirror	mm
e	Eccentricity	-	r_{int}	Internal radius of the pointing mirror	mm
F	Focal length	mm	TID	Total Ionizing Dose	rad
f	Focal ratio	-	T	Atmosphere temperature	K
f_{ac}	Acquisition frequency	Hz	T_{Mars}	Mars temperature	K
f_{typ}	Typical acquisition frequency	Hz	T_{surf}	Surface temperature	K
f_v	View factor	-	α	Absorptivity	-
f_x	Element x optical depth spectral dependence	-	Δv	Manoeuvre cost	-
G	Shear modulus	MPa	ϵ	Emissivity	-
h	Orbit altitude	km	η	Efficiency of the optical system	-
h_{pn}	Thickness of the pointing mirror	mm	η_{int}	Efficiency of the interferometer	-
i	Inclination	deg	λ	Wavelength	m
I	Observed monochromatic radiance	W/m^2-sr	μ	Cosine of emission angle	-
$KIPS$	Throughput	KIPS	ν	Poisson's ratio	-
$KIPS_{typ}$	Typical throughput	KIPS	ν_e	Spectral frequency	Hz
L	Coherence length	mm	ρ	Density	kg/m^3
L_s	Solar longitude	deg	σ	Stefan-Boltzmann constant	W/m^2K
M	Dust mass	kg	σ_t	Tensile yield strength	MPa
			τ	Optical depth	m

Acronyms

Acronym	Description
<i>ACQ</i>	Acquisition Mode
<i>BOT</i>	Boot Mode
<i>CAL</i>	Calibration Mode
<i>CCSDS</i>	Consultative Committee for Space Data Systems
<i>CM</i>	Closure Mechanism
<i>COSPAR</i>	Committee on Space Research
<i>ConOps</i>	Concept of Operations
<i>DLaTGS</i>	Deuterated L-alanine doped triglycine sulfate
<i>DSN</i>	Deep Space Network
<i>EOP</i>	Early Operation Phase
<i>EPS</i>	Electrical Power Subsystem
<i>FFT</i>	Fast Fourier Transform
<i>FOV</i>	Field of View
<i>FTIR</i>	Fourier Transform Infrared spectroscopy
<i>GM</i>	Gimbal Mirror
<i>GMA</i>	Gimbal Mirror Assembly
<i>GSD</i>	Ground Sampling Distance
<i>GUI</i>	Graphical User Interphase
<i>IFOV</i>	Instantaneous Field Of View
<i>IRF</i>	Instrument Response Function
<i>KIPS</i>	Kilo Instructions Per Second
<i>LRPT</i>	Low-Rate Picture Transmission
<i>MM</i>	Moving Mirror
<i>MOI</i>	Mars Orbit Insertion
<i>NOZ</i>	No Nadir Observation Zones
<i>OBC</i>	On-Board Computer
<i>OBDH</i>	On-Board Data Handling
<i>OS</i>	Observation Sequence
<i>PSG</i>	Power Spectrum Generator
<i>RTD</i>	Thermoresistances
<i>RoD</i>	Review of design
<i>SAF</i>	Safe Mode
<i>SLP</i>	Sleep Mode
<i>SNR</i>	Signal to Noise Ratio
<i>STB</i>	Stand-by Mode
<i>STR</i>	Structure
<i>SWU</i>	Software Update Mode
<i>TCM</i>	Telecommands
<i>TCS</i>	Thermal Control Subsystem
<i>VCSEL</i>	Vertical-Cavity Surface-Emitting Laser

1 | Introduction

1.1 Dust storms on Mars

The dust cycle is the most influential process affecting Martian meteorology on the short time scales as well as its climate across seasons and years. The Martian dust storms are classified according to their dimension and duration [1]. In particular

- Local dust storms: events in which high concentrations of dust are created on a region limited to $1.6 \times 10^6 \text{ km}^2$ for a maximum duration of 3 sols.
- Regional dust storm: these events are extended on an area larger than 10^6 km^2 and last up to 20 sols. Dust is moved for large portion of the planet surface and it can form an extended band that covers all latitudes.
- Global dust storms: these events are created by the connection of several regional storms. The planetary phenomena covers all latitudes and the dust concentration typically returns to nominal values only after 80-100 sols after the onset of the storm.

The current state of knowledge of Mars climatology does not allow to predict the onset of local or regional dust storms and how they can evolve in a short time frame to planetary-scale events. They don't originate from a preferential location of origin and the time interval between two global events was not constant during the years as can be observed in Figure 1.1.

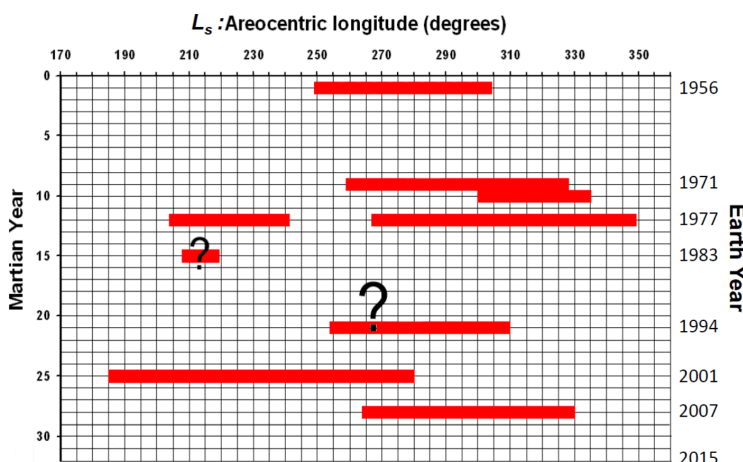


Figure 1.1: Distribution of directly confirmed and dubious global dust storms from 11th April 1955 (MY 1) to 18th June 2015 (end of MY 32). The event in Martian year 15 dust storm. Between the end of Viking mission and the beginning of Mars Global Surveyor (1983-1999) information is fragmented and only acquired from Earth observations

The dust has a key role in the present climate of Mars and achieving a deep understanding of dust storms is essential to enable the future possibility of performing weather forecasting on Mars, a requirement for human exploration missions (Goal IV, Sub-Objective B3 in the "Mars Science Goals, Objectives, Investigations, and Priorities 2020 Version" document). The capability to forecast dust storms sols in advance could allow to actuate specific mitigation activities for human and robotic missions, such as preserving power if a regional storm is expected to impact or avoiding performing EVAs.

The current fleet of spacecraft orbiting around Mars is able to provide a good picture of Mars' climate by performing a mapping activity, but in order to focus on weather monitoring, as a precursor to forecasting activities, continuous and simultaneous observations of the whole Martian surface are required [2].

1.2 Regions of interest for future human missions on Mars

The selection of candidate regions for future human missions is based on several constraints: the presence of ice deposits, preference for low latitude locations for increased solar power generation, and planar and rock-free surfaces for safe landing manoeuvres. The most promising areas identified by JPL and SpaceX [3] are Arcadia Planitia, Erebus Montes and Phlegra Montes, highlighted in the top panel of Figure 1.2. In the zoomed bottom panel 22 prospective landing sites are reported in the three regions. Based on this analysis, to provide valuable meteorological information for future human missions, it is sufficient to continuously monitor a limited latitude region, identified by the horizontal dashed lines in Figure 1.2 and spanning $[-70^\circ, 70^\circ]$.

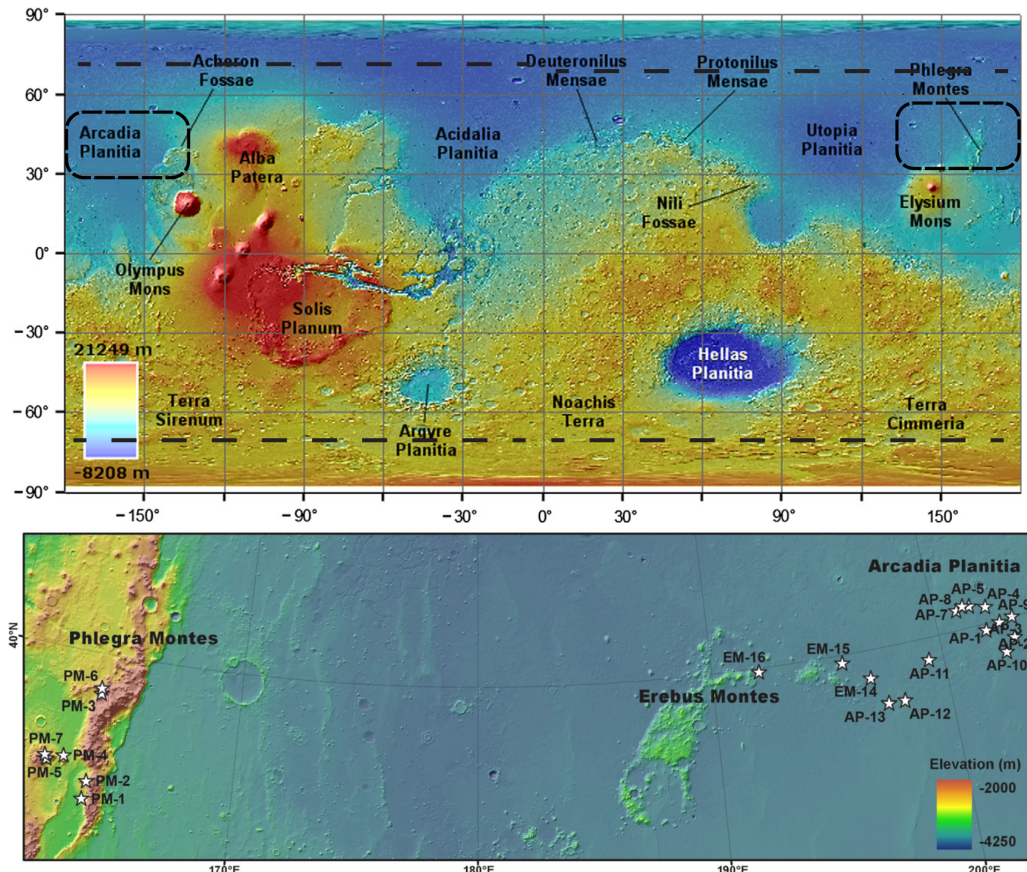


Figure 1.2: Selected landing sites for future Starship missions

1.3 Introduction to dust opacity observation

The key physical parameter to identify a dust storm in the Martian atmosphere from nadir pointing and to quantify the amount of dust that moves is the Column (vertically-integrated) Dust Optical Depth (CDOD) τ_{dust} [4]: it describes the amount of radiation at a specific wavelength absorbed by airborne dust during its path through the Martian atmosphere. This opacity can be directly linked to the dust mass M in the vertical column of the atmosphere that is observed by

$$M = \frac{4\tau_{dust}(\nu)r_{eff}}{3Q_{abs}}$$

with ρ density of dust material (typically 2500 kg m^{-3}), r_{eff} the effective radius of dust (typically $1.5\text{-}2 \mu\text{m}$ in the lower atmosphere) and Q_{abs} the absorption parameter for each dust particle encounter, modelled in [5].

To avoid the large scattering effect by dust particles and be able to observe the lower layers of the atmosphere even with a high amount of airborne dust, the analysis is focused on a spectral band

with wavelengths larger than the typical size of dust particles, so in the mid-infrared band. In order to obtain the CDOD τ_{dust} , the same method adopted by the instruments TES on Mars Global Survey mission [6], THEMIS on 2001 Mars Odyssey mission [7] and EMIS on Hope mission [8] is followed. The first step is the retrieval of the temperature profile along the Martian atmosphere. In order to obtain this measurement, the method developed by [9] is adopted, which requires high spectral sampling around the $15 \mu\text{m}$ absorption band of CO₂: the required bands, shown in Figure 1.3, are separated by 10 cm^{-1} . The resulting temperature profile has a vertical resolution of 10km and it extends from the Martian surface up to 0.1 mbar ($\sim 40\text{ km}$).

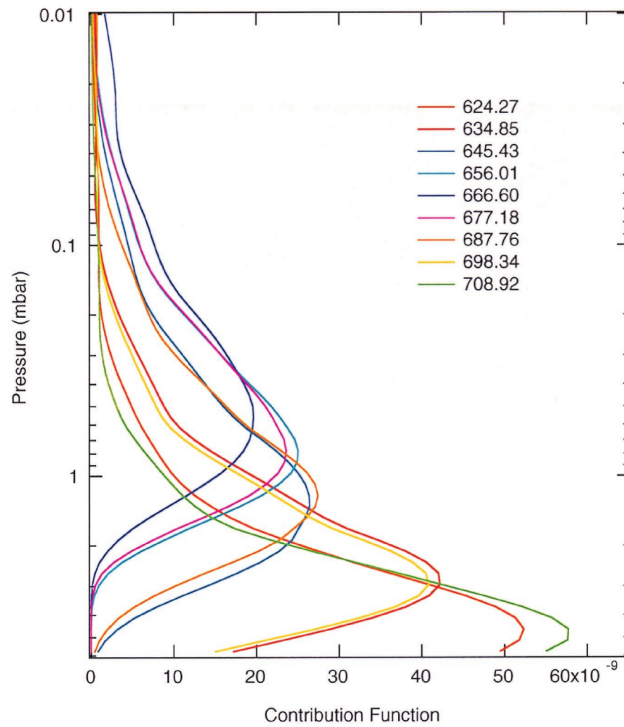


Figure 1.3: Contributing functions for the wavenumbers used in the temperature retrievals. These contributions can be obtained with a spectral resolution of 10 cm^{-1} around the $15 \mu\text{m}$ band

The second step is the retrieval for total aerosol optical depth τ_0 from the measured radiance

$$I_{\text{observed}}(\nu) = \epsilon(\nu)B(T_{\text{surf}}, \nu)e^{-\tau_0(\nu)/\mu} + \int_0^{\tau_0(\nu)} B(T, \nu)e^{-\tau/\mu} d\tau \quad (1.1)$$

where I is the observed monochromatic radiance, $\epsilon(\nu)$ is the surface emissivity at frequency ν , $B(T, \nu)$ is the Planck function, T_{surf} is the surface temperature, τ_0 is the total optical depth, μ is the cosine of the emission angle, T is the atmosphere temperature for the considered layer and the integral is performed from the spacecraft with $\tau=0$ to the surface with $\tau = \tau_0$.

The first term in the equation represents the radiance contribution from the planetary surface, while the second one is the radiance contribution from the different atmospheric layers. The total optical is composed of three contributions: absorption from dust, from water ice clouds and from CO₂ in the atmosphere

$$\tau_0(\nu) = \tau_{dust} + \tau_{ice} + \tau_{CO2} = A_{dust}(lat, long)f_{dust}(\nu) + A_{ice}(lat, long)f_{ice}(\nu) + A_{CO2}(lat, long)f_{CO2}(\nu) \quad (1.2)$$

where f_{dust} , f_{ice} and f_{CO2} contain the spectral dependence of the optical depth and A_{dust} , A_{ice} and A_{CO2} describe the variation of the opacities from spectrum to spectrum due to the amount of corresponding component observed.

Similarly, the surface emissivity is expressed as

$$\epsilon(\nu) = 1 - A_{\text{surf}}f_{\text{surf}} \quad (1.3)$$

where A_{surf} is the amplitude of the surface emissivity and f_{surf} is its spectral dependence.

The spectral contributions to the optical depth f_{dust} , f_{ice} , f_{CO_2} and f_{surf} are shown in Figure 1.4 and are assumed to remain the same for all the observations [10]. The amplitude of the CO_2 opacity contribution is also assumed to be constant and equal to 0.025.

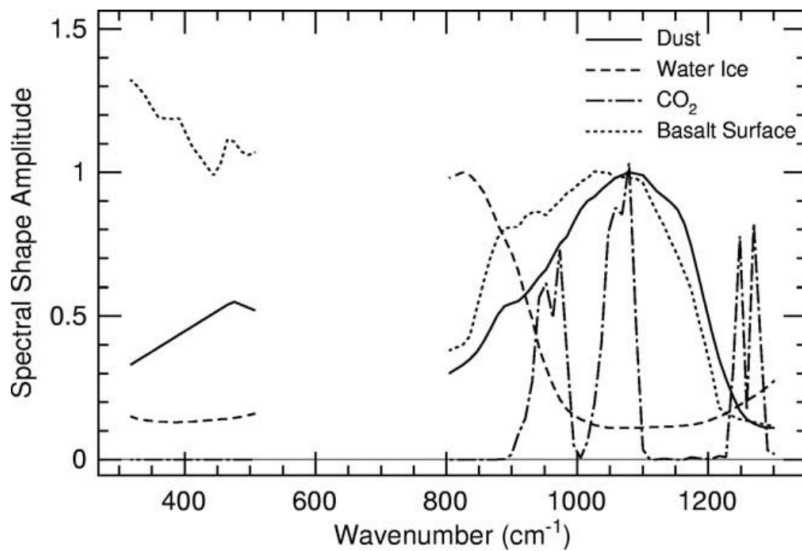


Figure 1.4: Spectral dependence of dust, water ice, CO_2 optical depth and of surface emissivity. Data in the region $500-800\text{ cm}^{-1}$ are not shown for the strong absorption by $15\mu\text{m}$ CO_2 band

For each opacity spectrum, given as input the measured radiance at each frequency, the surface temperature and atmospheric temperature at each considered layer, a minimization algorithm is used on Equation 1.1 to obtain A_{dust} , A_{ice} and A_{surf} . In Figure 1.5 spectra of the Martian atmosphere are shown for different measurement conditions [8]. In the dust storm spectrum, it is clearly visible the radiance drop at $9.3\mu\text{m}$ ($\sim 1100\text{ cm}^{-1}$) in correspondence with the higher spectral dependence of f_{dust} , shown in Figure 1.4. Analogously, the blue spectrum, corresponding to high content of water ice clouds, shows a drop around $12.5\mu\text{m}$ ($\sim 800\text{ cm}^{-1}$) where the f_{ice} has its maximum value.

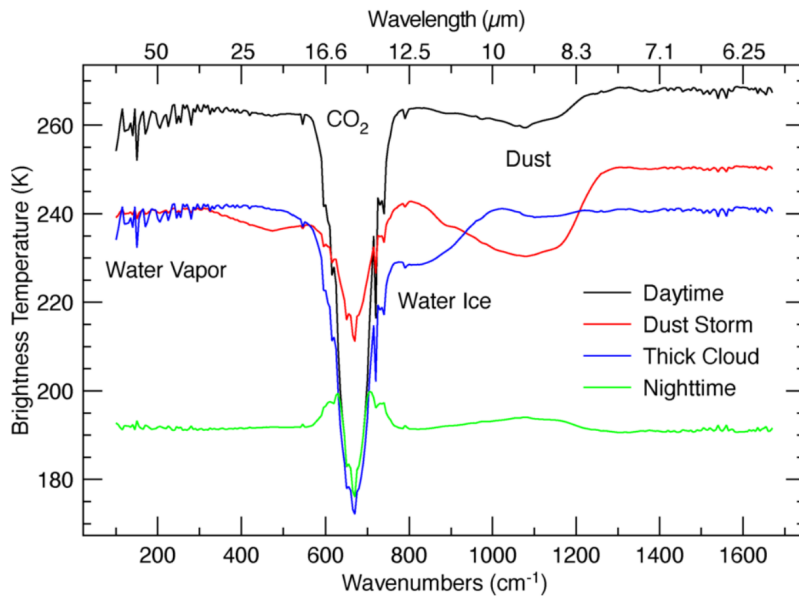


Figure 1.5: Spectra of Martian atmosphere for observation performed at local noon with clear sky, during a diurnal dust storm, during passage of thick water ice clouds and at local midnight

This analysis underlines that the wavelength band of interest for a dust monitoring mission ranges between $7\mu\text{m}$ to $15\mu\text{m}$.

2 | Concept definition

2.1 Mission Statement

The main scientific objective of the mission is to provide a diurnal continuous view of the lower atmosphere of Mars in order to monitor the time evolution of dust storms in the band of latitude between $\pm 70^\circ$.

The increasing number of Mars missions and the potential for future human colonization on the planet underscore the critical need for robust weather forecasting capabilities to ensure their success. Within this scope, D.U.S.T.I.N. (Dust Understanding and Storm Tracking INvestigator on Mars), aims to provide a diurnal continuous view of the lower atmosphere of Mars to monitor the time evolution of dust storms. In addition to enhancing Mars weather forecasting, D.U.S.T.I.N. will provide insight into short-time scale events, clarifying the formation and transformation of local dust storms into regional or global-scale phenomena.

In order to retrieve the optical depth of dust, the atmospheric and surface temperatures are necessary parameters to be acquired.

2.2 High Level Requirements

Table 2.1 displays the High-Level Requirements derived from the mission statement of the mission. In Section A.1, additional information about parent and children requirements for these HLR can be found.

Table 2.1: *High level requirements*

Identifier	Description	Type	Verification
DUS-HLR-0001	The payload shall observe the formation of dust storms covering at least the surface of Mars between latitude $+70^\circ$ and latitude -70°	Functional	Children
DUS-HLR-0002	The payload shall be capable of detecting dust presence in the Martian lower atmosphere	Functional	Children
DUS-HLR-0003	The payload shall be capable of computing the dust storms location in Martian lower atmosphere	Functional	Children
DUS-HLR-0004	The payload shall be capable of measuring the quantity of dust in the Martian lower atmosphere	Functional	Children
DUS-HLR-0005	The payload shall be capable of operating for at least 12 terrestrial years	Functional	Children
DUS-HLR-0006	The payload shall have an acquisition temporal resolution of less than 1 hour during diurnal observation	Functional	Children
DUS-HLR-0007	The payload shall have an on-ground spatial resolution of less than 100 km during diurnal observation	Functional	Children
DUS-HLR-0008	The payload shall survive the environmental conditions suffered during its whole lifetime	Functional	Children

2.3 Drivers

The design of D.U.S.T.I.N. is driven by several key drivers that influence both the architecture and operations of the instrument. Table 2.2 presents these drivers, highlighting their limitations and the impact they have on the system's design.

Table 2.2: *D.U.S.T.I.N. design drivers*

Driver	What limits the driver	What the driver limits
Data Storage	Number of payloads; Antenna; Orbit, GS availability; Solar conjunction	OBC Memory; Operation modes
Temporal Resolution	FoV; iFoV; Communication windows; Acquisition time; Processing time	Instrument Architecture; OBDH
Spatial Resolution	FoV; iFoV; Communication windows	Instrument Architecture; Orbit Selection; OBDH
Continuous Diurnal Coverage	Power, Orbit, Communication Windows	Instrument Architecture; Orbit Selection; OBDH

Data Storage is a critical driver that is influenced by the number of payloads on board, the capabilities of the antenna, the orbit parameters, and the availability of ground stations, as well as periods of solar conjunction when communication is not possible. This driver, in turn, places constraints on the On-Board Computer (OBC) memory and the operational modes of the instrument. A balance between storage capacity and data prioritisation is needed.

Temporal Resolution, defined by the Field Of View (FOV), Instantaneous Field Of View (IFOV), communication windows, acquisition time, and processing time, determines the data acquisition and processing capabilities of D.U.S.T.I.N. It impacts the instrument's architecture and the OBDH, demanding a design that can accommodate the required speed and efficiency of data handling.

Spatial Resolution is constrained by the FOV and IFOV, as well as the available communication windows. This driver shapes the instrument's architecture, which needs careful orbit selection to optimise coverage and resolution. It also has implications for the OBDH's data processing and storage strategies.

Continuous Diurnal Coverage is driven by the available power, the chosen orbit, and the communication windows. It challenges the instrument's architecture to ensure uninterrupted diurnal operation, influencing orbit selection and the OBDH's role in data handling.

Each driver interconnects with the others, creating a complex web of design considerations that must be carefully balanced to achieve the mission's objectives. The choices made in response to these drivers will ultimately determine the success of D.U.S.T.I.N. in its goal to track and analyze Martian dust storms.

2.4 Mission Phases

The mission is divided into operational phases. Table 2.3 summarizes all the mission phases, with their principal objectives:

Table 2.3: D.U.S.T.I.N. Operational Mission Phases

Operational Phase	Objectives
Launch Phase	During the launcher ascension the spacecraft and payload are in sleep mode. The s/c has to fulfill the driver to survive to the loads due to the launch.
EOP	After the separation from the upper stage, the central computer is booted up, it turns on the heaters to prevent fuel freezing, it deploys the solar panels, and through the sun sensor, orienting towards the Sun to charge the batteries. After this, the probe enters into contact with the DSN to communicate health and safety to the Ops Team. After the initial commissioning of the s/c and the aliveness testing of the science instruments, another task will be the trajectory correction, if needed, through TCMs.
Cruise Phase	After LEOP, the spacecraft is traveling toward Mars. Here will occur telemetry exchange and trajectory corrections, in preparation for the Mars orbit insertion (MOI). The criticalities in this phase are related to the harsh space environment and solar radiation.
Mars Orbit Insertion Phase	The objective of this phase is to ensure that the s/c reaches a stable orbit around Mars that meets the COSPAR Planetary Protection requirements[11]. The maneuver of MOI will start only after contact with the Earth, to see the probe from the DSN at least when the s/c is not behind Mars.
Transition Phase	The s/c enters in its design orbit and checks the health status of the instruments onboard.
Science Phase	This phase begins when the s/c enters the design orbit. After the check and the calibration of the instruments, the s/c starts to its observation campaign. It is designed to last 12 years but it can be extended.
Disposal	This phase begins at the end of the life of the mission. The objective of this phase is to ensure a safe decommissioning of the s/c, according to the Planetary Protection requirements [11].

In order to understand better the evolution in time of the mission, in Figure 2.1 is possible to see a first attempt of timeline (in months) of the mission (Figure 2.1).

Dust storms tend to occur near planetary perihelion that coincides with the Southern Summer Solstice (transition between yellow and red bar in Figure 2.1). Due to the intense summertime radiation, there is a higher probability to trigger dust storms that may last for several months, with optical depth value τ capable of obscuring the entire surface of the planet.

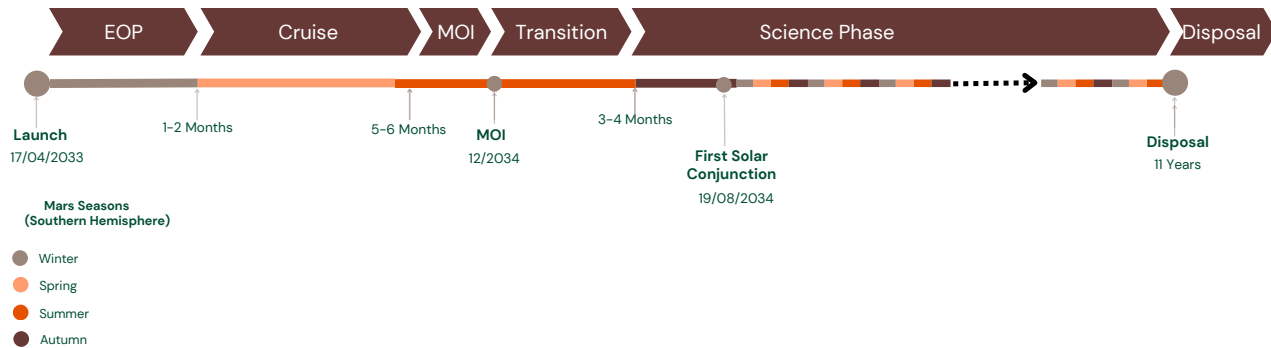


Figure 2.1: Timeline of the mission. The top timeline shows the phases of the mission, the bottom timeline illustrates the season cycle of Mars.

2.5 Payload Modes & ConOps

The payload has to operate in several modes, reported in Table 2.4. These modes should be seen as subroutines that are made to manage all the possible scenarios that can occur during the mission, from simple tasks to non-nominal conditions. This flexibility allows the payload to dynamically adapt its operations, ensuring robust performance and effective handling of unexpected situations.

Table 2.4: D.U.S.T.I.N. Operational Modes

Modes	Description
Sleep Mode (SLP)	This mode is activated when the Sun is approaching the FOV of the instrument, to avoid a direct Sun exposure of the optical system. The payload enters in SLP also during the eclipse, launch and cruise phase. In this mode, the payload is capable of receiving commands to enter in different modes.
Software Update Mode (SWU)	During this mode there is the possibility of uploading new software for controlling the payload in case of anomalies and failures.
Boot Mode (BOT)	In this mode the flight software is booted and the instrument searches for the pointing mirror home location.
Safe Mode (SAF)	This is an emergency mode, in which the payload will be switched off. This mode is activated automatically by some critical situation, like down of the power provided by the platform, temperature of the instrument beyond the admissible limit. Moreover, this mode can be also manually activated from ground, to restart the operations after an anomaly.
Acquisition Mode (ACQ)	During this mode the instruments acquires data needed to study the dust storm and processes them. This mode is activated after the end of the Calibration Mode.
Calibration Mode (CAL)	In this mode the instrument is calibrated. The spectrometer is calibrated by using two calibration measurements: observation of internal calibration blackbody target and of deep space.

The concept of operations (ConOps) for the payload are designed to get all the scientific observations needed to meet the science objectives of the mission. In the acquisition mode, the fundamental block of the ConOps of D.U.S.T.I.N. is the Observation Sequence (OS). This sequence is composed of two phases: the calibration of the instrument and the scanning observation, made through a gimbal mirror that scans the martian surface in a predefined range of latitude and longitude. In particular, ACQ mode starts after the calibration mode, where the spectrometer is calibrated by combining two calibration measurements: observation of deep space and internal calibration with a blackbody target. The full observation sequence requires approximately \sim 20 minutes as described in Section 4.10.2. This time interval is selected based on the fast temporal variability of dust storm on Mars.

The instrument is nadir-pointing and in order to avoid that the Sun enters in the FOV of the payload, a Sun-to-instrument boresight angle is regularly computed. When the observation enters in a exclusion cone with Sun at its vertex, called “No Nadir Observation Zones” (NOZ) [12], the scanning is interrupted and the instrument is put in SLP mode. In order to shield the internal optics, the gimbal mirror at the entrance of the instrument is pointed towards the internal calibration body, closing the path for the external radiation to the internal components of the instrument.

The ConOps retains the flexibility to define and implement new observation sequences, apart from the OS, like observations specifically designed to perform new science identified by the science team.

Once the modes are defined, it is possible to relate one or more of them to every single phase of the mission Table 2.5:

Table 2.5: Possible modes for each mission phases

Operational Phase	Possible Modes
Launch Phase	SLP - SAF
EOP	SLP - SAF - BOT
Cruise Phase	SLP - SAF
Mars Orbit Insertion Phase	SLP - BOT - SAF - SWU
Transition Phase	SLP - SAF
Science Phase	SWU - BOT - ACQ - CAL - SAF
Disposal	SLP

3 | Mission Analysis

3.1 Potential Launch Window

To select an appropriate launch window, the most critical point is the time duration of the mission as stated in requirement DUS-HLR-0005. D.U.S.T.I.N. aims to monitor Mars for a duration that exceed a whole solar cycle, equivalent to 11 years approximately. In this perspective, the launch window should be such that the total radiation received during the transfer, when the instrument is close to the Sun, is reduced while keeping both transfer cost and time as minimal as possible. Figure 3.1 [13] shows the prediction of solar activity for current solar cycle. As can be seen, it is expected to reach a minimum between 2030 and 2035. Therefore, it would be interesting to set the launch around those dates from radiation's perspective.

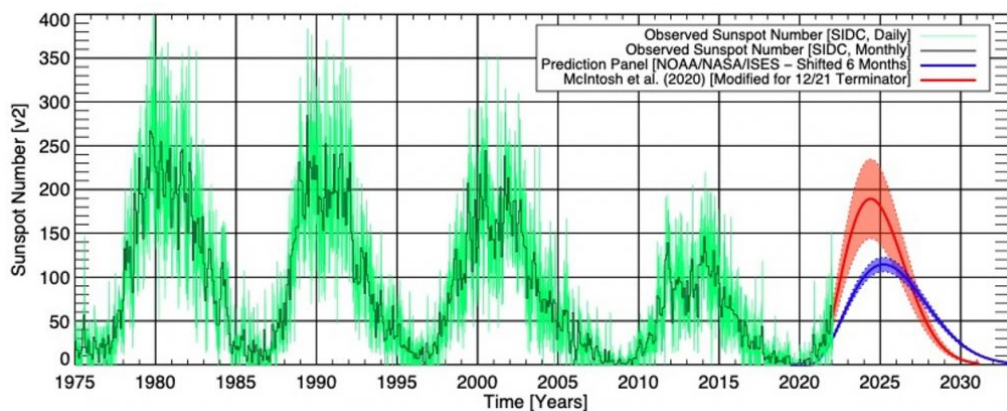


Figure 3.1: Solar cycle prediction

Additionally, Figure 3.2 [14] provides a set of possible launch windows based on transfer cost, transfer duration and Earth departure date. As mentioned above, it is interesting to select a short transfer in time and the scope will be focused on those points under 180 days of transfer time. Within these conditions and aiming to minimise the manoeuvre cost, the optimal solution is found to be launching on April 17th 2033. This time remains in the optimal range derived from a radiation perspective and, therefore, it is selected as D.U.S.T.I.N.'s potential starting date.

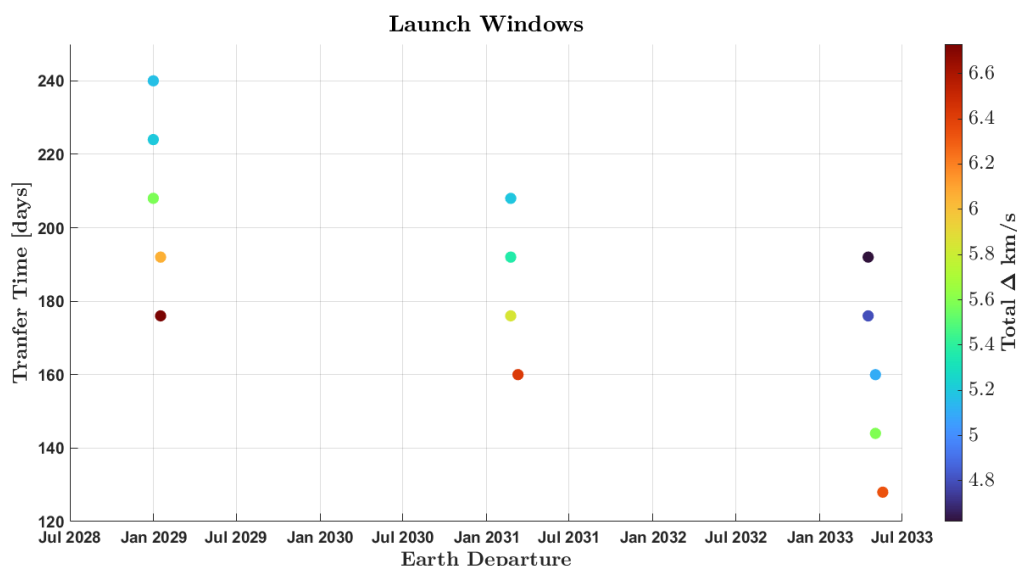


Figure 3.2: Possible Mars launch windows

Table 3.1: Transfer characterisation

Earth Departure	Mars Arrival	Departure Δv [km/s]	Injection Δv [km/s]	Total Δv [km/s]
Apr 17 2033	Oct 10 2033	3.6	1.2	4.8

3.2 Launcher Selection

In order to deploy the entire areostationary system in orbit around Mars, it is needed to select a launcher capable of deploying the four spacecrafts to Mars simultaneously. The parameters considered for the trade-off process are:

- Payload Capacity
- Reliability
- Cost-Effectiveness
- Availability and Schedule
- Flexibility

This trade-off process led to the selection of two possible choices: SpaceX's Falcon 9 and Falcon Heavy. The selection between these two options is based on their payload capacity.

Based on the table from mass preliminary breakdown from "Space Mission Analysis and Design" book [15], which provides a rough percentage value of the payload mass with respect to the overall mass of the spacecraft, the spacecraft mass for D.U.S.T.I.N.'s mission can be estimated. For example, for a Planetary mission, the payload typically corresponds to approximately 11% of the overall spacecraft mass. Given the instrument payload mass of approximately 24 kg, as derived in Section 9.3, it can be calculated that the spacecraft mass would be approximately 24 kg divided by 0.11, resulting in an estimated spacecraft mass of around 218 kg. However, it's important to note that a forecasting mission may involve multiple payloads, so is possible to select a reference overall payload mass of around 120 kg considering 5 payloads of similar mass. Using the same reasoning, the overall spacecraft mass is estimated to be around 1090 kg.

Considering that the mission is composed of 4 spacecrafts, the total mass will exceed 4020 kg, which is the maximum mass capability of the Falcon 9 launcher for Mars orbit. Therefore, the Falcon Heavy emerges as the optimal choice, offering a blend of reliability, cost-effectiveness, and performance that aligns seamlessly with the mission objectives.

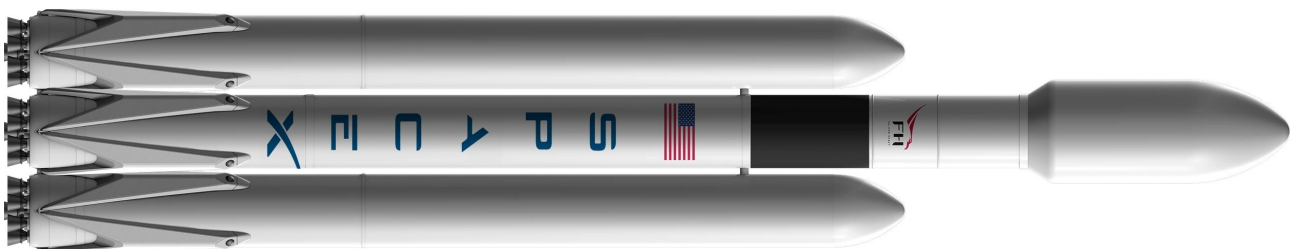


Figure 3.3: SpaceX's Falcon Heavy launcher

3.3 Nominal Orbit Trade-Off

As for the nominal orbit selection, three different options are studied:

- Polar orbit: Near circular low altitude orbit.
- Areostationary: Geostationary equivalent orbit on Mars.
- High elliptical orbit: High eccentricity orbit with a high-altitude apogee around the expected location of future colonies.

All of them can provide continuous monitoring of the target area, therefore, a trade-off analysis is needed for its selection.

Table 3.2: *Polar orbit analysis*

Polar Orbit	
Advantages	Disadvantages
<ul style="list-style-type: none"> • Better resolution on ground • Able to cover all of Mars' surface, including the caps • Possibility of having a smaller instrument • Easy to identify vertical dust storm variations thanks to continuous limb pointing • Easy to identify horizontal dust storm variations thanks to continuous nadir pointing 	<ul style="list-style-type: none"> • Constellation made of a high number of satellites to achieve continuous diurnal monitoring • More complex Mission Analysis procedure to understand the number of satellites needed • More complex Conceptual Operations to understand how the constellation is going to be carried to Mars and how is going to be deployed • More complex software, On-Board Data Handling and data processing to coordinate the data created by the whole constellation

The first orbit type to be removed is the Polar Orbit since the satellite would be in a low altitude and a high number of satellites would be needed to reach coverage of the desired area. Even if the time and spatial resolution that can be achieved with a low-altitude constellation are superior to the other two options, the amount of data that must be processed, both on-board and on-ground, and the complexity of coordinating the constellation makes it less interesting with respect to the other two orbits.

The next orbit to be discarded is the High Elliptical Orbit, the motivation derives from the high altitude reached during apogee and the long orbit period. In this case, the focal distance would need to be high to achieve a proper on-ground resolution, deriving in a big instrument with a narrow field of view, increasing the number of satellites needed. This last feature originates a more complex data process and satellite coordination. Additionally, as stated above, different types of orbits would need to be designed to cover the desired surface.

Therefore, the final selection is the areostationary orbit. It is a good compromise between the two options previously discussed and only three satellites are needed to cover the Martian area of interest [2]. The mission Hope, when at its periapsis is placed at a distance very close to areostationary orbit, provides a good example of the measurement that could be obtained. In particular, the time and spatial resolutions are acceptable when looking at Hope instrument EMIRS (Emirates Mars InfraRed Spectrometer) performances [8].



Table 3.3: Areostationary orbit analysis

Areostationary Orbit	
Advantages	Disadvantages
<ul style="list-style-type: none"> Only 3 satellites are needed for the monitoring of the desired area [2] Fixed satellite relative position with respect to Mars Global view of Mars's surface No need to coordinate satellites Less processing of data needed to combine all the measurements Easy to identify horizontal dust storm variations thanks to continuous nadir pointing 	<ul style="list-style-type: none"> Less resolution on-ground compared with Polar Orbit Bigger optics with respect to a Polar orbit Impossibility of performing limb pointing to asses vertical variations due to fixed relative position More complex measurement of vertical dust storm variations No caps coverage The implementation of an IR spectrometer is more complex as its field of view is typically small

Table 3.4: High elliptical orbit analysis

High Elliptical Orbit	
Advantages	Disadvantages
<ul style="list-style-type: none"> Less amount of satellites needed with respect to a Polar orbit Reduced data processing needs, when compared with a Polar orbit, as measurements are coming from fewer satellites More time spent around possible future colony locations, improving the time resolution Coverage of the whole of Mars' surface if the orbits are properly selected Easy to identify vertical dust storm variations thanks to continuous limb pointing Easy to identify horizontal dust storm variations thanks to continuous nadir pointing 	<ul style="list-style-type: none"> Design of different orbits needed to provide monitoring of the wanted area Long orbit period, meaning that a wide field of view or a high number of satellites will be needed to observe the desired area Worst resolution on-ground among the three options due to a very high altitude during the apogee More complex coordination of the orbiting satellites than in Areostacionary as different orbits are needed The implementation of an IR spectrometer is more complex as its field of view is typically small

3.3.1 Areostationary Orbit

An areostationary orbit is a circular and equatorial orbit around Mars with a semi-major axis of $a = 20428$ km, corresponding to an altitude of 17031.5 km. Its period of 24.65 hours is the same as the Martian sidereal day (sol) and allows to observe continuously the same position over the planet's surface.

Table 3.5: Orbital parameters

Orbit	a [km]	h [km]	e [-]	i [°]
Aerostationary	20428	17031.55	0	0

The areostationary orbit presents two stable and two unstable longitudes, respectively at 17.92°W , 167.83°E , 75.34°E and 105.55°W . The dominant perturbations for a satellite in areostationary orbit are due to:

- The non-spherical gravitational field of Mars causes a change of the semi-major axis of the orbit, producing a longitudinal drift of the spacecraft.
- The gravitational attraction of the Sun and of two moons Phobos and Deimos causes a change of orbit inclination, producing latitudinal oscillations.

The longitudinal station-keeping manoeuvres to maintain the areostationary orbit requires a higher Δv with respect to geostationary as shown in Figure 3.4 [16], while the north-south Δv would be smaller than the corresponding one for geostationary manoeuvres because of the small moons and the increased distance from the Sun.

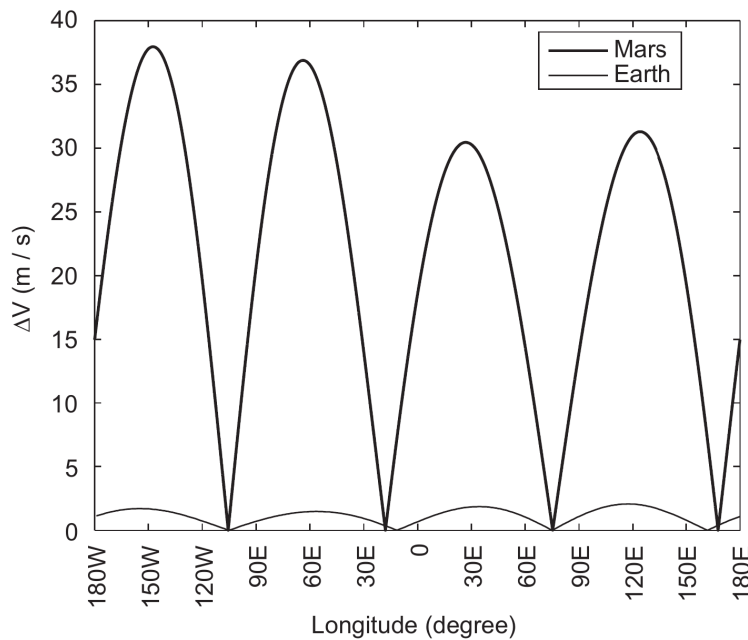


Figure 3.4: Annual Δv for longitudinal station keeping manoeuvres for areostationary and geostationary orbits

Finally, Figure 3.5 [17] shows the achievable coverage with 4 satellites placed in an areostationary orbit, centred at 180°W , 90°W , 0° and 90°E . This configuration, in which 4 identical D.U.S.T.I.N. payloads are used onboard 4 aerostationary satellites, is selected to provide a simultaneous coverage of Mars' surface in the latitude range of interest, as described in the requirement DUS-HLR-0001.

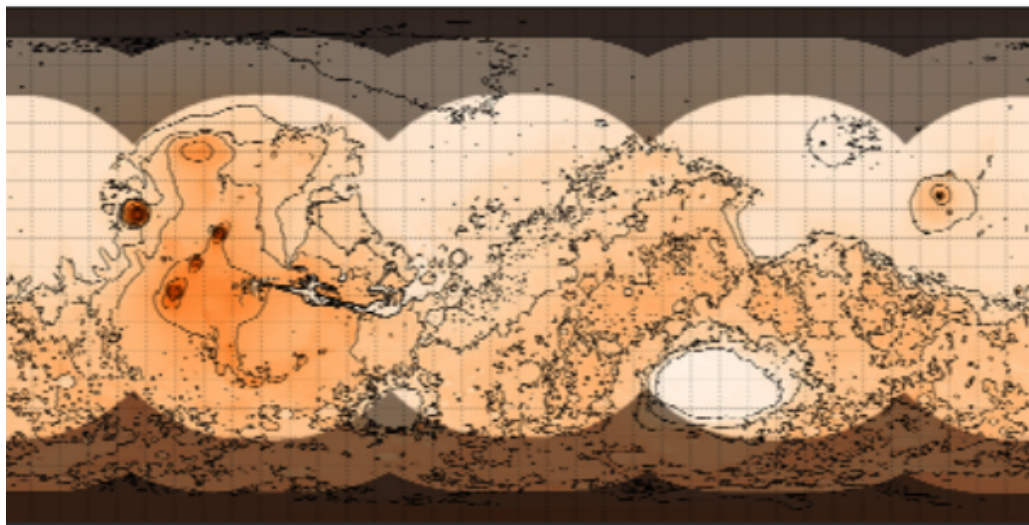


Figure 3.5: Mars surface coverage from a four-platform areostationary constellation

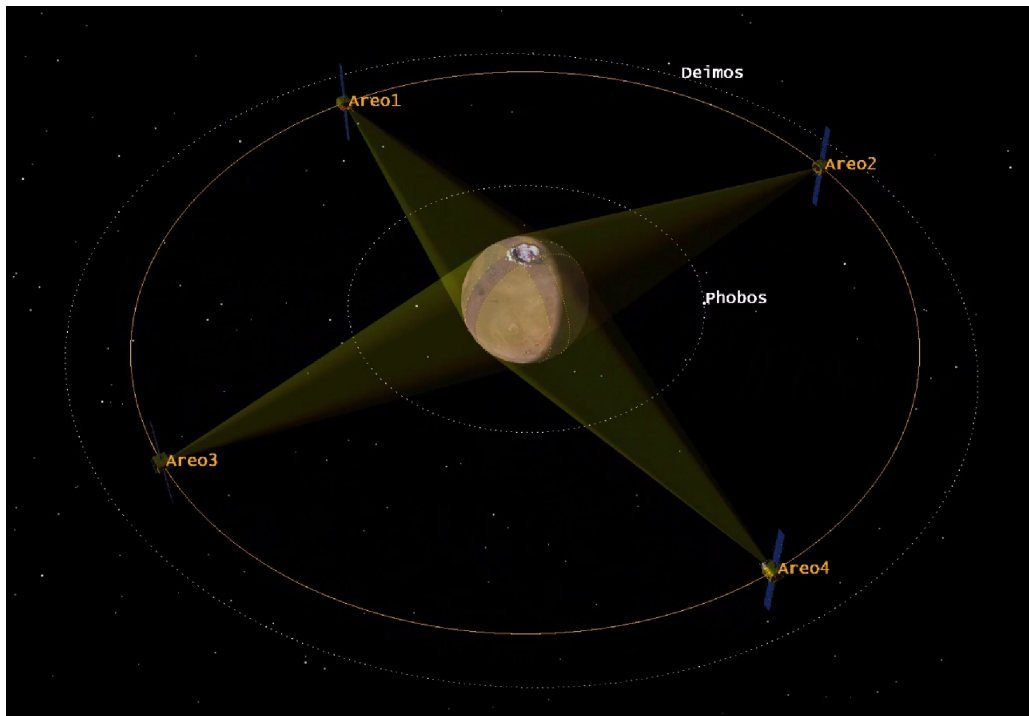


Figure 3.6: Mars observed from a constellation of 4 satellites from an areostationary orbit

3.4 Environmental Analysis

3.4.1 Main Assumptions

A preliminary assessment of the environment associated with the orbit selected is performed in order to provide guidelines for the design definition and the trade-off analysis. Particular attention is given to the radiation environment.

The analysis is performed with SPENVIS software and takes into account the effects of both Solar Particles fluxes (note that the departure date has been set during a minimum of solar activity) and Cosmic Rays to assess the Total Ionizing Dose (TID) and the Single Event Effect rates.

The overall trajectory designed for the mission is split into two portions: the interplanetary travel and the areocentric orbit for the operations.

3.4.2 Interplanetary Transfer

The transfer orbit is split into three segments and for each one, a mean distance from the Sun is considered for the computations:

Table 3.6: Segmentation of the transfer orbit for environmental analysis

Starting Date	Arrival Date	Distance from the Sun [AU]
April 17,2033	June 16,2033	1.09 AU
June 16,2033	August 16,2033	1.26 AU
August 16,2033	October 10,2033	1.44 AU

During the Transfer to Mars, D.U.S.T.I.N. is expected to be in sleep mode, hence only the TID is evaluated. The results are based on the SHIELDOSE-2 model implemented in SPENVIS, where D.U.S.T.I.N. is modelled as entirely made of Silicon and shielded by a sphere of Aluminium with varying thicknesses. Figure 3.7 reports the TID estimated in each segment and the total TID, as a function of the shield thickness.

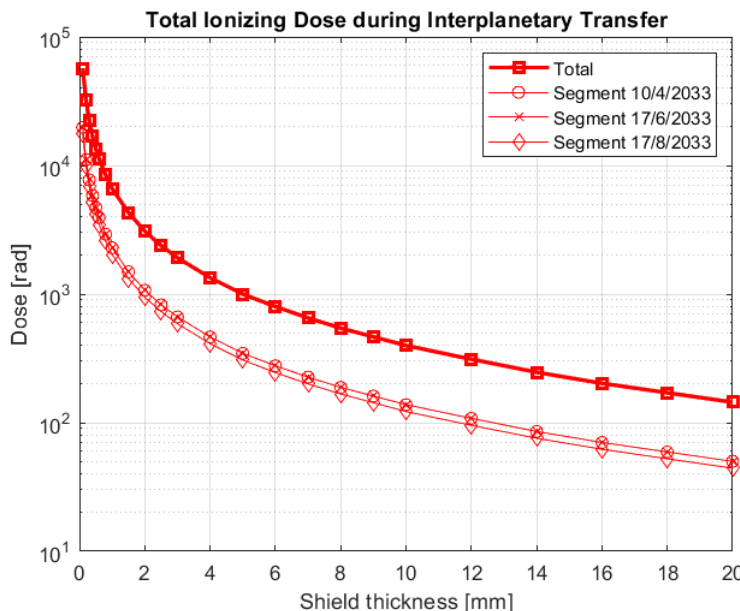


Figure 3.7: Total Ionizing Dose as function of shield thickness for the Interplanetary Segment

Hence, it is clear that one possibility is to adopt a thicker shielding to reduce the TID accumulated during transfer but so augmenting the inert mass of the system. Another possible solution would be to reduce the shielding (and so its mass), allowing the TID to grow, thus having to select components with better rad hardness properties.

3.4.3 Areostationary Orbit

D.U.S.T.I.N. is expected to perform its operations from areostationary orbit. This choice will allow for a constant observation of a specific region of Mars's surface. Computations are done considering the payload operational life of 12 terrestrial years (a Solar cycle), as specified in requirements DUS-HLR-0005. It is important to notice that Mars' magnetic field is extremely weak, hence the effect of trapped radiation is neglected by the models in SPENVIS.

The analysis in SPENVIS is conducted to assess the main aspects of the Martian areostationary radiation environment in terms of TID, SEU, and LET spectrum expected in order to have proper estimations for the design.

The evaluation of the Total Ionizing Dose is carried on again with the SHIELDOSE-2 model built in SPENVIS, considering the instrument as entirely in Silicon, shielded inside a sphere of Aluminium with varying thickness. Results are reported below:

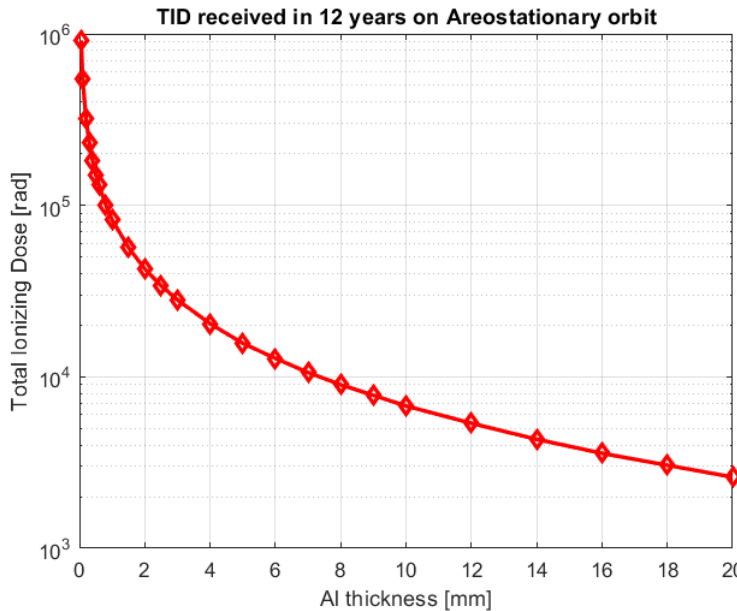


Figure 3.8: TID received by D.U.S.T.I.N. in its 12 year operations

It is possible to see that the TID associated with 12 Martian years of activity is larger than the TID absorbed during the interplanetary leg. This is due to the duration considered for this phase.

Given the long time of operations expected and the radiation environment of the nominal orbit, an assessment of the SEU rate is performed considering both the Galactic Cosmic Rays flux (ISO 15390 Standard model) and the high energy protons flux (CREME-96 model), which are the two main causes of single event effects. The analysis is launched considering an Aluminium shield of thickness 1 mm:

Table 3.7: Expected short-term SEU rates for high energetic protons flux

Effect	(bit ⁻¹)	(bit ⁻¹ s ⁻¹)	(bit ⁻¹ day ⁻¹)
Direct Ionization	5.8998E+04	1.5590E-04	1.3470E+01
Proton Induced Ionization	1.5647E+02	4.1347E-07	3.5724E-02
Total	5.9154E+04	1.5631E-04	1.3506E+01

Table 3.8: Total mission SEU due to GCR

Effect	(bit ⁻¹)
Direct Ionization	1.9308E+01
Proton Induced Ionization	2.8096E-01
Total	1.9589E+01

It is possible to see that the major contribution to SEU comes from the solar particles rather than GCR. Those parameters can be employed in the trade-off analysis and in the design phases related to the definition of the electronic architecture of the system [18].

It is reported below the average LET spectrum for a segment of the mission corresponding to one entire orbit and considering a shielded Si target, in order to assess the minimum LET that D.U.S.T.I.N. electronics shall withstand [18]:

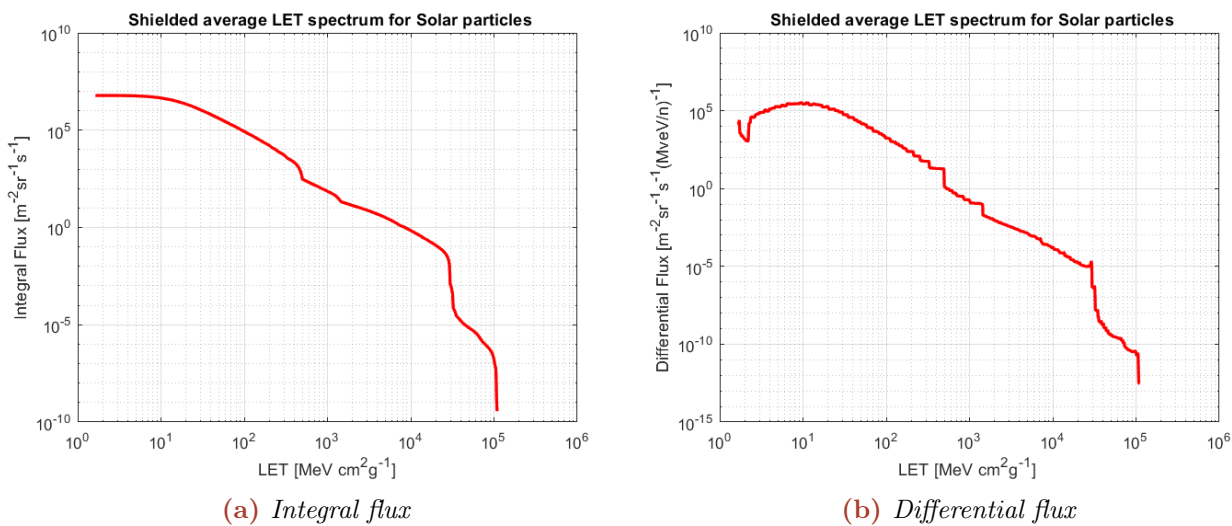


Figure 3.9: LET integral and differential fluxes for the areostationary orbit

After an iterative process, the final shielding thickness is set to 2 mm, considering aluminium as the material, to have a compliant design with all the components' radiation tolerance.

3.4.4 Areostationary Orbit Thermal Environment

Now, from the point of view of the thermal environment, three main heat flux sources are identified: direct heat flux from the Sun, flux due to Martian Albedo, and finally the thermal radiation from Mars surface.

As for the first one, its intensity decreases with the square of the distance from the Sun, hence, at Mars, it can be evaluated as:

$$q_{Sun} = 586.2 \text{ W/m}^2$$

Instead, for the flux due to Albedo, by considering a view factor f_v around 0.1 and the altitude h of the areostationary orbit, the flux is estimated as:

$$q_{Albedo} = f_v q_{Sun} al \left(\frac{R_{Mars}}{h} \right)^2 = 2.74 \text{ W/m}^2$$

Where the Albedo al of the surface is approximated as constant, around 0.17.

Finally, the thermal IR radiative flux is modelled as the emission from a black body at temperature $T_{Mars} = 209$ K, measured at the distance of the areostationary orbit:

$$q_{IR} = \sigma T_{Mars}^4 \left(\frac{R_{Mars}}{h} \right)^2 = 2.98 \text{ W/m}^2$$

where σ is the Stefan-Boltzmann constant.

It is clear that the direct heat flux from the Sun strongly dominates the thermal environment considered, hence being able to deal with it will dramatically affect the development of the TCS system.

3.5 Eclipse Analysis

To assess the eclipse analysis, the data is obtained using NASA GMAT and then processed with Matlab. To have a complete understanding of the eclipse evolution, the orbit is propagated for the whole mission duration. Figure 3.10 introduces both the total time and the total number of eclipses per day during the mission time span. It has a periodic behaviour, with a maximum eclipse duration of 77.26 minutes. This last value is crucial for EPS design.

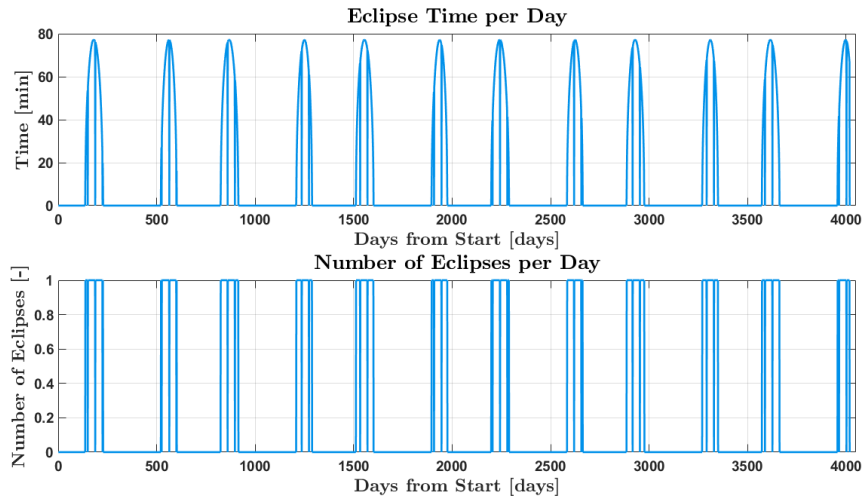


Figure 3.10: Total eclipse time per day and number of eclipses per day over the whole mission span

3.6 Visibility Windows Analysis

The Deep Space Network (DSN) is selected as one of the possible candidates for transmitting the data to Earth. The DSN is NASA's main communication ground segment facility for deep space missions. It is composed of the following three ground stations [19]:

Table 3.9: DSN ground stations

Parameter	Madrid	Goldstone	Canberra
Latitude [deg]	40° 25' 53" N	35° 25' 36" N	35° 24' 05" S
Longitude [deg]	4° 14' 53" W	35° 25' 36" N	148° 58' 54" E

As in the previous Section 3.5, the data is obtained using NASA GMAT and processed with Matlab. Figure 3.11 shows the total visibility time and number of visibility windows for each ground station during the whole mission lifetime. There is, at least, one window with each facility every day, with a minimum contact time of 5 hours. This analysis suggests that, if the DSN is the final ground segment selected, the data transmission will not be limited in any case.

Based on the above plots, D.U.S.T.I.N. memory sizing will be relieved by the possibility of transmitting all the generated data every day. However, GMAT does not consider the superior solar conjunction effects. During that time the payload is assumed to be out of reach for about two weeks [20]. Therefore, the payload's data generation during that period needs to be properly addressed, and its importance is already taken into account by the drivers.

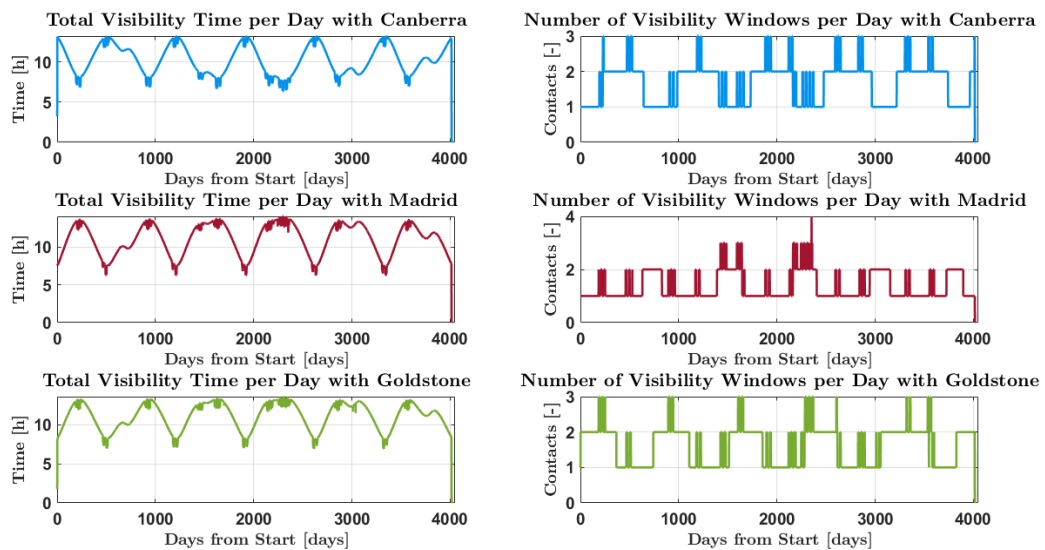


Figure 3.11: *Visibility windows analysis*

3.7 Orbital Technical Requirements

Table 3.10 displays the orbital technical requirements. In Section A.2.1, additional information about parents and children can be found.

Table 3.10: *Orbital technical requirements*

Identifier	Description	Type	Verification
DUS-ORB-0001	The payload shall be operated in an areostationary orbit around Mars	Mission	Inspection
DUS-ORB-0002	The payload shall point towards Nadir	Mission	Inspection
DUS-ORB-0003	Four simultaneous payloads shall be operated around Mars	Mission	Inspection
DUS-ORB-0004	The four payloads should be located centered at 180°W, 90°W, 0° and 90°E	Mission	Inspection

4 | Optics and Detector

4.1 Architecture Selection

In order to perform the spectroscopy study described in the Section 1.3, several options are considered. The first possibility is to use stripe filters on the detector, similarly to THEMIS payload of 2001 Mars Odyssey [7] which has 10 strip filters of $1 \mu\text{m}$ bandwidth. These strip filters could be selected in order to observe in the spectral region of interest for D.U.S.T.I.N.'s mission ($7\text{-}15 \mu\text{m}$). The problem with this solution is the broad band of each spectral filter: the first issue is that to be compliant with requirement DUS-OPT-0002, a spectral resolution of 10 cm^{-1} ($\sim 0.1 \mu\text{m}$) is required around $15 \mu\text{m}$ in order to retrieve the temperature profile of the Martian atmosphere. In addition to that, the similar behaviour of the spectral shape for dust absorption and surface emissivity requires such resolution also around $9 \mu\text{m}$ to be able to distinguish the two contributions. Another mission that used strip filters is Mars Reconnaissance Orbiter with Mars Climate Sounder [21] that, even using wide bands similar to THEMIS, is able to perform dust optical depth retrieval thanks to limb observations. Differently from nadir pointing, this approach allows to directly observe the temperature of the different layers of atmosphere. The LEO orbit that allows this kind of measurement is not selected from nominal orbit trade-off analysis.

A second option is the use of Echelle spectrometer. This solution, even if capable of providing the required resolution (requirement DUS-MIS-0014), is mostly used in the visible and near-infrared bands, so outside the spectral region needed by requirement DUS-OPT-0001 and DUS-FUN-0003. Its use for different frequency bands would need a substantial increment of complexity of the payload design.

The last solution considered is the use of a Fourier Transform InfraRed (FTIR) spectrometer. This instrument is capable of operating in the required bands and of providing the resolution to create the temperature profile of the atmosphere. An FTIR spectrometer contains an interferometer whose output is an interferogram produced at different discrete positions of an internal moving mirror: applying a Fourier transform to the interferogram, the actual radiance spectrum is obtained. FTIR spectrometers have a wider operating spectrum range with respect to the Echelle spectrometer, without decreasing the spectral resolution below the requirement of the mission. Past missions that used FTIR solution for studying the Martian atmosphere are Mars Global Surveyor with TES [9], Mars Express mission with PFS [22], ExoMars 2016 Trace Gas Orbiter with TIRVIM and Hope mission with EMIR [8]. The long heritage in mapping the Martian atmosphere in the mid-infrared band with FTIR spectrometer together with the capability of being compliant with all the payload requirements make the choice of FTIR spectrometer the most suited for D.U.S.T.I.N.'s scientific purposes.

Table 4.1: Trade-off for optical architecture

Architecture	Broad bandwidth	High resolution
Stripped filter	✓	X
Echelle spectrometer	X	✓
FTIR spectrometer	✓	✓

4.2 Interferometric System Trade-Off

Three different interferometers are analysed: Mach-Zehnder, Sagnac and Michelson.

The Mach-Zehnder configuration is the simplest, most robust and reliable solution. It minimises vibrations using stationary mirrors. For an FTIR spectrometer, however, it is not suitable, due to the thousands of measurements needed, each one with a different path, leading to thousands of medium needed.

The Sagnac interferometer addresses the challenge of altering the optical path without changing the medium, but moving the mirrors. This setup avoids also possible problems due to undesired

reflection on the secondary mirror, generating off-axis interference. Indeed, this kind of reflection is avoided with the use of a second beam splitter. However, this solution is more complex because, in order to obtain the different paths, at least two mirrors have to be moved, with a possible increment of vibrations and weight. This interferometer would also need more space.

The Michelson interferometer allows a continuous reading like the Sagnac setup while maintaining a lightweight and compact profile. It needs only one moving mirror, reducing the amount of vibrations with respect to the Sagnac counterpart. However, potential secondary reflections to the telescope's secondary mirror must be carefully considered to avoid unintended interference.

Due to the long duration of the mission, high reliability is requested. Thanks also to its lightness and its simpler design, the Michelson interferometer solution is chosen. The secondary reflection problem should be taken into account more deeply with a more detailed design of the optical system. Possible solutions involve the use of baffles and a stop to absorb the undesired rays.

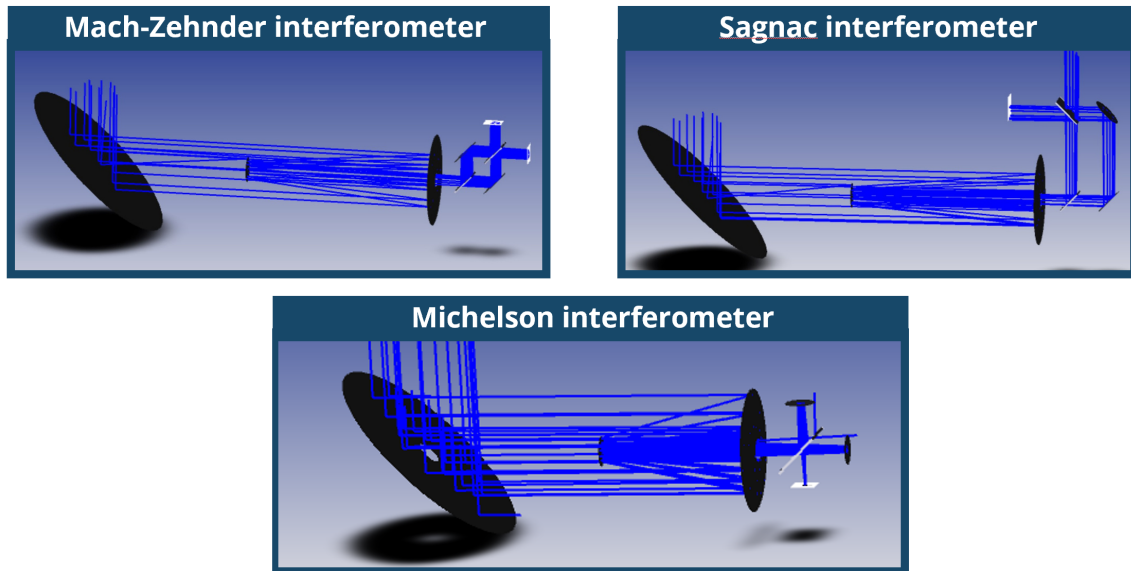


Figure 4.1: Different interferometric solutions

4.3 Pin-Hole Model

The pin-hole model is used to provide estimates of some key parameters of the optics, such as the focal length, the FOV and the IFOV. The selection of $GSD = 50$ km has the aim of improving the current resolution of the Mars climate model, which currently operates at a resolution in the range of 300-400 km. From the GSD and the altitude of an areostationary orbit, $h = 17031.5$ km the $IFOV = 0.168^\circ$ is obtained. Selecting a 5x5 pixels grid, each of 1.6 mm, the effective focal length results in $F = 0.477$ m. The size of the image radius at the Mars equator is $R = 250$ km, which combined with the areostationary orbit altitude, provides the $FOV = 0.841^\circ$. Selecting for this preliminary analysis a diameter of 0.17cm, the minimum IFOV to fully contain the Airy disk is 0.013° , ≈ 10 times smaller than the retrieved IFOV.

Table 4.2: Pin Hole model

h [km]	R [km]	GSD [km]	r_{pixel} [mm]	FOV [°]	IFOV [°]	F [m]	r_{det} [mm]	# pixels
17031.5	250	50	1.6	0.841	0.168	0.477	8	25

4.4 Optical Model

To have a lightweight small instrument, a reflector telescope is preferred. It is also better to avoid dispersion, potentially affecting the accuracy of the interferometric measurements. Moreover, reflectors can work over a broader range of wavelengths, making them versatile for different spectral regions [23].

The reflective telescope solution adopts a Cassegrain telescope configuration, which is more compact compared to a Newtonian system. The primary mirror is parabolic, while the secondary mirror is hyperbolic and serves to collimate the light rather than focusing it, thus facilitating interference. With the collimated beam, the error caused by the beam splitter thickness decreases significantly, eliminating the need to assume a thin beam splitter. Lastly, a paraxial mirror is used to focus the interference on the detector.

The first design of the optical system is performed using Zemax®. In Section 4.9 it is determined that the system requires an equivalent aperture d_{eq} of 200mm. To compute the value, it is considered the obstruction caused by the secondary mirror d_{sm} :

$$d_{pm} = \sqrt{d_{sm}^2 + d_{eq}^2}$$

Given a secondary mirror diameter equal to 50 mm, this results in a primary mirror with a diameter equal to 206.2 mm. Opting for a smaller secondary mirror introduces challenges in the collimation, generating more aberrations. Furthermore, the small reduction of the primary mirror diameter does not justify the resolution sacrifice. A mirror with the equivalent aperture would weigh just 40 g less than the primary mirror.

Following the Michelson interferometer, the light is focused using an off-axis paraxial mirror, represented in this preliminary design.

No margins are added since they are taken into account in Section 4.9. Further improvements, like a cold Lyot stop, could notably enhance the SNR[23]. However, such solutions are not considered in this preliminary design phase.

The design is shown in Figure 4.2:

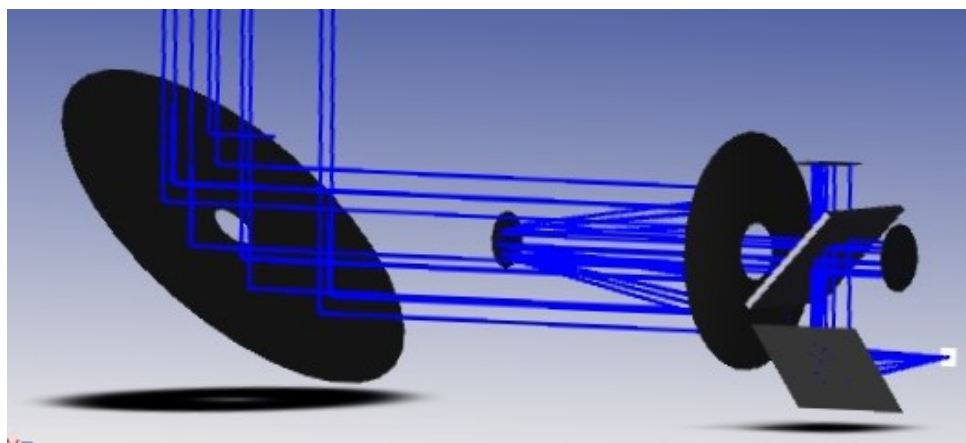


Figure 4.2: Optic design

The system uses a gimbal mirror to raster scan the Mars's atmosphere. The diameter of the pointing mirror d_{pn} is calculated as:

$$d_{pn} = \frac{d_{pm}}{\cos(45^\circ + \theta)}$$

where $\theta = 12^\circ$, equal to half the apparent diameter of Mars from an areostationary orbit. This allows to enlighten the entire primary mirror for each pointing angle of the raster scan, resulting in a pointing mirror of 376 mm.

Table 4.3: Optical model

Equivalent aperture [mm]	d_{pn} [mm]	d_{sm} [mm]	d_{int} [mm]	f	F [m]
200	376	50	60	2.39	0.477

4.5 Materials

To retrieve the best material for the mirrors, the main features considered are the reflectivity and the density.

A substrate of fused silica is considered for the mirror, due to its relatively low density, equal to about 2.3 g/cm^3 , and to its significant heritage in optical instruments and in space applications. Three different coatings among the most used in IR astronomy are considered: aluminium, silver and gold. The reflectivity spectra are provided by ThorLabs®:

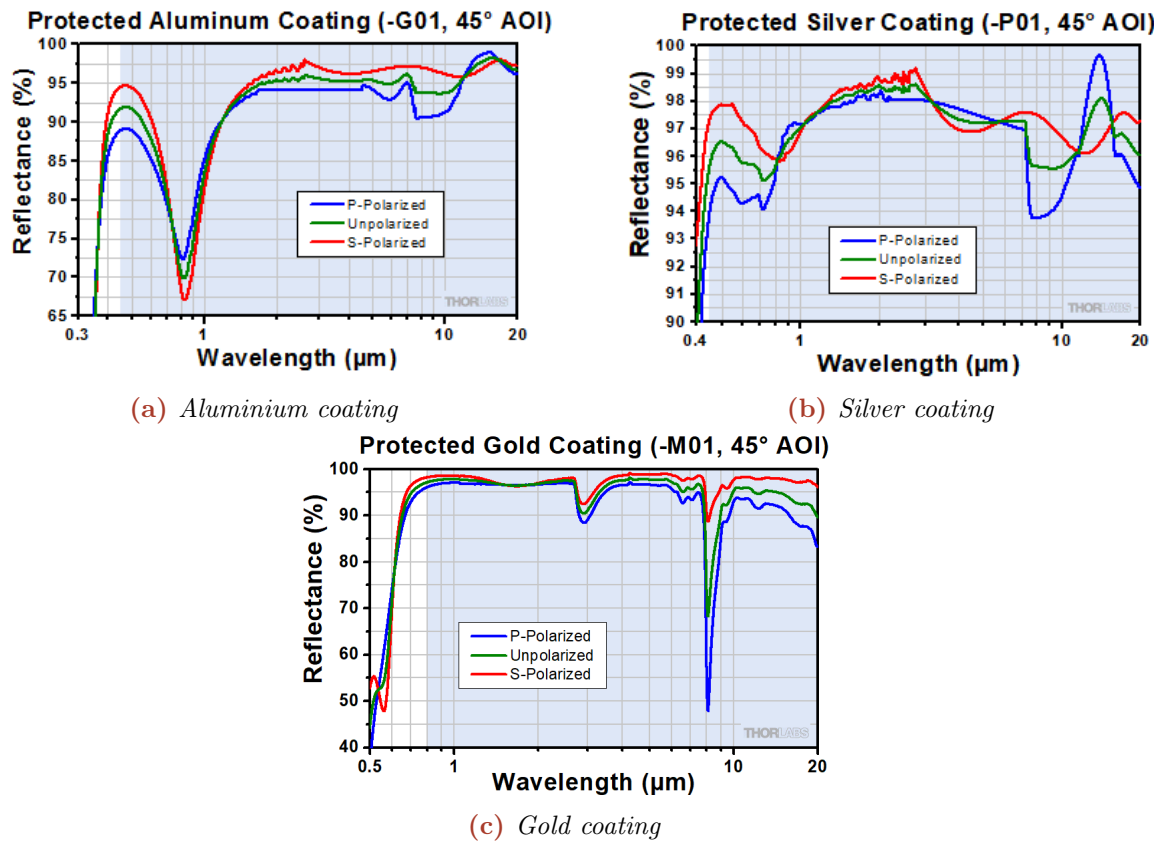


Figure 4.3: Different coatings for IR mirrors by ThorLabs, Inc.

Considering the wavelength range of interest equal to $8 - 16 \mu\text{m}$, the two best solutions are aluminium and silver since the gold coating shows a low reflectivity at $8 - 10 \mu\text{m}$, a region of interest to observe the CO_2 absorption line of the dust. The silver coating, Figure 4.3b, is chosen as coating for each mirror due to its highest reflectivity.

Considering that the maximum value of light polarization degree is very low ($< 2-3\%$) [24, 25], it is possible to compute a first approximation of the system efficiency considering the reflectivity of unpolarized light. From Figure 4.3b, the minimum reflectivity in the wavelength interval of interest is equal to $R=0.955$. The light is reflected five times before the measurement and only half creates the interference and reaches the detector, due to the 0.5 efficiency of the Michelson interferometer. The minimum efficiency η of the system can then be determined as:

$$\eta = R^5 \eta_{int}$$

resulting in a minimum efficiency equal to about 0.4.



The efficiency calculation does not currently incorporate the transmission coefficient of the IR filter of the detector. This data remains unavailable due to the need for customising the filter to meet mission requirements. However, given that a 100% margin is already factored into the diameter of the primary mirror and the transmissivity coefficient in the wavelength range of interest typically exceeds 95%, this coefficient can be disregarded at this stage without significant error.

4.6 Mass Budget

An estimation of the weight is provided considering the generic IR mirror with silver coating provided by ThorLabs®. The Table 4.4 reports the mass of each element without margins. Margins are added in the following sections to compute the TCS analysis. For this preliminary estimation, the interferometer mirrors, the secondary mirror and the beamsplitter are considered to have the same thickness equal to 6 mm. The pointing and the primary mirrors have a thickness equal to 12 mm. Each mirror is made of a fused silica substrate and a silver coating to enhance the reflectivity.

Table 4.4: *Mass budget of the optical system*

Element	Diameter [mm]	Estimated Mass[kg]
d_{pm}	206	0.914
d_{pn}	376	3.118
d_{sm}	50	0.027
d_{int}	60	0.039
l_{bs}	120	0.198
Total	-	4.296

4.7 Additional Components

4.7.1 Laser Diode

Considering a resolution of 10 cm^{-1} , the $\Delta\lambda$ is equal to 63.49 nm. It is possible to calculate the coherence length of the Michelson interferometer L . To calculate the movement of the moving mirror the following equation is employed:

$$L = \frac{\lambda^2}{n\Delta\lambda}$$

where n is the refractive index. This results in a coherence length of 1.008mm, leading to a maximum mirror travel $\frac{L}{2}$ equal to about $\pm 0.5 \text{ mm}$ [23].

From Subsection 4.10.2, the wavelength of the laser is equal to $0.846 \mu\text{m}$ at 25°C and the number of samples is at least 1120. Considering equidistant steps, the size of each step results in being equal to $0.9 \mu\text{m}$. The wavelength of the laser slightly changes with temperature, with a variation of 0.07 nm/K from the nominal temperature [26]. With a $\pm 20 \text{ K}$ variation, the change in the optical path is two orders of magnitude lower than the step size. From a resolution point of view, the shift of wavelength leads to a spectral sampling difference of about 0.1875 cm^{-1} , negligible with respect to the resolution of the instrument of 10 cm^{-1} .

4.7.2 Gimbal Mirror

Upon initial optical system design, the gimbal mirror boasts a substantial diameter of 376 mm, with a fused silica substrate and silver coating contributing to a mass of 3.118 kg. The gimbal mount must facilitate rotations of at least 102° , in order to allow both calibration and measurements. Movement precision should surpass the Instantaneous Field of View (IFOV) by at least an order of magnitude, ensuring a precision of at least $60'$.

The inertia matrix of the pointing mirror can be easily calculated as

$$I_z = \frac{1}{2} m_{pn} (r_{pn}^2 + r_{int}^2)$$

$$I_x = \frac{1}{12} m_{pn} [3(r_{pn}^2 + r_{int}^2) + h_{pn}^2]$$

leading to $I_z = 0.0542 \text{ kg/m}^2$ and $I_x = 0.0271 \text{ kg/m}^2$.

Given the significant size of the pointing mirror, robust support structures are required. Despite its considerable diameter, the mirror's weight remains relatively low. The optimal solution is then provided using a tailored gimbal mount. The selected motors are the ANT95R, allowing an accuracy of 3', fulfilling the precision requirement [27].

4.7.3 Paraxial Mirror

After the Michelson interferometer, the light is focused using a paraxial mirror. An off-axis parabolic mirror can be a valid solution to focus the light in the detector. However, in this preliminary design, a paraxial mirror is considered to have the desired focal length. Like the other mirrors of the system, the paraxial mirror is considered made of fused silica with an argent coating.

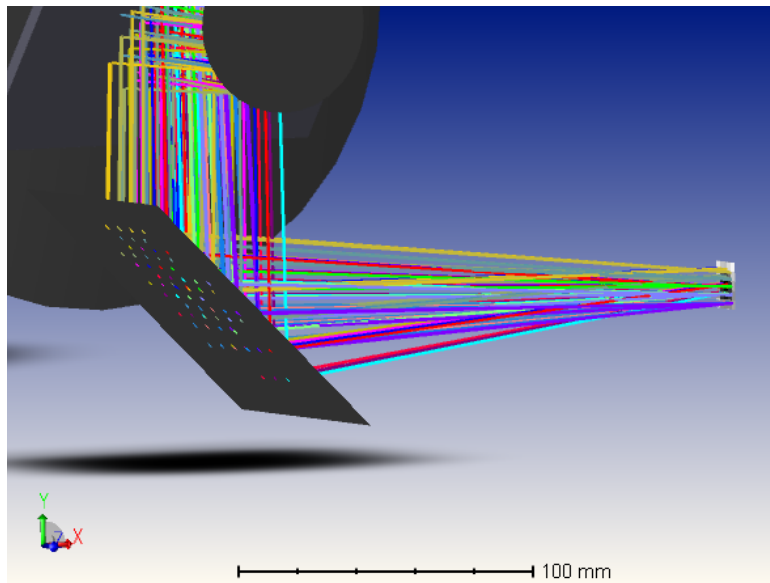


Figure 4.4: Paraxial mirror

4.7.4 Bandpass filter

To obtain the interferogram using FTIR technology, it is essential to filter it before acquiring spectra. Currently, it is considered an ideal bandpass IR filter with a low cutoff wavelength of $8 \mu\text{m}$ and a high cutoff wavelength of $16 \mu\text{m}$. Standard bandpass filters in this wavelength range can have a transmission coefficient higher than 90% [28]. Customized filters with thinner layers can achieve even higher transmission coefficients. To optimize performance, these filters should be positioned above the detectors. This placement minimizes dimensions and prevents undesired rays from reaching the detector, ensuring more precise spectroscopic measurements.

4.8 Detectors trade-off

For the selection of the detector, several options are considered and Table 4.5 summarises the key features of potential detector candidates. In other words, the table provides a concise overview of the critical characteristics taken into account during the detector selection process.

Table 4.5: *Detector's properties*

	Wild Spectral Range	High SNR	High Sensitivity	Reliability	Dynamic Range	No Cooling	Heritage
Thermocouples & Bolometers	✓	X	X	✓	X	X	THEMIS
DTGS	✓	X	X	X	X	✓	Mars Express
Photoconductive	✓	X	✓	X	X	✓	Akari
DLaTGS Pyroelectric	✓	X	✓	X	✓	✓	Cassini-Huygens
Mercury Cadmium Telluride	✓	✓	✓	X	✓	X	Venus Express
InSb	X	✓	✓	X	✓	X	Juno
Silicon	X	X	X	✓	X	✓	ISO

Clearly evident from the table, the preferred choice is the DLaTGS Pyroelectric detectors (Deuterated L-alanine doped triglycine sulfate Pyroelectric Detectors). Another viable option in terms of performance is the MCT detectors, albeit requiring an active cryogenic cooling system. The decision leans towards DLaTGS due to its advantage of not needing an active cooling system.

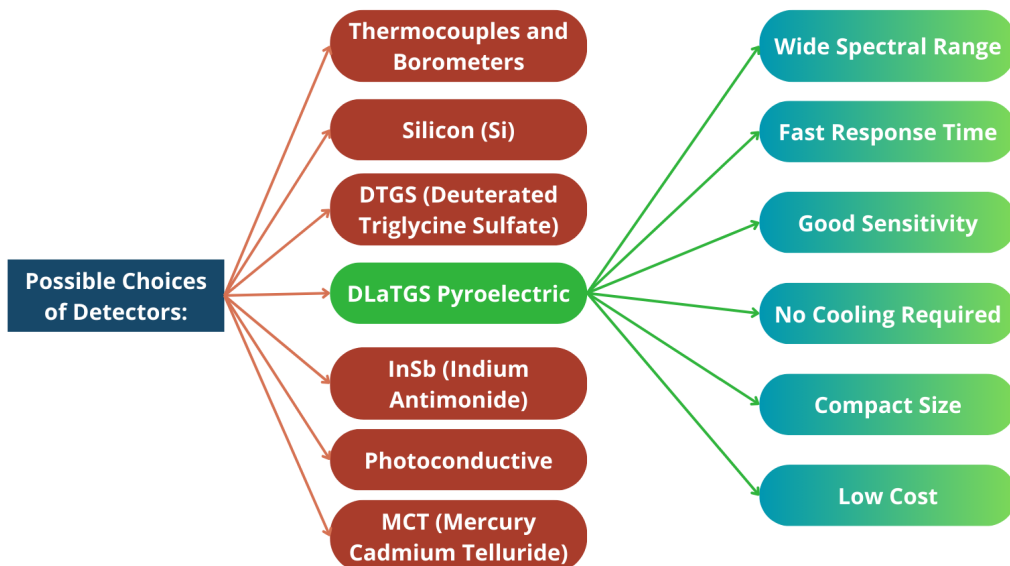


Figure 4.5: *Detectors trade off*

This detector has the peculiarity of measuring only the light, discarding other signals (like thermal noise), which don't produce any signal. The detector comprises a 5x5 pixel configuration, effectively covering an area of 250x250 km with a spatial resolution of 50 km.

The DLaTGS pyroelectric detectors selected are the ones from Series 99 by Leonardo company [29]. These detectors are characterized by a high energy level, providing for an acquisition frequency of 500 Hz a detectability $D = 5.08 \times 10^8 \text{ cm} \sqrt{\text{Hz}}/\text{W}$ and a responsivity $R = 150 \text{ V/W}$. Figure 4.6 [29] illustrates the relative trends in detectability, responsivity, and noise equivalent power (NEP) of these detectors.

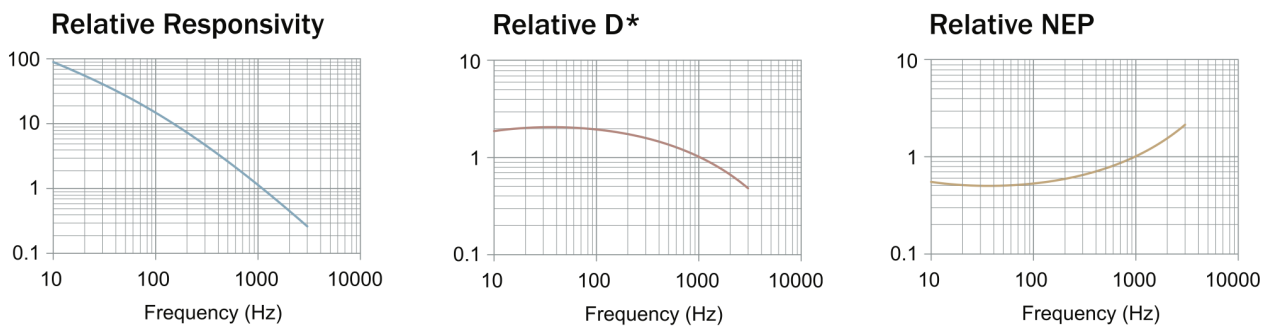


Figure 4.6: Typical relative responsivity, D^* and NEP for detector series 99 by Leonardo company

4.9 Radiometric Analysis

In order to assess D.U.S.T.I.N.'s Signal-to-Noise ratio (SNR), an analysis based on the Planetary Spectrum Generator (PSG) from NASA is performed. From its GUI, shown in Figure 4.7, it is possible to select the observation geometry and all properties of the spectrometer. In particular, this radiometric analysis considers a pyroelectric detector with an acquisition frequency of 500 Hz and a detectability of $D = 5.08 \times 10^8 \text{ cm} \sqrt{\text{Hz}}/\text{W}$. Figure 4.8a shows that for a diameter of the primary mirror major than 20 cm, SNR is bigger than 100 for the whole observation bands [8 μm , 16 μm], considering a 100% margin. Inside this band, the contribution to the reduction of the transmittance due to the dust peaks at 9 μm and the one related to CO₂ is placed 15 μm .

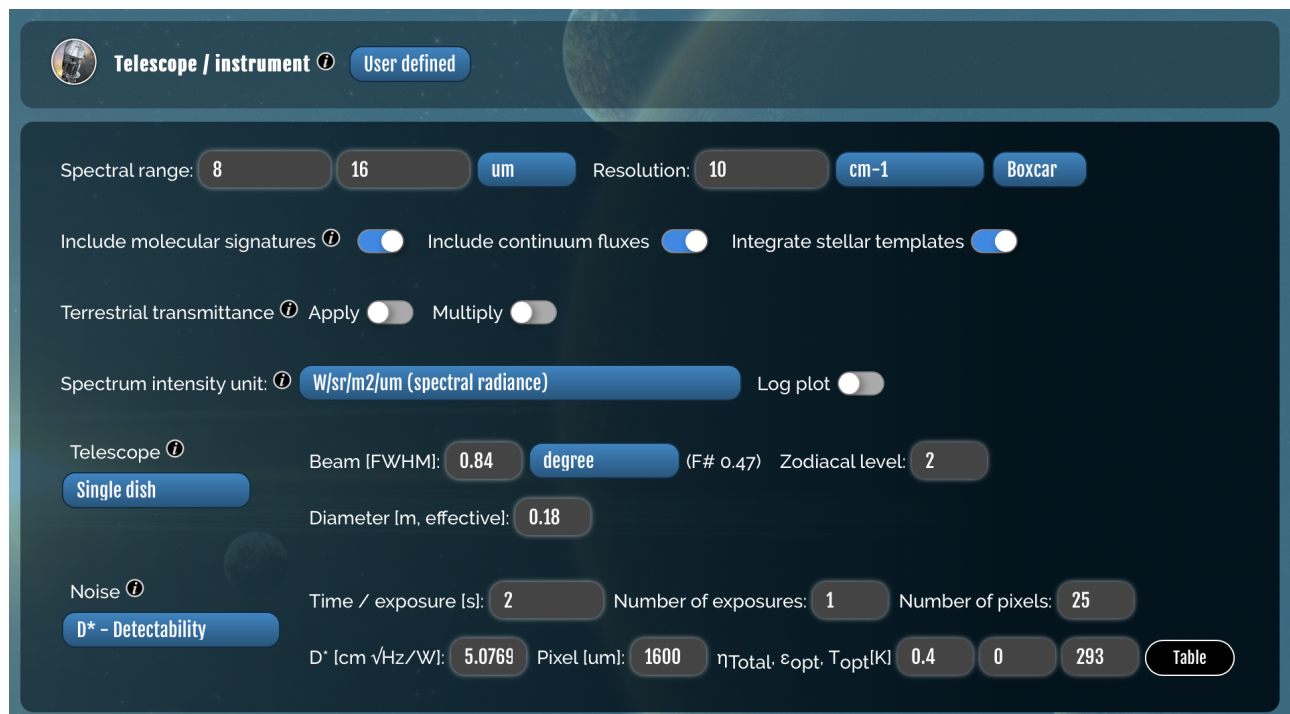


Figure 4.7: GUI of the NASA Planetary Spectrum Generator

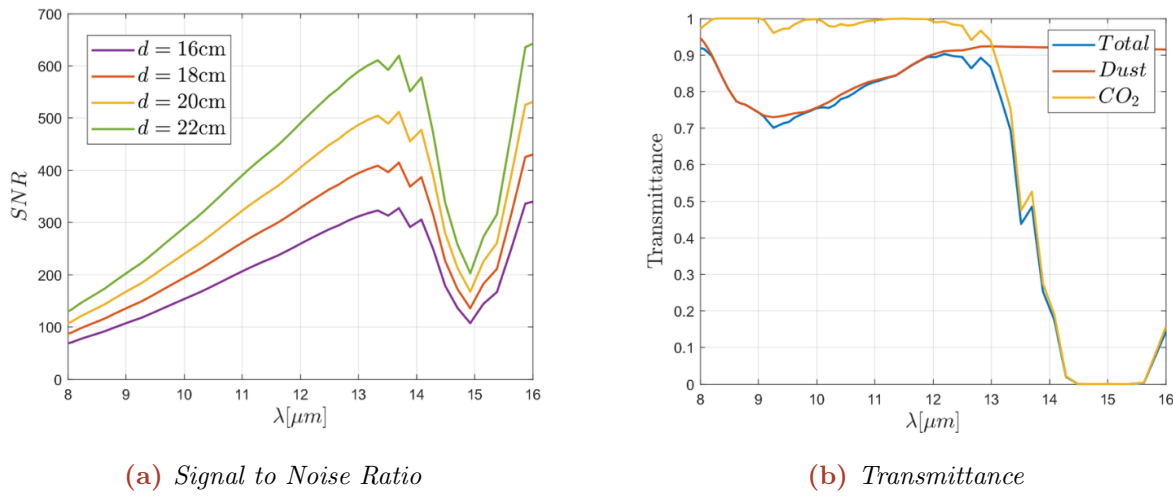


Figure 4.8: Radiometric analysis results from PSG

4.10 Observation Strategy

The acquisition strategy of D.U.S.T.I.N. is divided into two phases:

- Calibration.
- Raster scan.

The calibration phase aims to obtain the unknown parameters that contribute to the measurement and that need to be disentangled from the physical quantity of interest. After these preliminary operations, a gimbal mirror, positioned at the aperture of the instrument, starts a raster scan of the Martian surface in a predefined range of latitude and longitude, according to the grid shown in Figure 4.10.

4.10.1 Calibration Strategy

The objective of the measurements is the retrieval of the radiance of the scene (so its brightness temperature) at different frequencies to assess the presence of dust in the Martian atmosphere. The output of the Michelson interferometer is an electric voltage given by the difference of two contributes:

- The external spectral radiance falling on the detector, composed of the radiation emitted by the planet and the one emitted by the optical system: ($R_{\text{scene}} + R_{\text{optics}}$).
- the radiance emitted by the detector itself (R_{detector}).

This difference is then multiplied by the instrument response function (IRF).

In order to reduce the number of unknowns in this procedure, the introduction of a calibration body is required, a target of known radiance. Two options are taken into account:

- Black body positioned beyond the telescope assembly: the advantage is that, since the light is focused, a small calibration body can be used. On the other hand, an additional set of mirrors is required to point towards the black body. In this case, the radiation from the calibration target and from the scene follow two different optical paths and the radiance contributions coming from each optical element (R_{optics}) need to be estimated [30].
- Black body positioned in the opposite direction to the aperture: the gimbal mirror, already used for the observation of different locations on the Martian surface, can be used also to point a calibration target positioned on the opposite side with respect to the aperture of the instrument. In this case, the optical paths for the black body observation and for the Mars observation are

the same. This allows to compensate the R_{optics} by combining different calibration observations without the need for additional temperature measurement [8]. The disadvantage of this option is related to the need for a bigger black body since the light is not focused yet.

The second option is selected due to the easier design that does not require additional optical elements and the capability to obtain better accuracy on the radiance of the scene, thanks to the removal of the radiance contribution of the optics. The selected black body has the dimension of the primary mirror and has a v-groove surface geometry to increase its emissivity up to 0.99. The location of the black body is shown in Figure 5.4. Its temperature is measured with Thermoresistances (RTD).

The resulting equation to solve to obtain the radiance of the scene is:

$$V_{scene} = (R_{scene} - R_{detector})IRF \quad (4.1)$$

The two additional equations are obtained by performing a corresponding number of calibration measurements:

- Deep space observation:

$$V_{space} = (R_{space} - R_{detector})IRF \quad (4.2)$$

where the voltage V_{space} is measured and R_{space} is known since the deep space temperature is known (2.73K). The unknowns are $R_{detector}$ and IRF.

- Black body observation:

$$V_{cal} = (R_{cal} - R_{detector})IRF \quad (4.3)$$

where the voltage V_{cal} is measured and R_{cal} is known since the temperature of the black body is measured by RTDs. The unknowns in this case are $R_{detector}$ and IRF

By combining Equations 4.2 and 4.3, IRF and $R_{detector}$ are retrieved. Finally, by substituting them in Equation 4.1, the radiance of the scene R_{scene} is obtained. The calibration procedure is schematised in Figure 4.9.

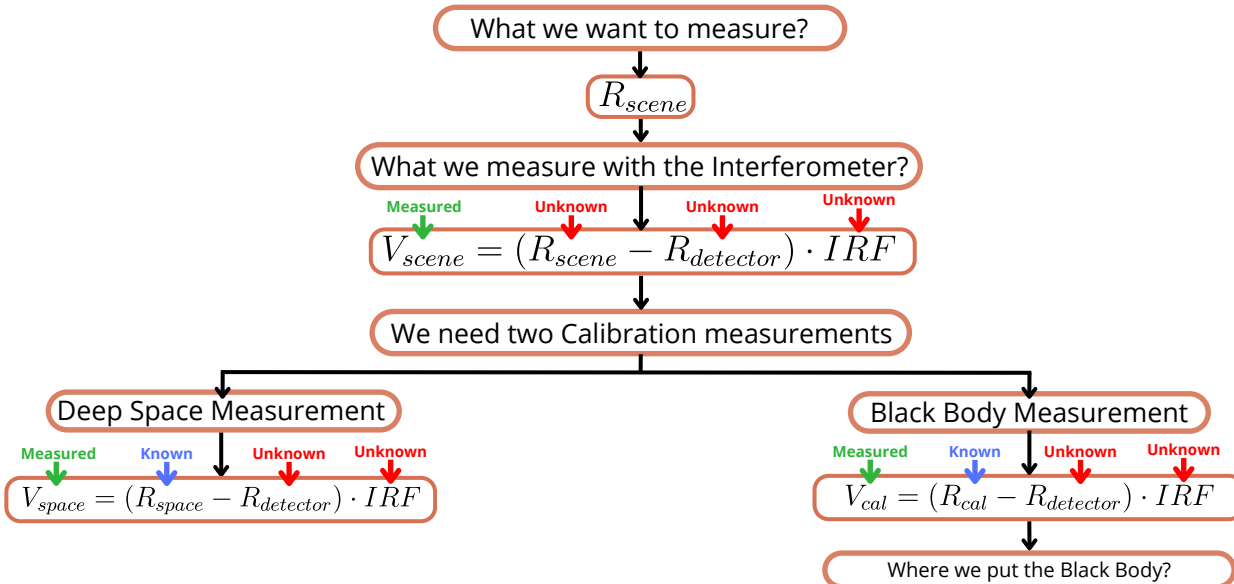


Figure 4.9: Conceptual scheme followed to perform the calibration of the instruments and to retrieve the desired output, the radiance of the scene R_{scene}

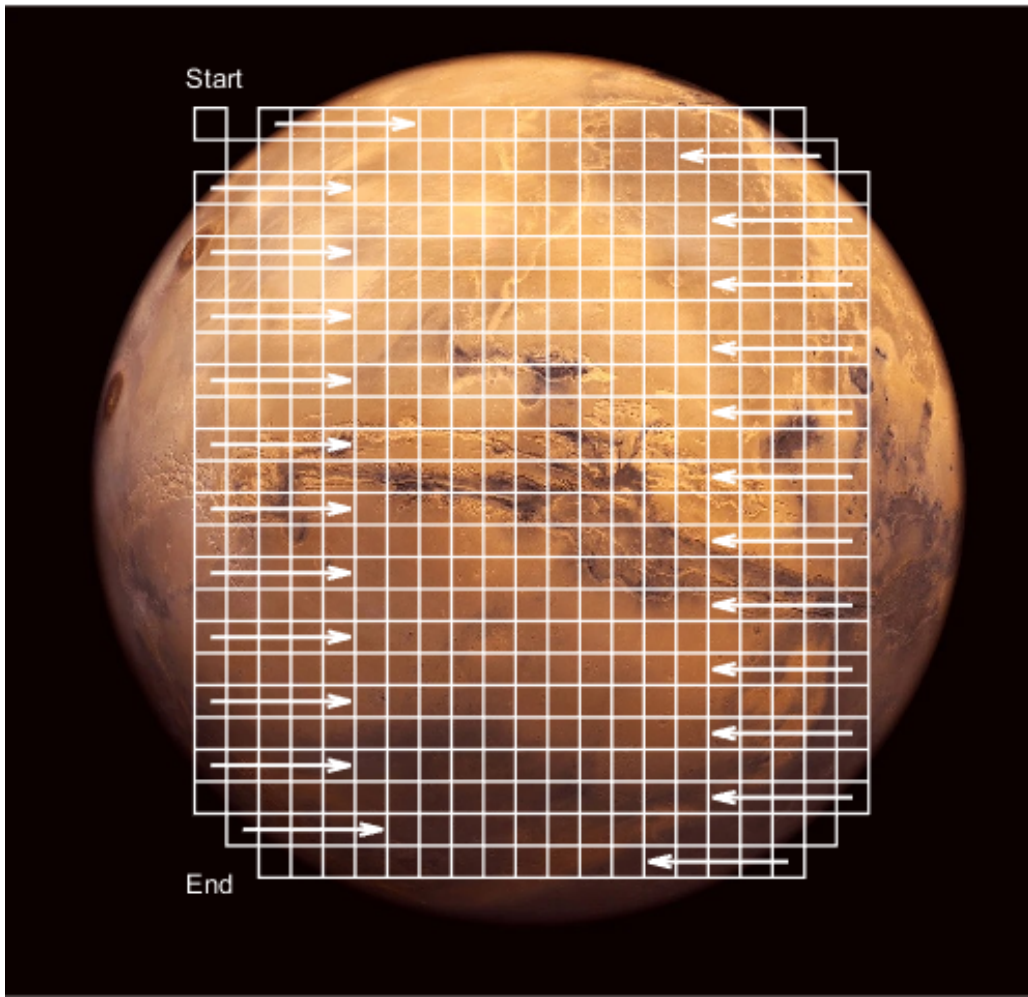


Figure 4.10: Acquisition strategy

4.10.2 Raster scan

A gimbal mirror placed as the first optical element after the aperture of the instrument is used to move the FOV of D.U.S.T.I.N across the Martian surface. The gimbal mirror is mounted on a side wall perpendicular to the instrument aperture to allow the observation of the calibration target and Mars. During each observation, one of the mirrors of the Michelson interferometer is moved at different positions: this generates a sequence of constructive/destructive interferences that are collected in an interferogram for each pixel of the detector. The Fourier transform of the interferogram as a function of the moving mirror position generates the spectrum of the observed scene.

Each acquisition requires 2 seconds to be performed: 1.8 seconds of proper observation during which the linear motor in the interferometer is actuated, after which 0.2 seconds are needed to position the moving mirror to its home position. The number of steps of the moving mirror (and so the number of points in the Fourier transform) needed to have a spectral sampling of $s_{sampling} = 10\text{cm}^{-1}$ is:

$$N_{points} = \frac{1}{s_{sampling}\lambda_{laser}} = 1120 \quad (4.4)$$

computed having the laser wavelength of $\lambda_{laser} = 0.846 \times 10^{-4} \text{ m}$.

The scanning grid is composed of 528 measurements. Each of them covers a region corresponding to 250 km at the Martian equator, as selected during the Pin-Hole model definition. The entire raster scan requires approximately $528 \times 2\text{s} \approx 18$ minutes to be completed.

The internal calibration measurement and the space observation, performed in correspondence with the "Start" square in Figure 4.10, are executed once at the beginning of each observation cycle. The observation grid covers the region of latitude $[-70^\circ, 70^\circ]$ and spans a total 110° of longitude.

This acquisition strategy, applied to 4 satellites in areostationary orbit, guarantees full coverage of the entire Martian surface every ≈ 18 minutes, with the exclusion of the polar regions.

4.11 Optics Technical Requirements

Table 4.6 displays the optics technical requirements. In Section A.2.2, additional information about parents and children can be found.

Table 4.6: *Optics technical requirements*

Identifier	Description	Type	Verification
DUS-OPT-0001	The payload detector shall measure wavelengths within the range of 8-16 μm	Functional	RoD
DUS-OPT-0002	The payload OPTICS solution shall have a spectral resolution of at least 10 cm^{-1}	Performance	Analysis, Test
DUS-OPT-0003	The payload OPTICS solution shall cover an area with a diameter of at least 250 km	Performance	Analysis
DUS-OPT-0004	The payload OPTICS solution shall be able to reconstruct the temperature profile of the Martian atmosphere	Functional	Analysis, Test
DUS-OPT-0005	The payload OPTICS solution shall measure the irradiance of the Martian atmosphere	Functional	Analysis, Test
DUS-OPT-0006	The payload OPTICS solution shall employ Fourier Transform Infrared Spectrometry	Functional	Inspection
DUS-OPT-0007	The payload OPTICS solution shall include a calibration target to perform the optical calibration of the instrument	Functional	Inspection
DUS-OPT-0008	The payload OPTICS solution shall be composed of the gimbal mirror assembly, the telescope assembly, the interferometer assembly and the detector assembly	Configuration	Inspection
DUS-OPT-0009	The payload telescope assembly shall be kept in the temperature range between 273.15 (TBC) K and 313.15 (TBC) K	Environment	Analysis, Test
DUS-OPT-0010	The payload interferometer assembly moving mirror shall be controlled at no lower than 5 (TBC) kHz	Performance	Test
DUS-OPT-0011	The payload interferometer assembly moving mirror shall be sampled at no lower than 40 (TBC) kHz	Performance	Test
DUS-OPT-0012	The payload interferometer assembly moving mirror shall travel a distance of ± 500.4 (TBC) μm	Performance	Test
DUS-OPT-0013	The payload interferometer assembly moving mirror shall travel at a speed of $560 \mu\text{m}/\text{s} \pm 28$ (TBC) $\mu\text{m}/\text{s}$	Performance	Test



Identifier	Description	Type	Verification
DUS-OPT-0014	The payload interferometer assembly shall be kept in the temperature range between 273.15 (TBC) K and 313.15 (TBC) K	Environment	Analysis, Test
DUS-OPT-0015	The acquired science data shall have a SNR higher than 80	Performance	Analysis, Test
DUS-OPT-0016	The payload detector shall acquire data with a frequency of at least 500 Hz	Performance	Test
DUS-OPT-0017	The payload detector should be able to operate at the temperature range imposed by the other components of the OPTICS solution	Functional	RoD
DUS-OPT-0018	The payload gimbal mirror assembly shall be able to cover, at least, the surface of Mars between latitude +70° and latitude -70°	Functional	Analysis
DUS-OPT-0019	The payload gimbal mirror assembly shall be able to cover, at least, the surface of Mars between longitude +55° and longitude -55°	Functional	Analysis
DUS-OPT-0020	The payload gimbal mirror assembly shall be kept in the temperature range between 273.15 (TBC) K and 323.15 (TBC) K	Environment	Analysis, Test
DUS-OPT-0021	The payload gimbal mirror assembly shall scan the desired surface of Mars in less than 30 (TBC) min	Performance	Analysis
DUS-OPT-0022	The platform shall avoid direct sunlight entering inside the payload through the OPTICS aperture	Interface	Inspection, Analysis
DUS-OPT-0023	The payload OPTICS solution shall include a closure mechanism to protect the optics from the external environment when needed	Functional	Inspection
DUS-OPT-0024	The payload detector shall always be kept in the temperature range between 253.15 (TBC) K and 343.15 (TBC) K	Functional	Inspection
DUS-OPT-0025	The payload calibration target shall be kept at a fixed and known temperature	Functional	Analysis, Test

5 | Subsystem Configuration

5.1 Configuration Description

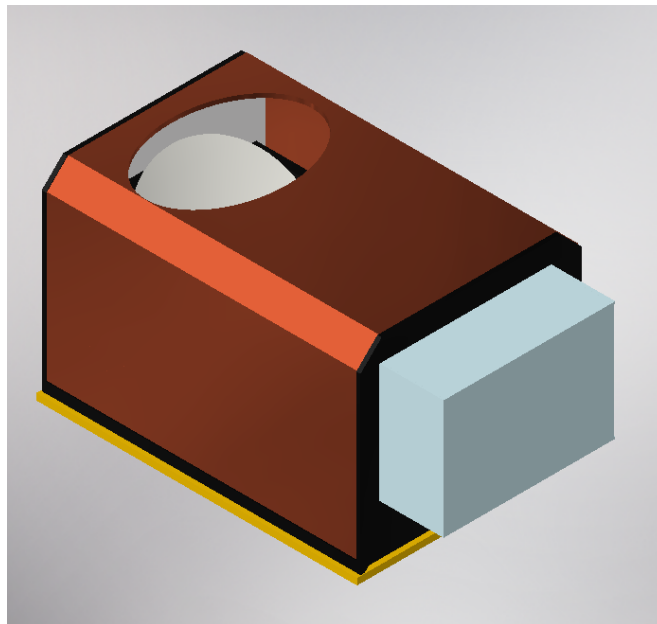


Figure 5.1: D.U.S.T.I.N. external view.

The primary structure is composed of a thick sandwich panel with a cavity in the centre (to reduce weight as much as possible), thus having an "O" shape, made by two plies enveloping a honeycomb core, everything in Al-7075. It acts as mechanical interface between D.U.S.T.I.N. and the spacecraft. On top of this plate, the main chassis is mounted; it is made by a thinner plate and two walls, where the various elements are mounted. The global encumbrance of the system corresponds to a parallelepiped of dimensions $75.5 \times 54 \times 47.5$ cm.

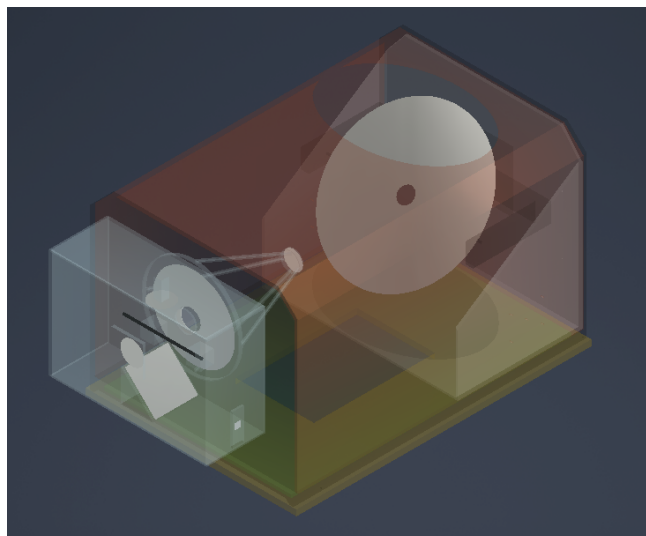


Figure 5.2: Semi-transparent representation of the system, the bottom plate is reported in yellow. It is possible to appreciate the interferometer external casing and the elements of the primary and secondary structure

The Cassegrain assembly is cantilevered on the internal face of one of the walls. The Michelson interferometer is mounted on the external face of the same wall, in axis with the optical path.

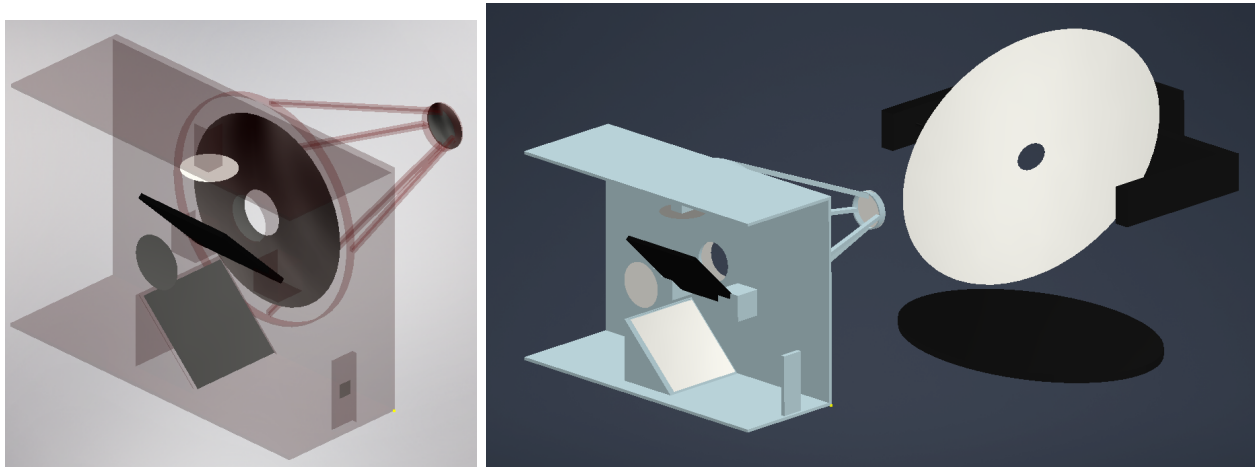


Figure 5.3: On the left: Cassegrain and interferometer assembly. On the right: components of the optical chain including the black body for calibration

On the other wall, a strengthening frame has been placed to deal with the interface loads of the rotating mirror assembly, mounted inside it, so that the light comes from the top aperture, is deviated towards the Cassegrain by the RMA, and finally enters in the interferometer and reaches the detector. The calibration black body lies below the RMA. A radiator has been placed onto the external face of the RMA wall, to minimise the thermal path from the RMA.

The electronics are placed into a plate that is located in an interspace between the chassis and the bottom plate, to be protected from the radiation environment and to ease the electrical and data interface with the platform. The calibration body is placed on the bottom plate of the chassis.

Finally, a thin (2 mm) Al-7075 cover envelopes the chassis and the interferometer to shield everything from the radiations and provide a surface for the application of the MLI.

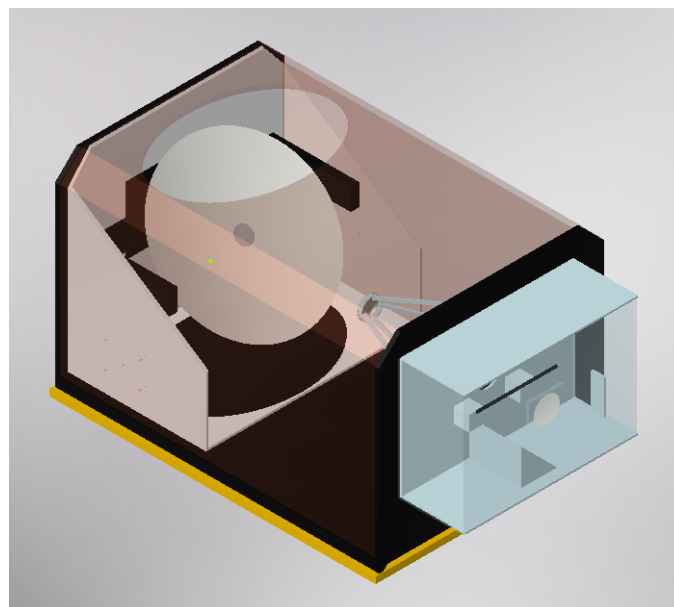


Figure 5.4: Isometric view of the main components of D.U.S.T.I.N.

5.2 Architecture Description

The diagram of Figure 5.5 represents the architecture of D.U.S.T.I.N., containing its subsystems, components, and the different interfaces among them and with the platform.

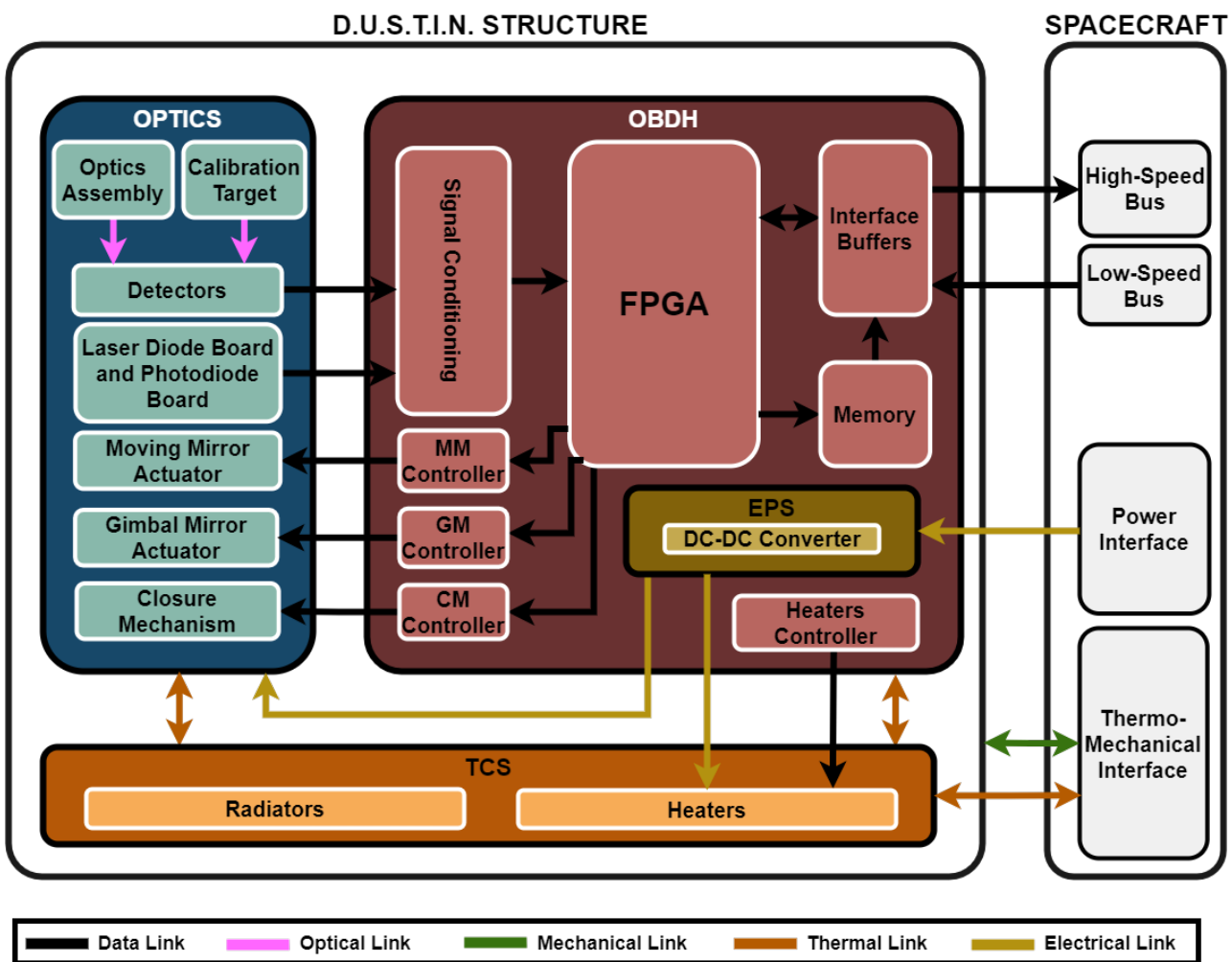


Figure 5.5: D.U.S.T.I.N. architecture

Five types of links are placed in the architecture, each denoted by a specific colour code as described in the diagram. The processing core of the payload is represented by the OBDH subsystem, which is contained in the control board PCB. This board centralises control, processing, memory, and data links. Additionally, the EPS subsystem, comprising several DC-DC Converters, is integrated within the control board to ensure a fast and reliable connection between the computer and the power converters.

The control board interfaces with the main spacecraft through two buses: a high-speed bus for transmitting telemetry data, and a low-speed bus for receiving telecommands and spacecraft updates. Data type interactions are maintained with the payload's other subsystems. The EPS interfaces with the spacecraft to manage electrical needs, regulating the input unregulated voltage and distributing power across D.U.S.T.I.N.'s components.

The optics subsystem houses all the components related to the interferometer and the optical elements for the correct focusing on the detector. The optics assembly and the calibration target communicate with the detectors through an optical link. Subsequent interactions are established with the control board via data links for each corresponding component.

TCS, consisting of radiators and heaters, maintains operational temperatures for both cold and hot scenarios. Through thermal links, it performs this function, while the heaters are connected to the control board's heater controller by a data link. The TCS also interfaces with the main spacecraft through the interface plate.

Holding all these subsystems is D.U.S.T.I.N.'s structure, which ensures the proper positioning of all components. It also protects the instrument against radiation and environmental conditions. Finally, it provides the necessary interfacing with the main platform.

6 | On-Board Data Handling

In the design of the OBDH for the D.U.S.T.I.N. project, two distinct strategies are considered for sizing. The first strategy is based on the estimation-by-similarity procedure, as described in the "Space Mission Analysis and Design" book [15]. This approach utilises tables that provide standard values for acquisition frequencies, throughput, and data and code for various functionalities. However, a limitation of this method is the outdated values, as the newer version of the book lacks this information. Consequently, the second strategy, which aligns with current trends, involves basing the OBDH sizing on heritage missions and selecting components that offer improved performance where possible.

Given the complexity and the challenges of early-stage sizing of the OBDH subsystem, the first approach is applied for the D.U.S.T.I.N. design, with an added margin of 400% to compensate for the method's accuracy limitations. Following this, the results are compared and validated with data from heritage missions, effectively implementing the second approach. This process ensures robust sizing by employing two different methodologies, ultimately converging on consistent outcomes.

6.1 Estimation-By-Similarity Considerations

The tables provided by the "Space Mission Analysis and Design" book [15] contain information about:

- Code in words: Number of words needed to code the functionality in the computer.
- Data in words: Number of data words generated when the functionality is being performed.
- Typical throughput in KIPS ($KIPS_{typ}$): Number of instructions per second that the processor needs to command to perform the functionality.
- Typical execution frequency in Hz (f_{typ}): Most common execution frequency of the functionality.

Given those parameters, the number of components, N , that need to perform the functionality, the selected acquisition frequency (f_{ac}) and the bits per word of the processor (bpw) the throughput ($KIPS$), ROM and RAM can be estimated by applying Equation 6.1.

$$KIPS = \frac{N KIPS_{typ} f_{ac}}{f_{typ}}, \quad \text{ROM [MB]} = \frac{\text{Code}_{tot} bpw}{8 \cdot 1024 \cdot 1024}, \quad \text{RAM [MB]} = \frac{(\text{Code}_{tot} + \text{Data}_{tot}) bpw}{8 \cdot 1024 \cdot 1024} \quad (6.1)$$

6.2 OBDH Functionalities

Before starting with the sizing procedure itself, the main functionalities that need to be performed by the payload are introduced, they are mostly based on EMIRS heritage [8]:

- Science data acquisition, compression and transmission/storage
- Housekeeping data acquisition, compression and transmission/storage
- Receive and decode commands from the platform OBC
- Receive spacecraft status and clock update message from the platform OBC
- Payload power conditioning control
- Control the optics gimbal mirror
- Control the interferometer moving mirror
- Control the payload closure mechanism

- Control the payload heaters
- Orchestrate data collection start, the timing of commands, and the sampling of all internal hardware interfaces
- Implement protection watchdogs

These are the main functionalities that need to be performed by D.U.S.T.I.N. OBDH solution. The solution selected will be discussed once the sizing is completed.

6.3 Sizing

6.3.1 Telemetry Data

The telemetry data is composed of housekeeping and science data. The sizing of the science data acquisition system uses a dual approach: the estimation-by-similarity technique coupled with anticipated payload performances. The data generation calculations are derived using the acquisition strategy described in Section 4.10, the detector characteristics specified in Section 4.8, and the acquisition frequency determined in Section 4.9.

To retrieve the science throughput and code requirements, the acquisition parameters are matched with the *Sun Sensor* functionality as referenced in [15]. Conversely, data compression and FFT processing are retrieved from *Math Utilities*.

The chosen compression algorithm is the CCSDS 121.0-B-3 standard, which uses a rice compression technique to deliver lossless data with a compression ratio of 11.47 [31].

Housekeeping data sizing is exclusively reliant on the estimation-by-similarity method and is correlated with *Telemetry Processing* functionality.

Table 6.1 presents the analysis of the OBDH for both science and housekeeping data acquisition. The science measurements data cell is unspecified as it is directly calculated from the anticipated performance of D.U.S.T.I.N..

Table 6.1: Science and housekeeping OBDH analysis

Functionality	<i>N</i>	Code [words]	Data [words]	Typical KIPS	Typical Frequency	Acquisition Frequency	KIPS
Science Measurements	25	500.0	–	1.0	2.0	500.0	250.0
Data compression/FFT	1	1200.0	200.0	0.5	0.1	500.0	2500.0
Housekeeping	1	1000.0	256.0	3.0	10.0	10.0	3.0

Subsequently, Table 6.2 examines the total data generation for both science and housekeeping activities, which must be sent to the spacecraft's OBC. Margins of 400% for housekeeping and 100% for science measurements are applied, the latter due to its higher degree of certainty. Total daily data and data for a solar conjunction period of 20 days are projected with an hourly time resolution, assuming measurements during all day as an additional safety margin.

6.3.2 EPS and TCS Control

The D.U.S.T.I.N. OBDH solution is responsible for the management and operation of both EPS and TCS subsystems. The sizing of these functionalities is entirely based on the estimation-by-similarity approach.

In this context, the control of the EPS is comparable to the *Power Management* functionality. Meanwhile, the TCS management is aligned with the *Thermal Control* function and it represents the only active thermal control method utilised by the payload. The outcomes of this arrangement are presented in Table 6.3.

Table 6.2: Science and housekeeping data generation

Parameter	Value	Unit
Number of Pixels	25	–
Data per Pixel	16	b
Acquisition Frequency	500	Hz
Data per acquisition	400	b
MM Cycle Duration	2	s
Data per MM Cycle (DMMC)	50000	B
Compression Rate	11.47	–
Number of points	530	–
Science Data (100% Margin)	4.41	MB
Science Data per Day	105.76	MB
Margined Housekeeping per MM Cycle	800	bytes
Housekeeping Data	0.40435791	MB
Housekeeping Data per Day	9.704589844	MB
Telemetry Data Solar Conjunction [20 days]	2.255178891	GB
Telemetry Data Solar Conjunction [20 days]	18.04143112	Gb

Table 6.3: EPS and TCS subsystems OBDH analysis

Functionality	N	Code [words]	Data [words]	Typical KIPS	Typical Frequency	Acquisition Frequency	KIPS
EPS Control	1	1200.0	500.0	5.0	1.0	1.0	5.0
TCS Control	1	800.0	1500.0	3.0	0.1	1.0	30.0

6.3.3 Interface and Autonomy

The entire procedure is based on the estimation-by-similarity method.

The payload is required to interface with the platform for receiving and decoding telecommands, acquiring spacecraft status, and synchronising the internal clock. This set of operations is encompassed under the *Command Processing* functionality. Additionally, the payload is responsible for transmitting telemetry data, a process analogous to the *Telemetry Processing* function.

Regarding autonomy, the payload must orchestrate the data collection start, the execution time of commands, and the sampling of internal hardware. They are considered as the *Simple Autonomy* functionality to effectively size these responsibilities.

Table 6.4 presents the results of this sizing procedure. The acquisition frequencies are derived entirely from heritage missions [8].

Table 6.4: Interface and autonomy OBDH analysis

Functionality	N	Code [words]	Data [words]	Typical KIPS	Typical Frequency	Acquisition Frequency	KIPS
Process TC, S/C Status and Clock Sync	1	1000.0	4000.0	7.0	10.0	2.0	1.4
Send Telemetry Data	1	1000.0	2500.0	3.0	10.0	1.0	0.3
Autonomy	1	2000.0	1000.0	1.0	1.0	1.0	1.0

6.3.4 Optics and Interferometer Control

The OBDH solution has the responsibility of controlling the optics gimbal mechanism, the interferometer's moving mirror, and the closure mechanism. To size these tasks, the estimation-by-similarity

approach is again used.

Each control control process is compared to the *Magnetic Control* functionality, considered the simplest method. Despite the fundamental differences in working principles, this comparison is deemed to be an overestimation, as the control performed by the payload primarily involves the mechanical movement of the mechanisms.

In addition, to control the moving mirror, the interferometer must be precisely sampled. This task is retrieved as *Rate Gyro Sensor Processing*, given that these sensors offer high precision and some of them employ laser technology.

The results of the sizing process are shown in Table 6.5. The acquisition frequencies for interferometer sampling and control, derived from the EMIRS mission [8], are selected to minimise vibrations in the moving mirror. This reduction is crucial for the optimal operation of the payload.

Table 6.5: Optics and interferometer control OBDH analysis

Functionality	N	Code [words]	Data [words]	Typical KIPS	Typical Frequency	Acquisition Frequency	KIPS
Interferometer Sampling	1	500.0	100.0	9.0	10.0	40000.0	36000.0
Interferometer Control	1	1000.0	200.0	1.0	2.0	5000.0	2500.0
Gimbal Mirror Control	1	1000.0	200.0	1.0	2.0	100.0	50.0
Closure Mechanism Control	1	1000.0	200.0	1.0	2.0	2.0	1.0

6.3.5 Operating System

Finally, the operating system needs to be considered in the sizing process. It is obtained entirely through the estimation-by-similarity approach, including the acquisition frequency selection. Table 6.6 shows the outcome of the process.

Table 6.6: Operating System OBDH analysis

Functionality	N	Code [words]	Data [words]	Typical KIPS	Typical Frequency	Acquisition Frequency	KIPS
I/O Device Handlers	1	2000.0	700.0	50.0	5.0	5.0	50.0
Test and Diagnostics	1	700.0	400.0	0.5	0.1	0.1	0.5
Math Utilities	1	1200.0	200.0	0.5	0.1	0.1	0.5
Executive	1	3500.0	2000.0	60.0	10.0	10.0	60.0
Run Time Kernel	1	8000.0	4000.0	60.0	10.0	10.0	60.0
Fault Detection	1	4000.0	1000.0	15.0	5.0	5.0	15.0
Fault Correction	1	2000.0	10000.0	5.0	5.0	5.0	5.0

6.3.6 Sizing per Mode

To determine the OBDH needs for each mode of operation, the required ROM, RAM, and total throughput are estimated. These calculations are based on Equation 6.1 and information from previous sections. The results are summarised in Table 6.7.

The ROM column in the table reflects the non-volatile memory used to store the code necessary for the instrument's operation. Additionally, the size of the telemetry data from a full scan is combined with the ROM to estimate the total non-volatile memory needed if this data is transmitted after collection. The RAM column indicates the amount of memory available for immediate use during operations. Finally, the throughput shows the total processing power of the system, measured in millions of instructions per second.

The Acquisition and Calibration modes require the most processing power due to the continuous operation of the interferometer and its control systems. The other modes, instead, require much less processing power. It is important to highlight that, to store the telemetry data from a complete scan,

Table 6.7: OBDH Sizing per Mode

Mode	ROM [Mb]	ROM+DATA [Mb]	RAM [Kb]	Throughput [MIPS]
Acquisition	6.836	45.324	11 290.000	237.514
Calibration	6.836	6.875	11 290.000	237.514
Sleep	4.517	4.517	8836.875	1.264
Software Update	4.517	4.517	8836.875	1.264
Boot	4.517	4.517	8836.875	1.264
Safe	4.333	4.333	8821.250	1.159

about 5.7 MB of memory would be needed. Lastly, the Safe mode is the one demanding the least resources in terms of ROM, RAM, and processing power because many functions and operations are either reduced or not running.

6.4 Heritage Solutions

Before selecting D.U.S.T.I.N.’s OBDH configuration, an analysis of the heritage adopted solution is done to validate the sizing results and have a better understanding of the typical needs of this kind of instrument. Four previous payloads are studied, EMIRS [8], OTES [30], THEMIS [32] and MSG TES [33]. The results of the literature review are retrieved in Table 6.8.

Table 6.8: Heritage OBDH Solutions

Mission	Solution	Processor	Throughput [MIPS]	Memory [Mb]
EMIRS	Only processor	Xilinx Vertex V with LEON 3	175.0	ROM: 49.200 RAM: 12.020
OTES	Only processor	FPGA	-	-
THEMIS	Only processor	Actel Field Programmable Gate Arrays	-	-
MSG TES	FFT Processor General processor	TMS320 Harris 80C86	12.5	0.625

The predominant chosen solution is only having a processor in the instrument with enough storage capability for the code and, eventually, some telemetry data. FPGAs appear to be the predominant selection as they are reliable and failure tolerant towards radiation.

The most relevant heritage mission of this project is EMIRS, which is the most recent instrument of the four and it is considered the baseline for D.U.S.T.I.N. development. Comparing the solution adopted by EMIRS with the results obtained in Table 6.7, the procedure is validated. In terms of internal memory, the expected values are within the internal memory of EMIRS solution. However, the throughput is higher with respect to the heritage mission. This can be explained by the outdatedness of the estimation-by-similarity tables, an overestimation of the functions to be performed by the subsystem or the 400% margin applied during the procedure.

6.5 OBDH Solution

Before selecting an OBDH solution, the function of D.U.S.T.I.N. inside a mission needs to be properly contextualised first. A forecasting mission usually involves multiple instruments, each of which should have the capability to process and package its telemetry data independently. This requirement ensures that the spacecraft’s OBC is not overwhelmed by data saturation. Therefore, the processing capability for D.U.S.T.I.N. is considered essential

The processor selection is inspired by the EMIRS mission and is chosen to agree with the results of the sizing procedure. The selected FPGA is the radiation-hardened Xilinx Vertex-5QV, which features a LEON 4 floating point processor with 32 bits per word. This selection improves the heritage solution and also meets the specific processing and memory requirements of the instrument. It represents a successful application of both heritage improvement and estimation-by-similarity strategies for OBDH sizing.

To ensure uninterrupted data acquisition during solar conjunctions or unexpected conditions, D.U.S.T.I.N. includes an internal memory component capable of storing the equivalent telemetry data of 20 days. The selected memory unit is the Teledyne e2V 4GB Radiation Tolerant DDR4 Memory, it offers 4 GB capacity, sufficient to store the required 2.26 GB. The additional memory is an efficient cold redundancy method while having minimal impact on power and mass.

Additionally, an A/D Converter is implemented to digitize data from the detector. The selected DDC 7809C converter aligns with the system's specifications.

Table 6.9 shows the specifications for the processor, memory, and A/D converter. The OBDH solution adequately balances performance to meet the payload's operational demands.

Table 6.9: Specifications of OBDH Components for D.U.S.T.I.N.

Parameter	Processor	Memory	A/D Converter
Component	Xilinx Vertex-5QV and LEON 4	Teledyne e2V 4GB Radiation Tolerant DDR4 Memory	DDC 7809C
Throughput [MIPS]	255	-	-
RAM [Kb]	12308	-	-
Storage Memory [MB]	6.15	4096.00	-
Temperature Range [°C]	0 - 85	-40 - 105	-40 - 85
Voltage [V]	1	1.14 - 1.26	0 - 5
Power [W]	8.5	1.5	0.1
Mass [g]	100	1.3	7.8
TID [krad]	1000	100	100

As it can be seen, by using an Aluminum shielding of 2 mm as explained in Section 3.4, all the OBDH components meet the requirements in terms of TID derived from the environmental analysis performed in Subsection 3.4.

6.6 Data Rate Analysis

The estimation of data rates for D.U.S.T.I.N. is focused on the connection between the control board and the instrument's various elements. The data rates for internal components communication within D.U.S.T.I.N.'s control board are not sized, as the board architecture already manages these interactions without the need for data buses.

The data rate for each component is calculated as the product of the acquisition frequency and the amount of data generated. This can be represented by the equation:

$$DR = f_{ac} \text{ Data} \quad (6.2)$$

Table 6.10 retrieves the data rates for various components interfacing with the spacecraft OBC, and the internal subsystems connected to the payload control board and between themselves. It includes data, acquisition frequencies, calculated data rates, data paths, and the selected data bus for each component. A margin of 400% is applied to these values to ensure reliability.

Table 6.10: D.U.S.T.I.N. Data rates

Component	Data [Kb]	f[Hz]	DR [Mb/s]	Path	Bus
Interface					
Commands and Updates	625	2	1.22	S/C to Interface Buffers	RS-422
Telemetry	39412	1	38.49	Interface Buffer to S/C	LVDS
Telemetry Solar Conjunction	18971812	0.01	184.74	Interface Buffer to S/C	LVDS
Internal Subsystems					
Detectors	2	500	0.98	Detectors assembly to A/D	RS-422
MM Sampling	16	40000	625.00	Photodiode to A/D	Ethernet
MM Control	31	5000	151.29	MM Driver to MM Actuator	Ethernet
GM Control	31	100	3.03	GM Driver to GM Actuator	RS-422
CM Control	31	2	0.06	CM Driver to CM Actuator	RS-422
Heaters Control	234	1	0.23	Heaters Driver to Heaters	RS-422

Table 6.11: Specifications for potential data buses

Parameter	RS-422 T	RS-422 R	LVDS TR	Ethernet TR
Component	DS26F31MQML	DS26F32MQML	SNLSV31-SP	DP83651-SP
Max Datarate [Mb/s]	10	10	400	1024
Temperature Range [°C]		-55/125		
Voltage [V]	7	2.5	3.3/3.6	2.5/3.3
Power [mW]	450	500	880	-
TID [krad]	300	100	150	300

The most demanding components are associated with the control and sampling of the interferometer's moving mirror, due to their significant acquisition frequencies. For these components, an Ethernet connection is necessary to fulfil the transmission requirements.

The second most demanding component is the telemetry transmission to the spacecraft's OBC. An LVDS bus, which is a one-directional channel used to compose the SpaceWire, is selected for this purpose. For all other data connections, an RS-422 bus is selected, meeting all necessary performance criteria.

Table 6.11 [34] contains examples of potential transmitters (T), receivers (R), and transceivers (TR) for each data bus solution. All of them are compatible with TID requirements and they are characterised by minimal power consumption. These components are not fixed as the nature of this project is a preliminary design.

Finally, to have a clearer view and understanding of the data rates, Figure 6.1 displays the values inside the architecture diagram.

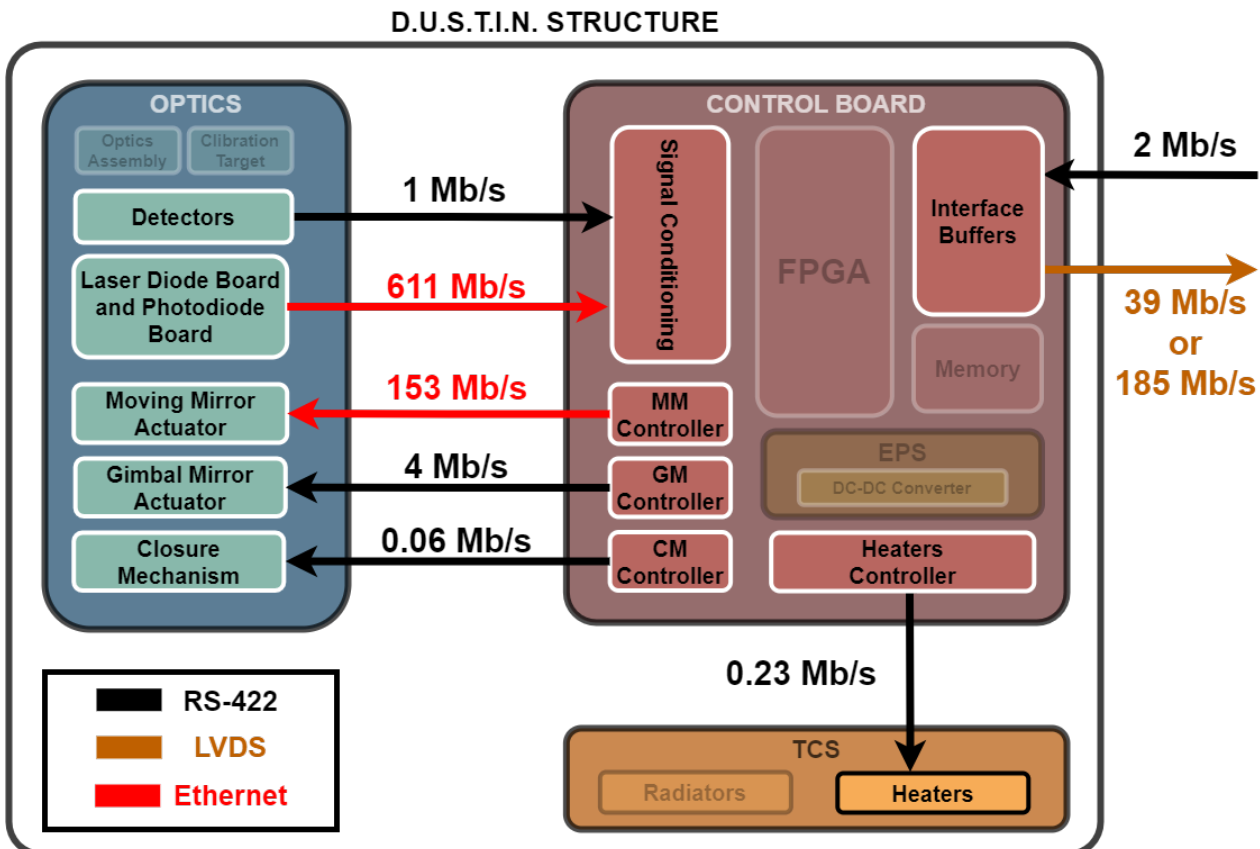


Figure 6.1: Data Rates Diagram

6.7 Science Data Acquisition Strategy

The OBDH subsystem's process for science data acquisition can be algorithmically described as stated in Algorithm 1:

Algorithm 1 Science Data Acquisition Process

- 1: The detector acquires interferometer data
 - 2: Transmit data to the A/D converter
 - 3: Data is sent to the processor
 - 4: **if** operation is nominal **then**
 - 5: Perform Fourier transform and data compression
 - 6: Store data in FPGA's internal memory
 - 7: Upon raster scan completion, send data to OBC
 - 8: **else if** operation is non-nominal or solar conjunction **then**
 - 9: Perform Fourier transform and data compression
 - 10: Store data in FPGA's internal memory
 - 11: Upon raster scan completion, send data to payload auxiliary memory
 - 12: Store data in auxiliary memory
 - 13: On non-nominal event end, send data to OBC when requested
 - 14: **end if**
-

6.8 OBDH Technical Requirements

Table 6.12 displays the OBDH technical requirements. In Section A.2.3, additional information about parents and children can be found.



Table 6.12: *On-board data handling technical requirements*

Identifier	Description	Type	Verification
DUS-OBDH-0001	The payload OBDH solution shall guarantee the proper functioning of the instrument during its whole lifetime	Functional	Inspection
DUS-OBDH-0002	The payload OBDH solution shall control the telemetry data acquisition, compression, storage and transmission to the platform OBC	Functional	Test
DUS-OBDH-0003	The payload OBDH solution shall acquire the instrument housekeeping data with a frequency of 10 (TBC) Hz	Performance	Test
DUS-OBDH-0004	The payload OBDH solution shall transmit the telemetry data of one gimbal mirror cycle to the platform OBC in less than 1 (TBC) s	Performance	Test
DUS-OBDH-0005	The payload OBDH solution shall transmit the telemetry data of 20 days to the platform OBC in less than 100 (TBC) s	Performance	Test
DUS-OBDH-0006	The payload OBDH solution shall have enough memory to store the generated telemetry data during 20 days	Functional	RoD
DUS-OBDH-0007	The payload OBDH solution shall receive and decode telecommands from the platform OBC with a frequency of 2 (TBC) Hz	Functional	Test
DUS-OBDH-0008	The payload shall receive the spacecraft status with a frequency of 2 (TBC) Hz	Performance	Test
DUS-OBDH-0009	The payload shall update its internal clock with the spacecraft's clock with a frequency of 1 (TBC) Hz	Performance	Test
DUS-OBDH-0010	The payload OBDH solution shall control the instrument power conditioning	Functional	Test
DUS-OBDH-0011	The payload OBDH solution shall control the gimbal mirror assembly	Functional	Test
DUS-OBDH-0012	The payload OBDH solution shall control the interferometer moving mirror	Functional	Test
DUS-OBDH-0013	The payload OBDH solution shall control the instrument active thermal actuators	Functional	Test
DUS-OBDH-0014	The payload OBDH solution shall orchestrate the data collection start	Functional	Test
DUS-OBDH-0015	The payload OBDH solution shall control the commands execution timing	Functional	Test
DUS-OBDH-0016	The payload OBDH solution shall control the sampling of all internal hardware interfaces	Functional	Test
DUS-OBDH-0017	The payload shall have a processing capability of at least 240 (TBC) MIPS	Performance	RoD



Identifier	Description	Type	Verification
DUS-OBDH-0018	The payload OBDH solution shall have a RAM of at least 1.4 (TBC) MB	Performance	RoD
DUS-OBDH-0019	The payload OBDH solution shall have a total memory of at least 2.3 (TBC) GB	Performance	RoD
DUS-OBDH-0020	The payload OBDH solution shall be kept in the temperature range between 273.15 (TBC) K and 358.15 (TBC) K	Environment	Analysis, Test
DUS-OBDH-0021	The payload OBDH solution shall be exposed to a maximum Total Ionizing Dose (TID) of 100 (TBC) krad during its lifetime	Environment	Analysis
DUS-OBDH-0022	The payload OBDH solution shall interface with the spacecraft OBC with a data bus capable of transmitting data at no less than 185 (TBC) Mb/s	Performance	RoD
DUS-OBDH-0023	The payload OBDH solution shall interface with the spacecraft OBC with a data bus capable of receiving data at no less than 2 (TBC) Mb/s	Performance	RoD
DUS-OBDH-0024	The payload OBDH solution shall interface with the instrument interferometer assembly with a bus capable of transmitting data at no less than 153 (TBC) Mb/s	Performance	RoD
DUS-OBDH-0025	The payload OBDH solution shall interface with the instrument interferometer assembly with a bus capable of receiving data at no less than 611 (TBC) Mb/s	Performance	RoD
DUS-OBDH-0026	The payload OBDH solution shall interface with the instrument detector assembly with a bus capable of receiving data at no less than 1 (TBC) Mb/s	Performance	RoD
DUS-OBDH-0027	The payload OBDH solution shall interface with the instrument gimbal mirror assembly with a bus capable of transmitting data at no less than 4 (TBC) Mb/s	Performance	RoD
DUS-OBDH-0028	The payload OBDH solution shall interface with the instrument active thermal actuators with a bus capable of transmitting data at no less than 1 (TBC) Mb/s	Performance	RoD



7 | Electric Power Subsystem

7.1 Architecture

The electronic Power Subsystem (EPS) of D.U.S.T.I.N. is constituted by a power conditioning module that regulates and distributes the power provided by the satellite bus. It uses a regulated architecture with a DET approach. It is assumed that the spacecraft supplies unregulated 28V that is converted to the regulated voltages needed for different components of the payload by using DC/DC converters.

In particular, the elements considered are the Xilinx Virtex 5 FPGA in the OBDH, the two 3-phase motors for the gimbal mirror control, the linear motor for the moving mirror of the interferometer, the laser diode to identify with precision the position of the moving mirror and the pyroelectric detector constituted by 25 pixels. In Tables 7.1, 7.2 and 7.3 it is reported the power consumption for the different modes of the payload. During Science mode, all the components are used at 100%, while in Sleep and Safe modes the interferometer is turned off. The motor power consumption does not go to 0W in any mode due to the need to keep a fixed position for the gimbal mirror and the moving mirror even when they are not used. During safe mode, heaters are needed due to the decrease of internal heat produced by OBDH and motors.

Table 7.1: EPS power budget - Acquisition/Calibration/Software Update mode

Components	Voltage [V]	Power [W]	Power (Margined 10%) [W]
OBDH	1	19	20.1
Dual-voice coil linear motor	3.3	2.5	2.8
Schaeffer 3-phase stepper motors [x2]	12	10.5	11.6
Laser Diode	2.5	0.02	0.022
Detector	12	0.05	0.06
Total		32.1	35.3
Total + 20% System margin			42.3

Table 7.2: EPS power budget - Sleep/Boot mode [75% OBDH, 25% Motors, Interferometer off]

Components	Voltage [V]	Power [W]	Power (Margined 10%) [W]
OBDH	1	14.3	15.7
Dual-voice coil linear motor	3.3	0.6	0.66
Schaeffer 3-phase stepper motors [x2]	12	2.6	2.9
Laser Diode	2.5	0	0
Detector	12	0	0
Total		17.5	19.3
Total + 20% System margin			23.1

Table 7.3: EPS power budget - Safe Mode [25% OBDH, 25% Motors, Interferometer assembly off]

Components	Voltage [V]	Power [W]	Power (Margined 10%) [W]
OBDH	1	4.8	5.3
Dual-voice coil linear motor	3.3	0.6	0.66
Schaeffer 3-phase stepper motors [x2]	12	2.6	2.9
Laser Diode	2.5	0	0
Detector	12	0	0
Heaters	-	7	7.7
Total		15	16.5
Total + 20% System margin			19.8



The selected DC/DC converters for the computation of the power budget are space-graded components from Crane Aerospace & Electronics [35] and their specifications are listed in Table 7.4.

Table 7.4: EPS DC/DC converters

Components	Efficiency	Input Voltage [V]	Output Voltage [V]
SMTR283R3S	73%	16 to 40	3.3
SMTR2812S	83%	16 to 40	12
MFP0507S	89%	3 to 6	1, 2.5

7.2 Technical requirements

Table 7.5 displays the EPS technical requirements. In Section A.2.4, additional information about parents and children can be found.

Table 7.5: EPS technical requirements

Identifier	Description	Type	Verification
DUS-EPS-0001	The payload EPS solution shall receive unregulated voltage from the spacecraft and condition it	Functional	Analysis, Test
DUS-EPS-0002	The payload EPS solution shall provide enough power to the active components for their correct operation	Functional	Analysis, Test
DUS-EPS-0003	The payload EPS solution shall distribute the power to the active components of the instrument	Functional	Analysis, Test
DUS-EPS-0004	The payload EPS solution shall be able to dissipate the excess of electric power	Functional	Analysis, Test
DUS-EPS-0005	The payload EPS solution shall be able to switch on and off each power line (TBC)	Functional	Analysis, Test
DUS-EPS-0004	The payload EPS solution shall supply 1 (TBC) V regulated power to the payload components	Performance	RoD
DUS-EPS-0005	The payload EPS solution shall supply 2.5 (TBC) V regulated power to the payload components	Performance	RoD
DUS-EPS-0006	The payload EPS solution shall supply 3.3 (TBC) V regulated power to the payload components	Performance	RoD
DUS-EPS-0007	The payload EPS solution shall supply 10 (TBC) V regulated power to the payload components	Performance	RoD
DUS-EPS-0008	The payload EPS solution shall supply 12 (TBC) V regulated power to the payload components	Performance	RoD



Identifier	Description	Type	Verification
DUS-EPS-0009	The payload EPS solution shall receive 28 (TBC) V unregulated input voltage from the spacecraft	Interface	Analysis, Test
DUS-EPS-0010	The payload EPS solution shall receive, at least, 40.36 (TBC) W of peak power from the spacecraft at EOL	Interface	Analysis, Test
DUS-EPS-0011	The payload EPS solution shall always operate between 218.15 (TBC) K and 398.15 (TBC) K	Environmental	Analysis, Test
DUS-EPS-0012	The payload EPS solution shall be exposed to a maximum Total Ionizing Dose (TID) of 100 (TBC) krad during its lifetime	Environmental	Analysis



8 | Thermal Control System

It is crucial for the correct functioning of the payload that all the components are allowed to operate inside their nominal temperature range. It is clear considering the expected environment and the architecture of D.U.S.T.I.N. that some form of thermal control is required.

8.1 Temperature Limits

In the following Table 8.1 the nominal temperature intervals of the components taken into account for the thermal analysis are reported:

Table 8.1: Temperature thresholds for the payload components

Component Name	Min Temp [K]	Max Temp [K]
Electronics	263.15	358.15
Detector	253.15	328.15
Gimbal Mirror Assembly	273.15	323.15
Cassegrain	273.15	313.15
Interferometer	273.15	313.15

From the previous survey it is possible to derive a first guideline for the temperature ranges that the payload must ensure: the sizing is carried on considering maintaining the temperatures of all elements inside the range 278.15K - 308.15K.

8.1.1 Internal heat sources

The payload electronics and motors are expected to produce heat. In order to have a first assessment of the heat that the TCS needs to dissipate, it is considered that all the required electrical power is converted into heat that must be disposed of. It is clear that the internal thermal power generation is not constant along the mission, but it varies with the modes. In particular, it appears that the most critical components from this point of view are the electronics and the motors of the Gimbal Mirror Assembly (GMA), as can be seen from the tables in the power budget. It is important to consider that the sources are located in different spots inside D.U.S.T.I.N (Electronics plate, GMA, interferometer assembly), thus making a multi-nodal approach unavoidable.

8.1.2 TCS Architecture

From the environmental analysis, in order to cut out the solar flux, which is the most intense heat source from the environment, D.U.S.T.I.N. is to be wrapped in an MLI, thus decoupling the system from the environment, the only heat flux entering the system being the small amount of flux hitting the mirror.

Secondly, the interface with the spacecraft adopts thermal washers avoiding conduction between the payload and the platform S/C. However, the bottom plate is developed to be radiatively coupled with the spacecraft. This allows for exploiting the platform as a thermal sink to stabilise the temperatures. For the analysis performed, two S/C temperatures are considered: 303.15K for the hot case and 278.15K for the cold one. The bottom plate is considered to have an emissivity around 0.77.

A radiator of dimensions 20 cm by 20 cm made in Al alloy honeycomb and covered in silvered Teflon is exploited to dump the heat into outer space. Its optical properties (emissivity, ϵ , and absorptivity, α) are [36]:

$$\alpha = 0.068$$

$$\epsilon = 0.808$$

The radiator is placed on the external face of the wall of the chassis where the GMA assembly is mounted, in order to ease the thermal connection with it.

The calibration body is considered as decoupled from the rest of the system (exploiting aerogel insulator), and also the GMA is thermally decoupled with respect to the chassis, and directly connected to the radiator exploiting copper braids. The electronics plate too is directly connected to the radiator since it is a quite strong internal source of heat. Finally, all the internal surfaces are considered as coated in "Aeroglaze Z306" paint, which grants high emissivity in IR, about 0.7 [8].

A set of heaters is implemented for dealing with those situations where the Electronics is not dissipating enough. These are simply resistors between two Kapton foils. They are placed on the Electronics plate and are capable of generating up to 7 W.

8.2 Thermal Simulation

The thermal net considered for the analysis is reported in Figure 8.1.

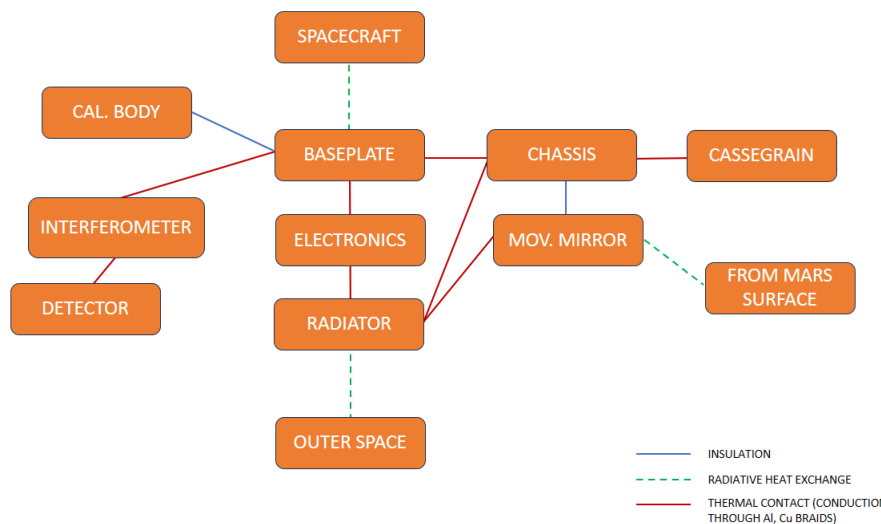


Figure 8.1: Thermal net developed, the thermal connections between nodes are highlighted

Where all the nodes are considered homogeneous elements in Al 7075 alloy. Now, the material properties utilised in the simulation are reported in Table 8.2:

Table 8.2: Thermal net characterization

Component	Material	Conductivity [W/mK]	Specific heat capacity [J/kgK]
Baseplate	Al-7075	129.7	963
Chassis	Al-7075	129.7	963
Electronics plate	Al-7075	129.7	963
Interferometer frame	Al-7075	129.7	963
Detector	Silicium	-	710
GMA	Al-7075	129.7	963
Cassegrain Assembly	Al-7075	129.7	963
Radiator	Al-7075	129.7	963
Cal. Body	Al-7075	129.7	963
Copper braids	Cu	400	-
Insulation	Aerogel silica	0.03	-

The simulation is conducted in Simulink Simscape, and only a steady-state conditions analysis is conducted. Two simulations are performed: hot case and cold case.

8.2.1 Hot Case Scenario

In the first simulation, the payload is considered to stay in acquisition mode (the most demanding in terms of heating generation) during daylight. The spacecraft is considered at 303.15 K. Under these assumptions, it is clear that, at steady state conditions, the system must guarantee that the temperatures are kept below the maximum allowed. This is reached by iterating on the thermal connection scheme between the nodes and on the radiator size.

By considering a 20x20 cm radiator, with an estimated thermal power of 35.3 W entering the system, the results are reported in Table 8.3:

Table 8.3: Steady state temperatures reached in hot case scenario

Component	Temperature [K]
Electronics	308.00
Detector	308.01
GMA	308.66
Cassegrain	307.87
Interferometer	308.01

It is possible to see that, with the configuration adopted, the TCS can keep all elements below their maximum temperature by exploiting only passive solutions (radiators and copper braids). It can be noticed that the GMA reaches a temperature slightly higher than the rest of the payload. This is because it receives a small amount of radiation from ground and also receives the heat from its motors. For these reasons, it is directly connected to the radiator through copper thermal paths. The temperature of the GMA is slightly outside the previously stated range, however, considering the component limit temperature being 323.15 K and the fact that it is insulated from the rest of the system, this is not considered a critical issue to impose a resizing of the TCS.

8.2.2 Cold case scenario

During Safe mode, the power consumption is dramatically reduced so the temperatures are expected to drop. To keep the temperatures above an acceptable threshold, heaters are implemented. By considering the spacecraft at 278.15 K, the simulation yields to the results displayed in Table 8.4:

Table 8.4: Steady state temperatures reached in cold case scenario

Component	Temperature [K]
Electronics	281.90
Detector	281.89
GMA	281.64
Cassegrain	281.72
Interferometer	281.89

Therefore, even in Safe mode, the TCS can maintain all the elements in the proper range indefinitely, by activating the heaters to dissipate those 7 W that allow thermal equilibrium at an acceptable temperature for each component.

8.3 TCS technical requirements

Table 8.5 displays the TCS technical requirements. In Section A.2.5, additional information about parents and children can be found.



Table 8.5: TCS technical requirements

Identifier	Description	Type	Verification
DUS-TCS-0001	The payload TCS solution shall be able to keep the instrument temperature range between 278.15 (TBC) K and 308.15 (TBC) K	Performance	Analysis, Test
DUS-TCS-0002	The payload structure shall thermally interface with the structure of the spacecraft	Interface	Analysis, Test
DUS-TCS-0003	The payload interface shall be conductive-isolated from the spacecraft	Functional	Analysis, Test
DUS-TCS-0004	The payload interface shall allow radiation heat exchange with the spacecraft	Functional	Analysis, Test
DUS-TCS-0005	The payload TCS solution shall be able to emit radiation outward	Functional	Analysis, Test
DUS-TCS-0006	The payload TCS solution shall include active thermal control	Functional	Inspection
DUS-TCS-0007	The payload gimbal mirror assembly shall be conductive-connected to the outward emitter	Functional	Inspection
DUS-TCS-0008	The payload control board shall be conductive-connected to the outward emitter	Functional	Inspection
DUS-TCS-0009	The thermal connections between components shall be achieved by employing conductive heat	Design	Inspection
DUS-TCS-0010	The payload calibration body shall be thermally isolated from the other components	Functional	Analysis, Test

9 | Structure

9.1 Structural Analysis

The Falcon 9 launcher user manual provides all the data to fully characterise the load environment, which is the most critical load situation. Since the S/C is not defined nor known, the launch loads are considered as directly injected into the payload mechanical interface.

The first one to be performed is a modal analysis, to ensure to be compliant with the requests of the launch authority in terms of primary and secondary modes [37]:

Payloads should consider maintaining the primary lateral frequency above 10Hz, primary axial frequency above 25Hz, and all secondary structure minimum resonant frequencies above 35Hz to avoid interaction with launch vehicle dynamics.

Then, a static analysis is performed considering the load envelope provided by the launch authority. Two different cases are analysed separately: maximum axial acceleration (and correspondent lateral acceleration) and maximum lateral (with corresponding axial load). A qualification factor of 1.25 is applied. From this analysis, the stresses on all the elements of the FEM model are assessed and checked to be below the allowed tensile strength. The acceleration envelope used is reported in Figure 9.1 [37].

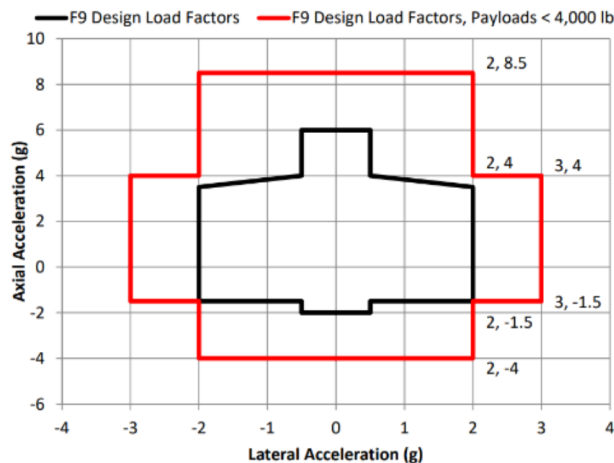


Figure 9.1: Static loads envelope as prescribed by the launcher user manual

Finally, a frequency response analysis is carried on, considering the two acceleration profiles expressed by the EQSL tables from the user manual and reported in Figure 9.2 [37].

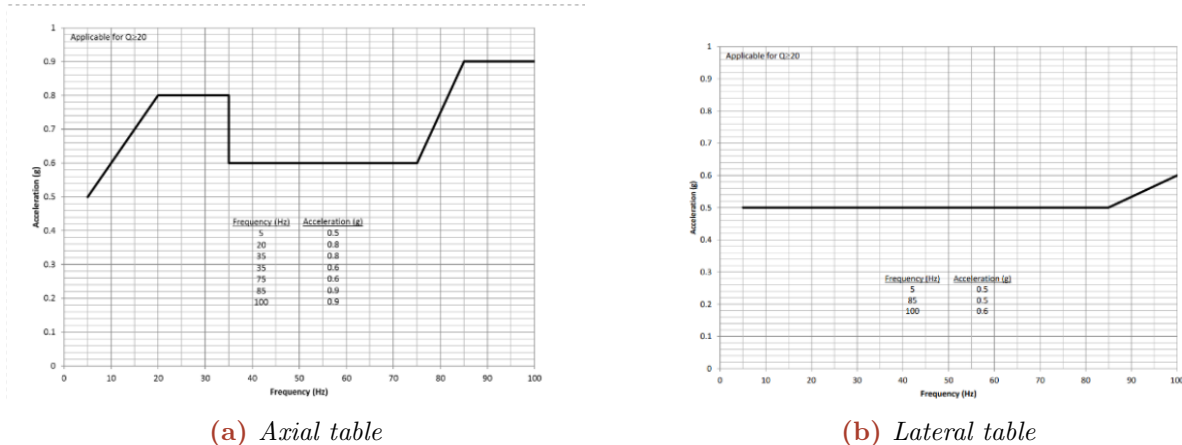


Figure 9.2: Sine test load histories (axial and lateral)

In this analysis stresses and accelerations are checked.

9.1.1 FEM Description

From the payload CAD, a FEM model is obtained by exploiting Inventor Nastran. The mesh comprises only tetrahedral elements. The lenses and connections are represented as point masses (with the values expressed in Section 4.6) connected to their frame via RBE2 links. A graphical representation of the FEM is reported in Figure 9.3.

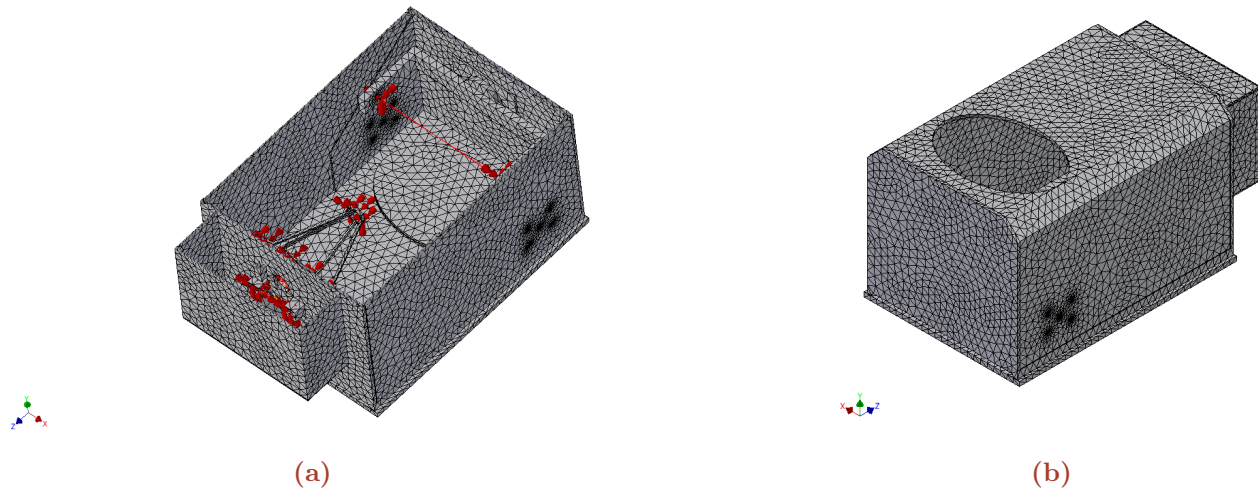


Figure 9.3: Cut view and external view of D.U.S.T.I.N. FEM model, the rigid elements that model the lenses have been highlighted)

As for the materials, all the structural elements are considered to be in Al-7075 alloy, except the bottom plate, where the properties of the sandwich panel(two Al 7075 plates encasing an Al 5056 honeycomb core) are applied. The mechanical properties of both materials are reported in Tables 9.1 and 9.2 respectively [38] [39].

Table 9.1: Al-7075 properties

Material	E [GPa]	ν [-]	σ_t [Mpa]	ρ [kg/m ³]
Al-7075	71.7	0.33	503	2810

Table 9.2: Honeycomb panel properties

E_x [MPa]	E_y [MPa]	E_z [MPa]	G_{xy} [MPa]	G_{xz} [MPa]	G_{yz} [MPa]	ν_{xy} [-]	ν_{xz} [-]	ν_{yz} [-]	ρ [kg/m ³]
3.3	3.3	2944.6	1.98	426	651.7	1	0	0	130

9.2 Results

9.2.1 Modal Analysis

The first 10 modes of the system considered grounded at the bottom plate are assessed:

Table 9.3: First 10 modes of the payload

Mode No.	1	2	3	4	5	6	7	8	9	10
Freq [Hz]	157.76	195.23	301.71	420.41	437.96	544.36	570.13	587.95	593.35	623.63

The first four modes are due mainly to the GMA structure so they can be considered secondary, while in modes number 5 and 6 the external cover of the instrument gets excited, as well as the

Cassegrain in mode 6. Finally, modes from 7 to 10 are secondary modes induced by the Cassegrain telescope. For this reason, since the first mode falls well above the required threshold of 35 Hz, it is possible to say that the payload fulfils the prescribed requirement DUS-STR-0005 from the launch authority.

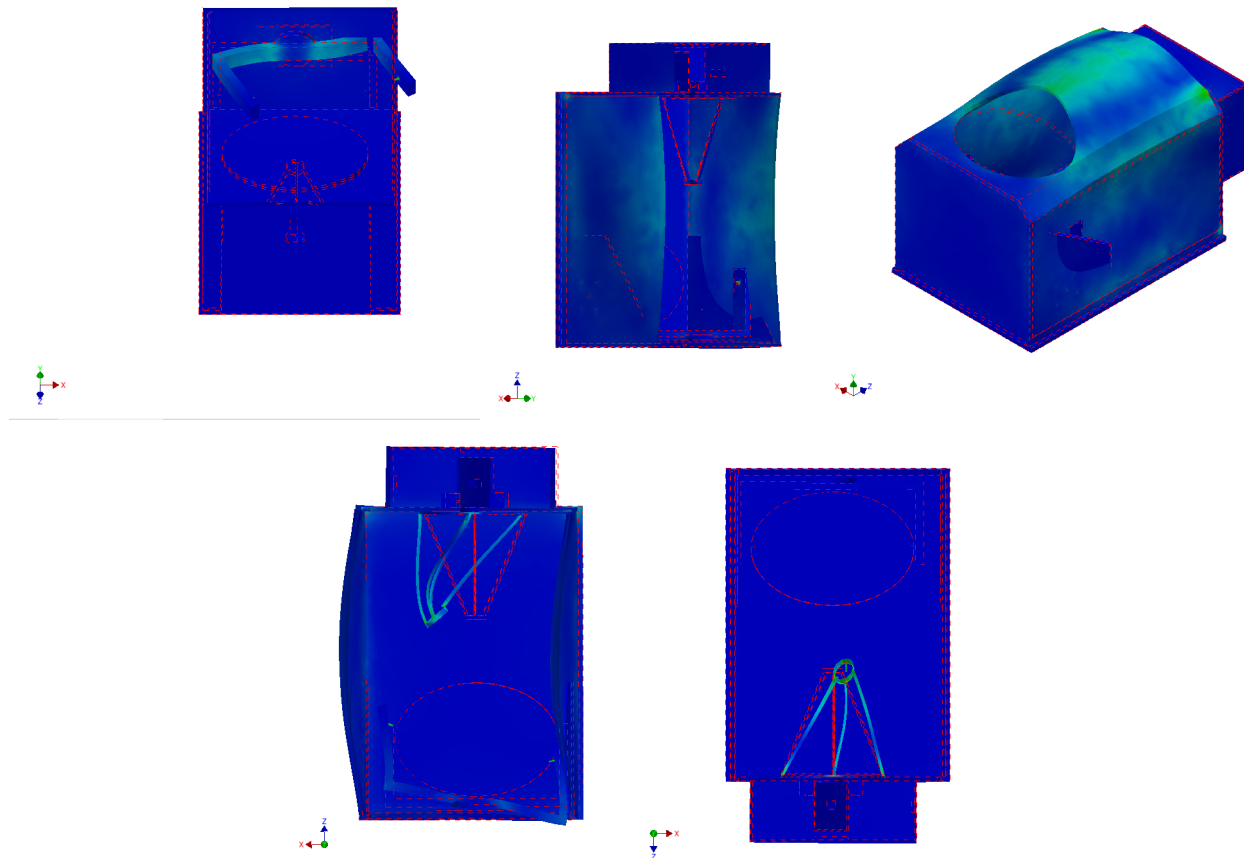


Figure 9.4: From left to right, from top to bottom: mode 1 (section), mode 5 (section), mode 5 (external view), mode 6 (section), mode 7 (section)

9.2.2 Static Analysis

Four different load cases are considered for the static analysis: 8.5 g in Y (axial) direction + 2 g in X (lateral) direction, 8.5 g in Y direction + 2 g in Z (lateral) direction, 4 g in Y direction + 3 g in X direction, and 4 g in Y direction + 3 g in X direction. It is expected that the behaviour of the system under these four load environments will be representative of all the possible load histories that can be reconstructed from the launcher-prescribed loads. An additional factor of 1.25 is applied to all the loads prescribed. In all the subcases considered, the displacements estimated by analysis are kept in the order of the micrometer. Even the two most critical components, the Cassegrain and the GMA structure, are seeing an acceptable displacement for the optical chain not to be disrupted. Regarding the interferometer assembly, it tends to move as a single unit and also its displacements are at an acceptable level. As for the stresses, in all the load situations considered the maximum value is kept way below the limit to avoid plastic deformation (the maximum value of all subcases being 1.7 MPa), with the most stressed regions being the pins that connect the rigid element representing the mirror to the GMA structure. Another component that is subjected to higher stresses is the Cassegrain telescope, although not at the levels of the GMA connections.

9.2.2.1 Case 1: Axial Load 8.5 g, Lateral Load 2 g in X Direction

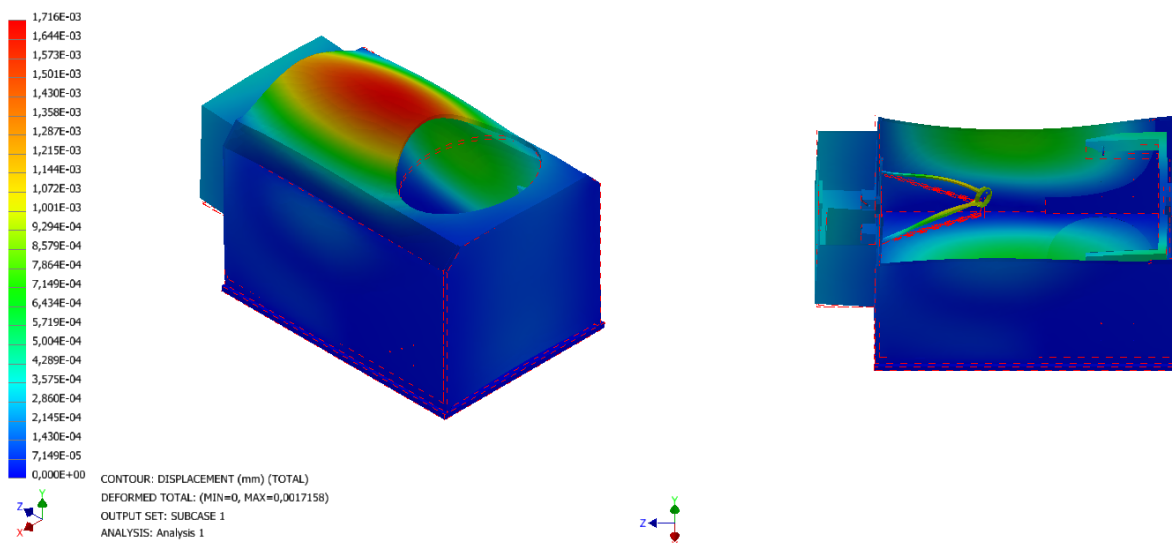


Figure 9.5: Displacements (mm) for load case 1

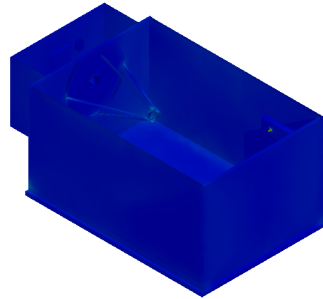
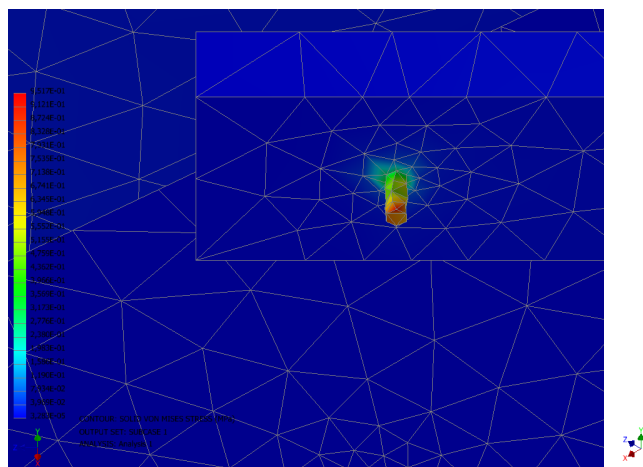


Figure 9.6: Stresses (MPa) evaluated for load case 1

9.2.2.2 Case 2: Axial Load 8.5 g, Lateral Load 2 g in Z Direction

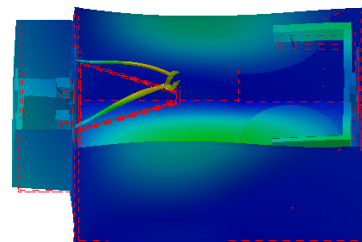
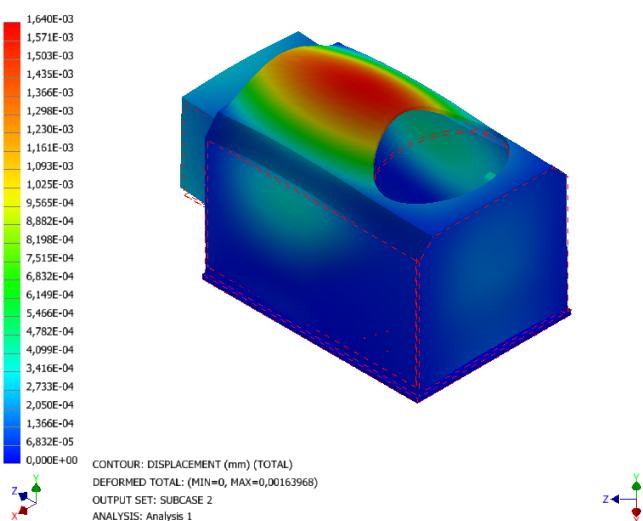


Figure 9.7: Displacements (mm) for load case 2

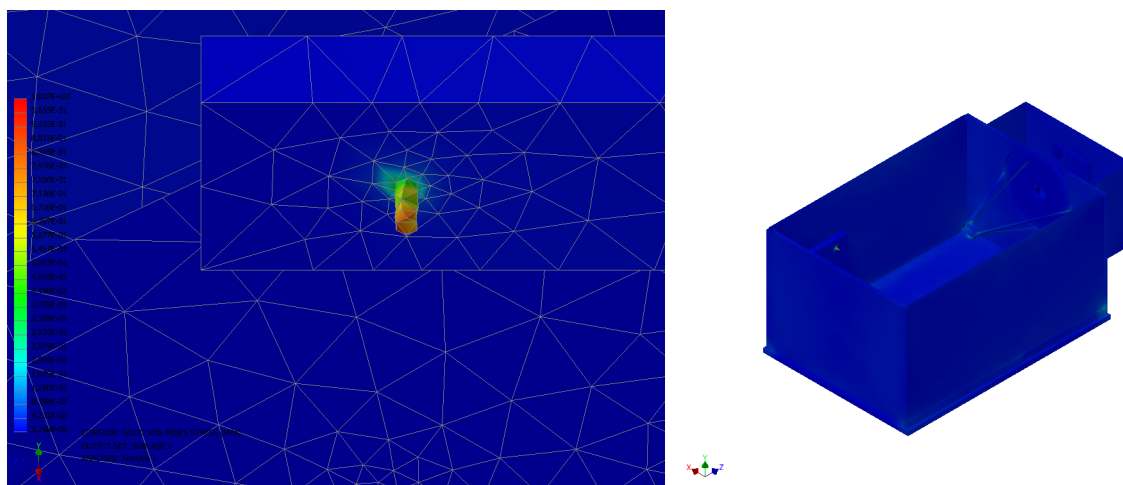


Figure 9.8: Stresses (MPa) evaluated for load case 2

9.2.2.3 Case 3: Axial Load 4 g, Lateral Load 3 g in X Direction

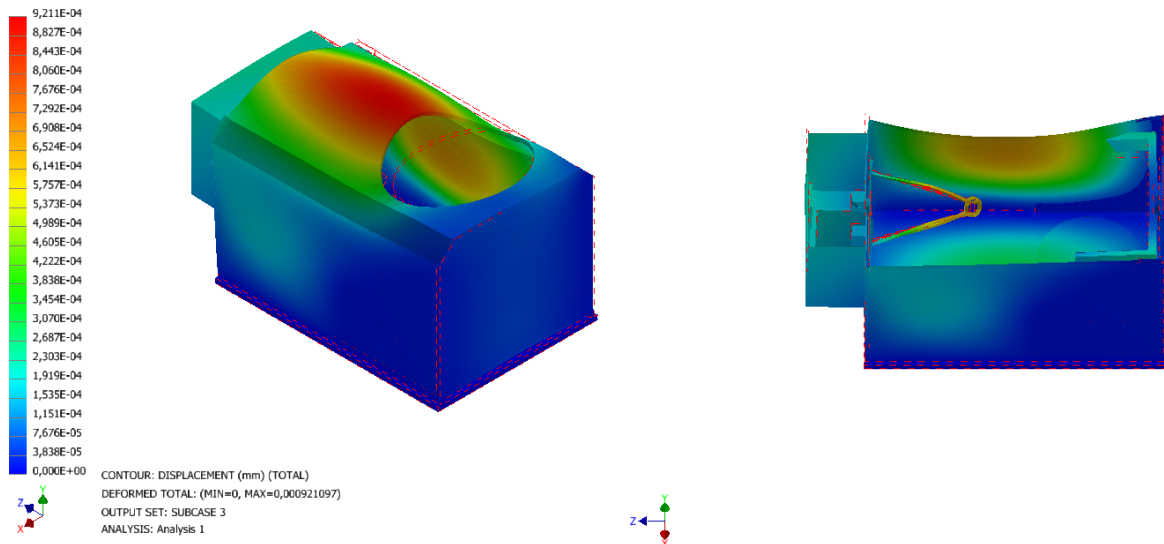


Figure 9.9: Displacements (mm) for load case 3

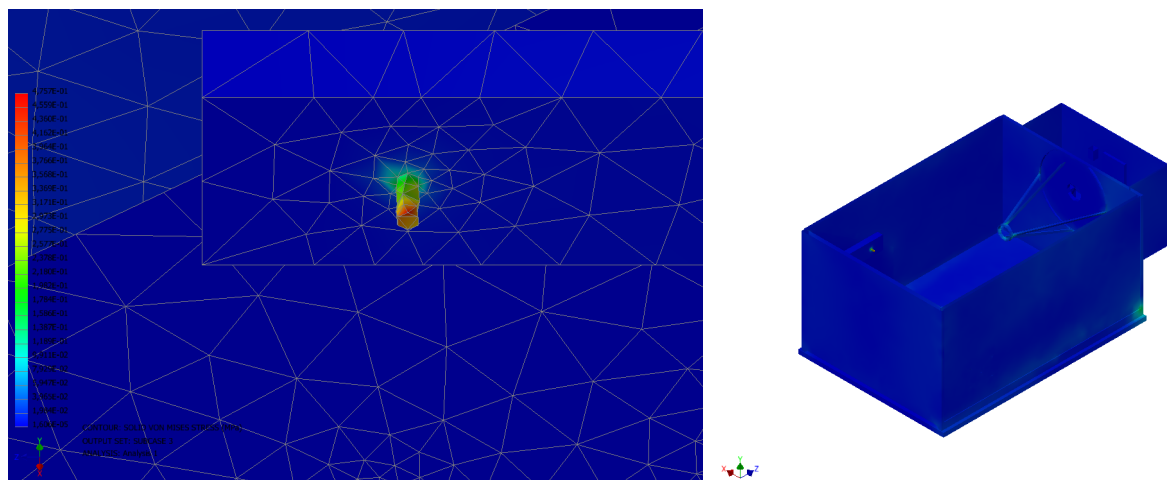


Figure 9.10: Stresses (MPa) evaluated for load case 3

9.2.2.4 Case 4: Axial Load 4 g, Lateral Load 3 g in Z Direction

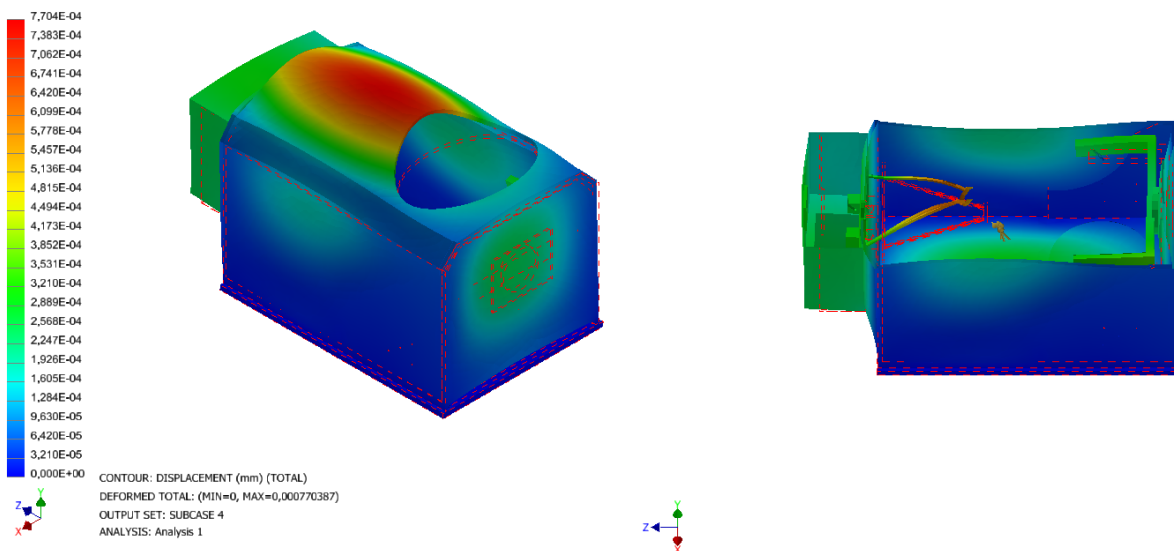


Figure 9.11: Displacements (mm) for load case 4

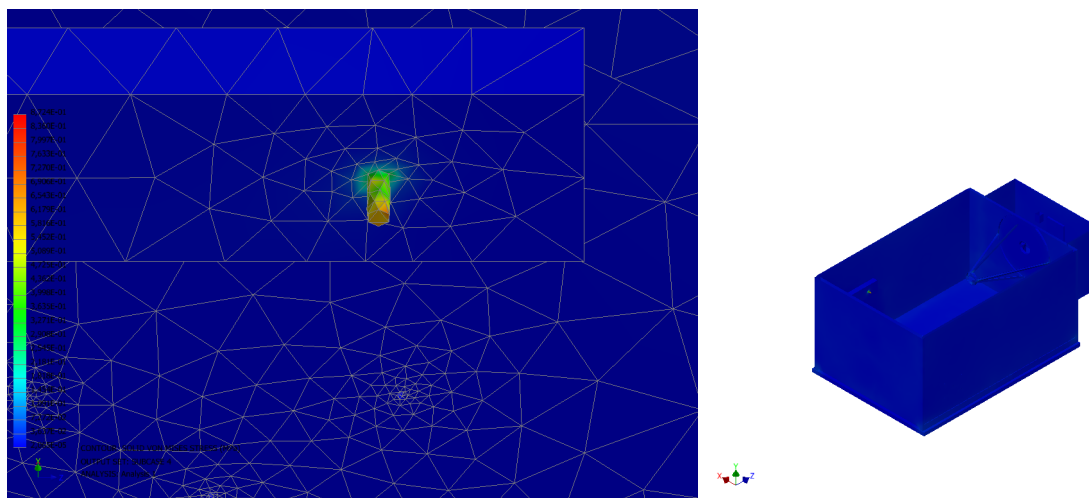


Figure 9.12: Stresses (MPa) evaluated for load case 4

9.2.3 Random Analysis

Three representative cases are tested: one with the axial load spectrum prescribed, and two with the lateral one, one time along the X axis and one time along Z. In all the simulations the stress is always kept at an acceptable level, with the GMA structure, the Cassegrain telescope and the bottom plate being the most solicited components. As for the accelerations, the structure does not appear to significantly amplify the accelerations imposed at the bottom plate, with the arms of the GMA seeing the highest accelerations.

9.2.3.1 Axial Accelerations

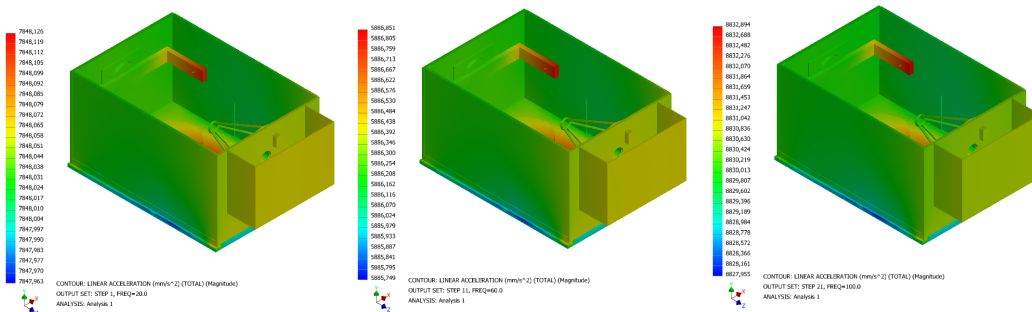


Figure 9.13: From left to right, computed accelerations [mm/s²] at 20 Hz, 60 Hz and 100 Hz

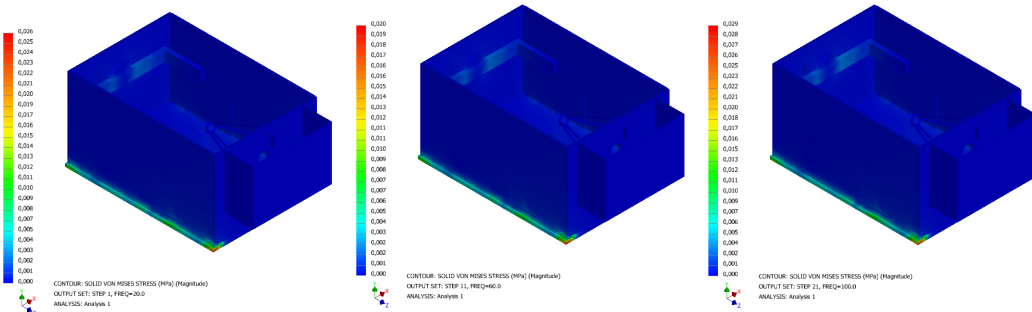


Figure 9.14: From left to right, computed stresses [MPa] at 20 Hz, 60 Hz and 100 Hz

9.2.4 Lateral Acceleration (X Direction)

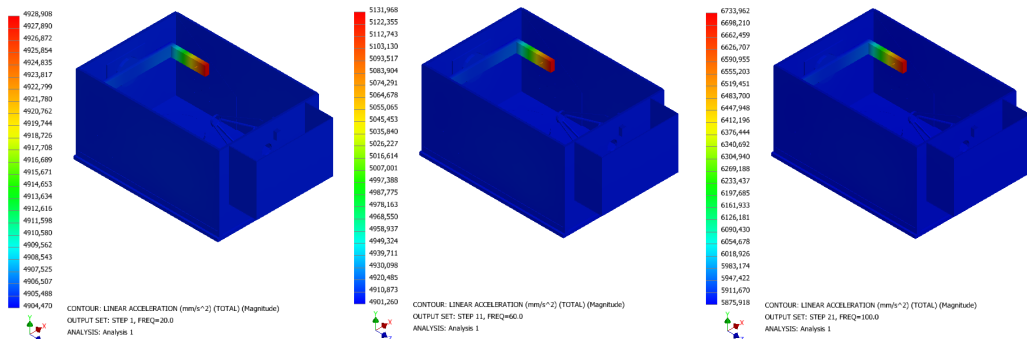


Figure 9.15: From left to right, computed accelerations [mm/s²] at 20 Hz, 60 Hz and 100 Hz

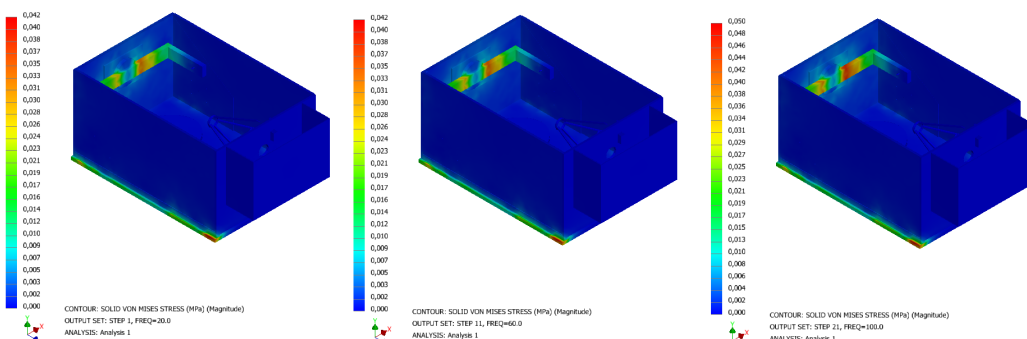


Figure 9.16: From left to right, computed stresses [MPa] at 20 Hz, 60 Hz and 100 Hz

9.2.5 Lateral Acceleration (Z Direction)

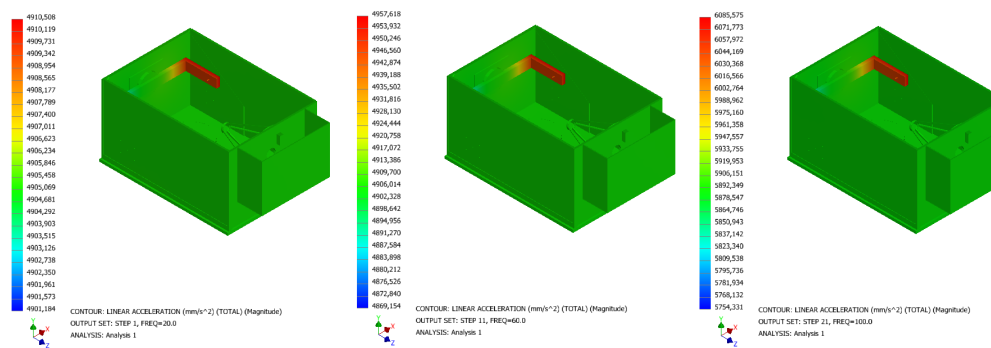


Figure 9.17: From left to right, computed accelerations [mm/s²] at 20 Hz, 60 Hz and 100 Hz

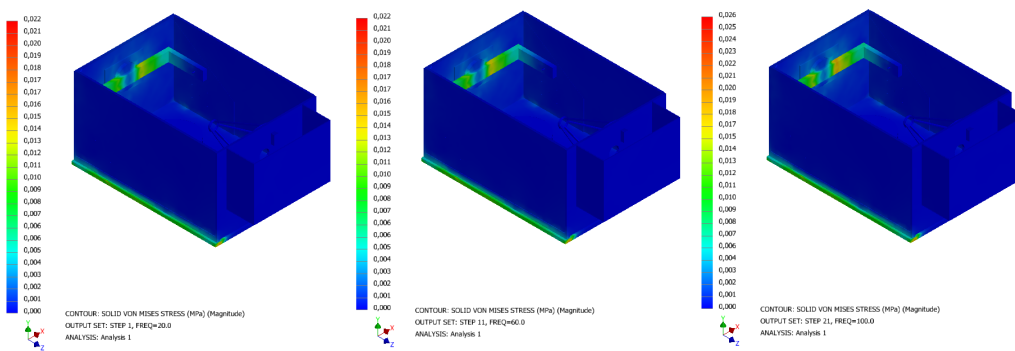


Figure 9.18: From left to right, computed stresses [MPa] at 20 Hz, 60 Hz and 100 Hz

In conclusion, the structural solutions adopted and tested demonstrate to be compliant with the launch authority requests.

9.3 Mass Budget

It is hereby reported the mass contribution of each subsystem to the overall mass budget of the system. It can be noticed that the two most demanding ones from the mass viewpoint are the structure and the optics (which includes also the masses of the motors controlling the mirrors). In particular, the mass of the structure is reduced by adopting a sandwich panel for the bottom plate, instead of a thick panel of Al alloy. This allows to save around 3 kg while maintaining acceptable mechanical behaviour. The mass budget is reported in Table 9.4

Table 9.4: Mass budget, computed and margined values, for D.U.S.T.I.N.

Subsystem	Mass [kg]	Mass, margined 10% [kg]
Structure	11.5	12.7
Optics	4.29	4.72
EPS	1.54	1.69
OBDH	0.11	0.12
TCS	0.45	0.5
Total	17.89	19.73
Total, 20% system margin	-	23.68

9.4 Structural technical requirements

Table 9.5 displays the structural technical requirements. In Section A.2.6, additional information about parents and children can be found.

Table 9.5: *Structural technical requirements*

Identifier	Description	Type	Verification
DUS-STR-0001	The payload shall survive to the load environment expected in any phase of the mission after launch	Functional	Test
DUS-STR-0002	The payload structure shall mechanically interface with the structure of the spacecraft	Functional	Inspection
DUS-STR-0003	The payload structure shall protect all the subsystems from the radiation environment	Functional	Analysis, Test
DUS-STR-0004	The payload structure shall be capable of accommodating all the components and subsystems, including their harnesses	Functional	Inspection
DUS-STR-0005	The payload shall survive to the launch environment prescribed by the launch authorities	Functional	Test
DUS-STR-0006	The payload first primary lateral frequency shall be above 20 Hz	Performance	Test
DUS-STR-0007	The payload first primary axial frequency shall be above 35 Hz	Performance	Test
DUS-STR-0008	The payload secondary minimum resonant frequencies shall be above 45 Hz	Performance	Test
DUS-STR-0009	The maximum displacement seen by the OPTICS subsystem elements shall be kept in the order of micrometres during the mission lifetime	Performance	Test
DUS-STR-0010	The payload primary structure shall hold the secondary and tertiary structures	Functional	Inspection
DUS-STR-0011	The payload primary structure shall act as thermo-mechanical interface with the spacecraft	Configuration	Inspection, Test
DUS-STR-0012	The payload primary structure shall hold the electronics plate	Configuration	Inspection
DUS-STR-0013	The payload secondary structure shall hold the Cassegrain telescope	Functional	Inspection
DUS-STR-0014	The payload tertiary structure shall protect the instrument components from the external environment	Functional	Analysis
DUS-STR-0015	The payload tertiary structure shall keep the Total Ionizing Dose (TID) in the components under 100 (TBC) krad	Performance	Analysis



Identifier	Description	Type	Verification
DUS-STR-0016	The payload tertiary structure shall include the elements and mechanisms to hold the instrument harness	Functional	Inspection



10 | Conclusion

The preliminary design of D.U.S.T.I.N. is complete, compressing a robust and multidisciplinary approach to studying Martian dust storms. The architecture includes an advanced optical subsystem, ensuring high-resolution data collection. The OBDH subsystem is optimised for processing and storing significant volumes of scientific data, based on heritage designs while including modern technology to enhance performance.

D.U.S.T.I.N.'s EPS deals with the demanding energy requirements for continuous diurnal observation, with the TCS designed to resist properly assessed temperature variations. The structural integrity is confirmed through rigorous analysis to withstand the stresses of launch and Martian operations. Each subsystem is integrated to ensure operational efficiency and scientific measurements.

While the payload is based on heritage technology, its innovative design introduces improvements in several key areas. The potential for D.U.S.T.I.N. to improve upon heritage performance is implicit in its design. It incorporates advanced technologies and improved both temporal and spatial resolution, contributing valuable insights into Martian meteorology. Future work could lead to the design of the tool and its validation and verification.

Bibliography

- [1] Luca Montabone and François Forget. On forecasting dust storms on mars.
- [2] Luca Montabone, Nicholas Heavens, Jose L. Alvarellos, Michael Aye, Alessandra Babuscia, Nathan Barba, J. Michael Battalio, Tanguy Bertrand, Bruce Cantor, Michel Capderou, Matthew Chojnacki, Shannon M. Curry, Charles D. Edwards, Meredith K. Elrod, Lori K. Fenton, Robin L. Fergason, Claus Gebhardt, Scott D. Guzewich, Melinda A. Kahre, Ozgur Karatekin, David M. Kass, Robert Lillis, Giuliano Liuzzi, Michael A. Mischna, Claire E. Newman, Maurizio Pajola, Alexey Pankine, Sylvain Piqueux, Ali Rahmati, M. Pilar Romero-Perez, Marc Sanchez-Net, Michael D. Smith, Alejandro Soto, Aymeric Spiga, Leslie Tamppari, Joshua Vander Hook, Paulina Wolkenberg, Michael D. Wolff, Ryan C. Woolley, and Roland M. B. Young. Observing Mars from Areostationary Orbit: Benefits and Applications. *Bulletin of the AAS*, 53(4), mar 18 2021. <https://baas.aas.org/pub/2021n4i281>.
- [3] M. Golombek, N. Williams, A. McEwen P. Wooster, A. Bramson N. Putzig, J. Head, J. Heldmann, M. Marinova, and D. Beaty. SpaceX starship landing sites on mars.
- [4] François Forget and Luca Montabone. Atmospheric dust on mars: A review.
- [5] J.B. Madeleine, F. Forget, E. Millour, L. Montabone, and M. J. Wolff. Revisiting the radiative impact of dust on mars using the lmd global climate model.
- [6] Michael D. Smith. Interannual variability in tes atmospheric observations of mars during 1999–2003.
- [7] Michael D. Smith, Joshua L. Bandfield, Philip R. Christensen, and Mark I. Richardson. Thermal emission imaging system (themis) infrared observations of atmospheric dust and water ice cloud optical depth.
- [8] G.L. Mehall C.S. Edwards, P.R. Christensen. The emirates mars mission (emm) emirates mars infrared spectrometer (emirs) instrument. *Space Sci Rev*, (227), 2021. <https://link.springer.com/article/10.1007/s11214-021-00848-1>.
- [9] Barney J. Conrath, John C. Pearl, Michael D. Smith, William C. Maguire, Philip R. Christensen, Shymala Dason, and Monte S. Kaelberer. Mars global surveyor thermal emission spectrometer (tes) observations: Atmospheric temperatures during aerobraking and science phasing.
- [10] Michael D. Smith, Joshua L. Bandfield, and Philip R. Christensen. Separation of atmospheric and surface spectral features in mars global surveyor thermal emission spectrometer (tes) spectra.
- [11] ESA. Planetary protection, 2016.
- [12] H.E. S. Amiri, D. Brain, O. Sharaf, P. Withnell, M. McGrath, and M. Alloghani et al. The emirates mars mission. *Space Science Reviews*, 2022.
- [13] Nicola Fox. Solar cycle 25 is exceeding predictions and showing why we need the gcd mission, 2022.
- [14] NASA Ames Research Center Trajectory Browser. Trajectory search, 2023.
- [15] J.R. Wertz and W.J. Larson. *Space Mission Analysis and Design*. Space technology library. Kluwer Academic, 1991.
- [16] Juan J. Silva and Pilar Romero. Optimal longitudes determination for the station keeping of areostationary satellites. *Planetary and Space Science*, 87:14–18, 2013.

- [17] L. Montabone, N. G. Heavens, A. Pankine, M. Wolff, A. Cardesin-Moinelo, B. Geiger, F. Forget, S. Guerlet, E. Millour, A. Spiga, S. D. Guzewich, M. D. Smith, O. Karatekin, B. Ritter, L. Ruiz Lozano, C. B. Senel, O. Temel, R. J. Lillis, K. S. Olsen, P. L. Read, A. C. Vandaele, F. Daerden, L. Neary, S. Robert, S. Aoki, J. M. Battalio, T. Bertrand, C. Gebhardt, B. Guha, R. M. B. Young, M. Giuranna, F. Oliva, P. Wolkenberg, S. J. Greybush, J. Hernández-Bernal, A. Sánchez-Lavega, A. Kleinboehl, M. A. Mischna, L. K. Tamppari, J. A. Holmes, S. R. Lewis, M. R. Patel, P. M. Streeter, P. Machado, F. Montmessin, H. Nakagawa, K. Ogohara, D. Titov, M. Vincendon, H. Wang, and R. J. Wilson. The Case and Approach for Continuous, Simultaneous, Global Mars Weather Monitoring from Orbit. In *Seventh International Workshop on the Mars Atmosphere: Modelling and Observations*, page 4406, June 2022.
- [18] Martha O'Bryan. Single event effects specifications.
- [19] Wikipedia contributors. Nasa deep space network — Wikipedia, the free encyclopedia. https://en.wikipedia.org/w/index.php?title=NASA_Deep_Space_Network&oldid=1190018835, 2023. [Online; accessed 11-January-2024].
- [20] Jane Platt. Mars in our night sky. <https://mars.nasa.gov/all-about-mars/night-sky/solar-conjunction/>. [Online; accessed 11-January-2024].
- [21] Armin Kleinböhl, John T. Schofield, David M. Kass, Wedad A. Abdou, Charles R. Backus, Bhaswar Sen, James H. Shirley, W. Gregory Lawson, Mark I. Richardson, Fredric W. Taylor, Nicholas A. Teanby, and Daniel J. McCleese. Mars climate sounder limb profile retrieval of atmospheric temperature, pressure, and dust and water ice opacity.
- [22] V. Formisano, F. Angrilli, G. Arnold, S. Atreya, G. Bianchini, D. Biondi, A. Blanco, M.I. Blecka, A. Coradini, L. Colangeli, A. Ekonomov, F. Esposito, S. Fonti, M. Giuranna, D. Grassi, V. Gnedykh, A. Grigoriev, G. Hansen, H. Hirsh, I. Khatuntsev, and A. Kiselev et al. The planetary fourier spectrometer (pfs) onboard the european mars express mission. *Planetary and Space Science*, 2005.
- [23] Jingquan Cheng. *The Principles of Astronomical Telescope Design*. Springer, 2010.
- [24] James B. Pollack and Carl Sagan. An analysis of martian photometry and polarimetry. 1968.
- [25] Bhavesh Jaiswal, G. Mahapatra, Anuj Nandi, M. Sudhakar, K. Sankarasubramanian, and V. Sheel. Polarization signatures of mars dust and clouds: Prospects for future spacecraft observations. *Planetary and Space Science*, 2021.
- [26] Laser diode, 2023.
- [27] Gimbal motor ant95r, 2023.
- [28] Filter ir edmund optics, 2023.
- [29] LEONARDO. *Performances of DLATGS Detectors*, 2017. DLATGS Detectors.
- [30] P. R. Christensen, V. E. Hamilton, G. L. Mehall, D. Pelham, W. O'Donnell, S. Anwar, H. Bowles, S. Chase, J. Fahlgren, Z. Farkas, T. Fisher, O. James, I. Kubik, I. Lazbin, M. Miner, M. Rassas, L. Schulze, K. Shamordola, T. Tourville, G. West, R. Woodward, and D. Lauretta. The osiris-rex thermal emission spectrometer (otes) instrument. *Space Science Reviews*, 214(5), July 2018.
- [31] CCSDS. *IMAGE DATA COMPRESSION*. CCSDS Secretariat, 2021.
- [32] Philip R. Christensen, Bruce M. Jakosky, Hugh H. Kieffer, Michael C. Malin, Harry Y. McSween Jr, Kenneth Nealson, Greg L. Mehall, Steven H. Silverman, Steven Ferry, Michael Caplinger, and Michael Ravine. *The Thermal Emission Imaging System (Themis) for the Mars 2001 Odyssey Mission*, pages 85–130. Springer Netherlands, Dordrecht, 2004.



- [33] P. R. Christensen, J. L. Bandfield, V. E. Hamilton, S. W. Ruff, H. H. Kieffer, T. N. Titus, M. C. Malin, R. V. Morris, M. D. Lane, R. L. Clark, B. M. Jakosky, M. T. Mellon, J. C. Pearl, B. J. Conrath, M. D. Smith, R. T. Clancy, R. O. Kuzmin, T. Roush, G. L. Mehall, N. Gorelick, K. Bender, K. Murray, S. Dason, E. Greene, S. Silverman, and M. Greenfield. Mars global surveyor thermal emission spectrometer experiment: Investigation description and surface science results. *Journal of Geophysical Research: Planets*, 106(E10):23823–23871, 2001.
- [34] Texas Instruments. *Buses Rad-hard*, 2023. TI Space Products Guide 2023.
- [35] Crane Aerospace Electronics. Power solutions interpoint dc-dc converters and emi filters space catalog. https://www.craneae.com/sites/default/files/documents/Standard_Power_Interpoint_Space_Cat_0.pdf.
- [36] R. L. Cox G. Bourland. Evaluation of non-specular reflecting silvered teflon and filled adhesives. *NASA Contractor Report 165657*, 1981.
- [37] SpaceX. *Falcon User's Guide*. September, 2021.
- [38] ASM Aerospace Specifications Metals Inc. Aluminum 7075-t6; 7075-t651. <https://asm.matweb.com/search/SpecificMaterial.asp?bassnum=MA7075T6>. [Online; accessed 11-January-2024].
- [39] Ali Aborehab, Mohammed Kassem, Ahmed Farid Nemnem, and M. Kamel. Mechanical characterization and static validation of a satellite honeycomb sandwich structure. 2020.

Appendix A

Requirements

A.1 High Level Requirements

Identifier	Description	Parents	Children	Type	Verification
DUS-HLR-0001	The payload shall observe the formation of dust storms covering at least the surface of Mars between latitude +70° and latitude -70°		DUS-ORB-0001, DUS-ORB-0002, DUS-ORB-0003, DUS-ORB-0004, DUS-OPT-0017, DUS-OPT-0018, DUS-OBDH-0001, DUS-OBDH-0002, DUS-STR-0004	Functional	Children
DUS-HLR-0002	The payload shall be capable of detecting dust presence in the Martian lower atmosphere		DUS-OPT-0001, DUS-OPT-0002, DUS-OPT-0004, DUS-OBDH-0001, DUS-STR-0002, DUS-STR-0004	Functional	Children
DUS-HLR-0003	The payload shall be capable of computing the dust storms location in Martian lower atmosphere		DUS-OPT-0001, DUS-OPT-0002, DUS-OPT-0004, DUS-OBDH-0001, DUS-STR-0002, DUS-STR-0004	Functional	Children
DUS-HLR-0004	The payload shall be capable of measuring the quantity of dust in the Martian lower atmosphere		DUS-OPT-0001, DUS-OPT-0002, DUS-OPT-0004, DUS-OBDH-0001, DUS-STR-0002, DUS-STR-0004	Functional	Children



Identifier	Description	Parents	Children	Type	Verification
DUS-HLR-0005	The payload shall be capable of operating for at least 12 terrestrial years		DUS-OPT-0008, DUS-OPT-0013, DUS-OPT-0016, DUS-OPT-0020, DUS-OPT-0024, DUS-OBDH-0001, DUS-OBDH-0020, DUS-EPS-0011, DUS-STR-0001, DUS-STR-0002, DUS-STR-0003, DUS-STR-0004	Functional	Children
DUS-HLR-0006	The payload shall have an acquisition temporal resolution of less than 1 hour during diurnal observation		DUS-ORB-0001, DUS-ORB-0002, DUS-ORB-0003, DUS-ORB-0004, DUS-OPT-0003, DUS-OBDH-0001, DUS-STR-0002, DUS-STR-0004	Functional	Children
DUS-HLR-0007	The payload shall have an on-ground spatial resolution of less than 100 km during diurnal observation		DUS-ORB-0001, DUS-ORB-0002, DUS-ORB-0003, DUS-ORB-0004, DUS-OPT-0003, DUS-OBDH-0001, DUS-STR-0002, DUS-STR-0004	Functional	Children
DUS-HLR-0008	The payload shall survive the environmental conditions suffered during its whole lifetime		DUS-OPT-0008, DUS-OPT-0013, DUS-OPT-0016, DUS-OPT-0020, DUS-OPT-0022, DUS-OPT-0024, DUS-OBDH-0001, DUS-OBDH-0020, DUS-EPS-0011, DUS-STR-0001, DUS-STR-0002, DUS-STR-0003, DUS-STR-0004	Functional	Children



A.2 Technical Requirements

A.2.1 Orbit Requirements

Identifier	Description	Parents	Children	Type	Verification
DUS-ORB-0001	The payload shall be operated in an areostationary orbit around Mars	DUS-HLR-0001, DUS-HLR-0006, DUS-HLR-0007	DUS-OPT-0017, OPT-0018	DUS- Mission	Inspection
DUS-ORB-0002	The payload shall point towards Nadir	DUS-HLR-0001, DUS-HLR-0006, DUS-HLR-0007		Mission	Inspection
DUS-ORB-0003	Four simultaneous payloads shall be operated around Mars	DUS-HLR-0001, DUS-HLR-0006, DUS-HLR-0007	DUS-OPT-0017, OPT-0018	DUS- Mission	Inspection
DUS-ORB-0004	The four payloads should be located centered at 180°W, 90°W, 0° and 90°E	DUS-HLR-0001, DUS-HLR-0006, DUS-HLR-0007		Mission	Inspection



A.2.2 Optics Requirements

Identifier	Description	Parents	Children	Type	Verification
DUS-OPT-0001	The payload detector shall measure wavelengths within the range of 8-16 μm	DUS-HLR-0002, DUS-HLR-0003, DUS-HLR-0004		Functional	Rod
DUS-OPT-0002	The payload OPTICS solution shall have a spectral resolution of at least 10 cm^{-1}	DUS-HLR-0002, DUS-HLR-0003, DUS-HLR-0004	DUS-OPT-0007, OPT-0010, DUS-OPT-0012, DUS-OPT-0013, DUS-OPT-0015, DUS-STR-0009	DUS- Performance	Analysis, Test
DUS-OPT-0003	The payload OPTICS solution shall cover an area with a diameter of at least 250 km	DUS-HLR-0001, DUS-HLR-0006	DUS-OPT-0021	Performance	Analysis
DUS-OPT-0004	The payload OPTICS solution shall be able to reconstruct the temperature profile of the Martian atmosphere	DUS-HLR-0002, DUS-HLR-0003, DUS-HLR-0004	DUS-OPT-0006, OPT-0008, DUS-OPT-0010, DUS-OPT-0012, DUS-OPT-0013, DUS-OPT-0015	DUS- Functional	Analysis, Test
DUS-OPT-0005	The payload OPTICS solution shall measure the irradiance of the Martian atmosphere	DUS-HLR-0002, DUS-HLR-0003, DUS-HLR-0004	DUS-OPT-0006, OPT-0008, DUS-OPT-0010, DUS-OPT-0012, DUS-OPT-0013, DUS-OPT-0015	DUS- Functional	Analysis, Test
DUS-OPT-0006	The payload OPTICS solution shall employ Fourier Transform Infrared Spectrometry	DUS-OPT-0004, OPT-0005	DUS-	Functional	Inspection
DUS-OPT-0007	The payload OPTICS solution shall include a calibration target to perform the optical calibration of the instrument	DUS-OPT-0002		Functional	Inspection
DUS-OPT-0008	The payload OPTICS solution shall be composed of the gimbal mirror assembly, the telescope assembly, the interferometer assembly and the detector assembly	DUS-OPT-0004		Configuration	Inspection
DUS-OPT-0009	The payload telescope assembly shall be kept in the temperature range between 273.15 K (TBC) and 313.15 (TBC) K	DUS-HLR-0005, DUS-HLR-0008	DUS-TCS-0001	Environment	Analysis, Test



Identifier	Description	Parents	Children	Type	Verification
DUS-OPT-0010	The payload interferometer assembly moving mirror shall be controlled at least at 5 (TBC) kHz	DUS-OPT-0002, OPT-0004, DUS-OPT-0005	DUS-OPT-0002, OPT-0004, DUS-OPT-0005	DUS-OBDH-0012	Performance Test
DUS-OPT-0011	The payload interferometer assembly moving mirror shall be sampled at least at 40 (TBC) kHz	DUS-OPT-0002, OPT-0004, DUS-OPT-0005	DUS-OPT-0002, OPT-0004, DUS-OPT-0005	DUS-OBDH-0012	Performance Test
DUS-OPT-0012	The payload interferometer assembly moving mirror shall travel a distance of $\pm 500.4\mu\text{m}$ (TBC) mm	DUS-OPT-0002, OPT-0004, DUS-OPT-0005	DUS-OPT-0002, OPT-0004, DUS-OPT-0005	DUS-OBDH-0012	Performance Test
DUS-OPT-0013	The payload interferometer assembly moving mirror shall travel at a speed of $560\mu\text{m}/\text{s} \pm 28$ ($\text{TBC}\mu\text{m}/\text{s}$)	DUS-OPT-0002, OPT-0004, DUS-OPT-0005	DUS-OPT-0002, OPT-0004, DUS-OPT-0005	DUS-OBDH-0012	Performance Test
DUS-OPT-0014	The payload interferometer assembly shall be kept in the temperature range between 273.15 (TBC) K and 313.15 (TBC) K	DUS-HLR-0005, DUS-HLR-0008	DUS-HLR-0005, DUS-HLR-0008	DUS-TCS-0001	Environment Analysis, Test
DUS-OPT-0015	The acquired science data shall have a SNR higher than 80	DUS-OPT-0002, OPT-0004, DUS-OPT-0005	DUS-OPT-0002, OPT-0004, DUS-OPT-0005	DUS-OPT-0016	Performance Analysis, Test
DUS-OPT-0016	The payload detector shall acquire data with a frequency of at least 500 Hz	DUS-OPT-0015	DUS-OPT-0015	DUS-OBDH-0002	Performance Test
DUS-OPT-0017	The payload detector should be able to operate at the temperature range imposed by the other components of the OPTICS solution	DUS-HLR-0005, DUS-HLR-0008	DUS-HLR-0005, DUS-HLR-0008	Functional R&D	
DUS-OPT-0018	The payload gimbal mirror assembly shall be able to cover, at least, the surface of Mars between latitude +70° and latitude -70°	DUS-HLR-0001	DUS-HLR-0001	DUS-OBDH-0011	Functional Analysis
DUS-OPT-0019	The payload gimbal mirror assembly shall be able to cover, at least, the surface of Mars between longitude +55° and longitude -55°	DUS-ORB-0001, ORB-0003	DUS-ORB-0001, ORB-0003	DUS-OBDH-0011	Functional Analysis



Identifier	Description	Parents	Children	Type	Verification
DUS-OPT-0020	The payload gimbal mirror assembly shall be kept in the temperature range between 273.15 (TBC) K and 323.15 (TBC) K	DUS-HLR-0005, DUS-HLR-0008	DUS-TCS-0001	Environment Analysis, Test	
DUS-OPT-0021	The payload gimbal mirror assembly shall scan the desired surface of Mars in less than 30 (TBC) min	DUS-OPT-0003, OPT-0018, DUS-OPT-0019	DUS-OBDH-0011	Performance Analysis	
DUS-OPT-0022	The platform shall avoid direct sunlight entering inside the payload through the OPTICS aperture	DUS-HLR-0008		Interface Inspection, Analysis	
DUS-OPT-0023	The payload OPTICS solution shall include a closure mechanism to protect the optics from the external environment when needed	DUS-HLR-0008		Functional Inspection	
DUS-OPT-0024	The payload detector shall always be kept in the temperature range between 253.15 (TBC) K and 343.15 (TBC) K	DUS-HLR-0005, DUS-HLR-0008	DUS-TCS-0001	Functional Inspection	
DUS-OPT-0025	The payload calibration target shall be kept at a fixed and known temperature	DUS-TCS-0010		Functional Analysis, Test	



A.2.3 OBDH Requirements

Identifier	Description	Parents	Children	Type	Verification
DUS-OBDH-0001	The payload OBDH solution shall guarantee the proper functioning of the instrument during its whole lifetime	HLR	DUS-OBDH-0002, DUS-OBDH-0007, DUS-OBDH-0008, DUS-OBDH-0009, DUS-OBDH-0010, DUS-OBDH-0011, DUS-OBDH-0012, DUS-OBDH-0013	Functional	Inspection
DUS-OBDH-0002	The payload OBDH solution shall control the telemetry data acquisition, compression, storage and transmission to the platform OBC	DUS-OBDH-0001, OPT-0016	DUS-OBDH-0003, DUS-OBDH-0004, DUS-OBDH-0005, DUS-OBDH-0014, DUS-OBDH-0017, DUS-OBDH-0018, DUS-OBDH-0019, DUS-OBDH-0026	Functional	Test
DUS-OBDH-0003	The payload OBDH solution shall acquire the instrument housekeeping data with a frequency of 10 (TBC) Hz	DUS-OBDH-0002	DUS-OBDH-0016, DUS-OBDH-0017, DUS-OBDH-0018, DUS-OBDH-0019	Performance	Test
DUS-OBDH-0004	The payload OBDH solution shall transmit the telemetry data of one gimbal mirror cycle to the platform OBC in less than 1 (TBC) s	DUS-OBDH-0002	DUS-OBDH-0022	Performance	Test
DUS-OBDH-0005	The payload OBDH solution shall transmit the telemetry data of 20 days to the platform OBC in less than 100 (TBC) s	DUS-OBDH-0002	DUS-OBDH-0022	Performance	Test
DUS-OBDH-0006	The payload OBDH solution shall have enough memory to store the generated telemetry data during 20 days	DUS-OBDH-0002	DUS-OBDH-0019	Functional	Rod
DUS-OBDH-0007	The payload OBDH solution shall receive and decode telecommands from the platform OBC with a frequency of 2 (TBC) Hz	DUS-OBDH-0001	DUS-OBDH-0015, DUS-OBDH-0017, DUS-OBDH-0018, DUS-OBDH-0019, DUS-OBDH-0023	Functional	Test



Identifier	Description	Parents	Children	Type	Verification
DUS-OBDH-0008	The payload shall receive the spacecraft status with a frequency of 2 (TBC) Hz	DUS-OBDH-0001	DUS-OBDH-0017, DUS-OBDH-0018, DUS-OBDH-0019, DUS-OBDH-0023	Performance	Test
DUS-OBDH-0009	The payload shall update its internal clock with the spacecraft's clock with a frequency of 1 (TBC) Hz	DUS-OBDH-0001	DUS-OBDH-0017, DUS-OBDH-0018, DUS-OBDH-0019, DUS-OBDH-0023	Performance	Test
DUS-OBDH-0010	The payload OBDH solution shall control the instrument power conditioning	DUS-OBDH-0001, DUS-EPS-0001, DUS-EPS-0002, DUS-EPS-0003, DUS-EPS-0005	DUS-OBDH-0017, DUS-OBDH-0018, DUS-OBDH-0019	Functional	Test
DUS-OBDH-0011	The payload OBDH solution shall control the gimbalmirror assembly	DUS-OBDH-0001, DUS-OPT-0019, DUS-OPT-0021	DUS-OBDH-0017, DUS-OBDH-0018, DUS-OBDH-0019, DUS-OBDH-0027	Functional	Test
DUS-OBDH-0012	The payload OBDH solution shall control the interferometer moving mirror	DUS-OBDH-0001, DUS-OPT-0011, DUS-OPT-0011, DUS-OPT-0013	DUS-OBDH-0017, DUS-OBDH-0018, DUS-OBDH-0019, DUS-OBDH-0024, DUS-OBDH-0025	Functional	Test
DUS-OBDH-0013	The payload OBDH solution shall control the instrument active thermal components	DUS-OBDH-0001, TCS-0006	DUS-OBDH-0017, DUS-OBDH-0018, DUS-OBDH-0019, DUS-OBDH-0028	Functional	Test
DUS-OBDH-0014	The payload OBDH solution shall orchestrate the data collection start	DUS-OBDH-0002	DUS-OBDH-0017, DUS-OBDH-0018, DUS-OBDH-0019	Functional	Test
DUS-OBDH-0015	The payload OBDH solution shall control the commands execution timing	DUS-OBDH-0007	DUS-OBDH-0017, DUS-OBDH-0018, DUS-OBDH-0019	Functional	Test
DUS-OBDH-0016	The payload OBDH solution shall control the sampling of all internal hardware interfaces	DUS-OBDH-0003	DUS-OBDH-0017, DUS-OBDH-0018, DUS-OBDH-0019	Functional	Test



Identifier	Description	Parents	Children	Type	Verification
DUS-OBDH-0017	The payload shall have a processing capability of at least 240 (TBC) MIPS	DUS-OBDH-0002, DUS-OBDH-0003, DUS-OBDH-0007, DUS-OBDH-0008, DUS-OBDH-0009, DUS-OBDH-0010, DUS-OBDH-0011, DUS-OBDH-0012, DUS-OBDH-0013, DUS-OBDH-0014, DUS-OBDH-0015, DUS-OBDH-0016		Performance	Rod
DUS-OBDH-0018	The payload OBDH solution shall have a RAM of at least 1.4 (TBC) MB	DUS-OBDH-0002, DUS-OBDH-0003, DUS-OBDH-0007, DUS-OBDH-0008, DUS-OBDH-0009, DUS-OBDH-0010, DUS-OBDH-0011, DUS-OBDH-0012, DUS-OBDH-0013, DUS-OBDH-0014, DUS-OBDH-0015, DUS-OBDH-0016		Performance	Rod
DUS-OBDH-0019	The payload OBDH solution shall have a total memory of at least 2.3 (TBC) GB	DUS-OBDH-0002, DUS-OBDH-0003, DUS-OBDH-0006, DUS-OBDH-0007, DUS-OBDH-0008, DUS-OBDH-0009, DUS-OBDH-0010, DUS-OBDH-0011, DUS-OBDH-0012, DUS-OBDH-0013, DUS-OBDH-0014, DUS-OBDH-0015, DUS-OBDH-0016		Performance	Rod
DUS-OBDH-0020	The payload OBDH solution shall be kept in the temperature range between 273.15 (TBC) K and 358.15 (TBC) K	DUS-HLR-0005, DUS-HLR-0008	DUS-TCS-0001	Environment Analysis, Test	
DUS-OBDH-0021	The payload OBDH solution shall be exposed to a maximum Total Ionizing Dose (TID) of 100 (TBC) krad during its lifetime	DUS-HLR-0005, DUS-HLR-0008		Environment Analysis	



Identifier	Description	Parents	Children	Type	Verification
DUS-OBDH-0022	The payload OBDH solution shall interface with the spacecraft OBC with a data bus capable of transmitting data at no less than 185 (TBC) Mb/s	DUS-OBDH-0004, OBDH-0005	DUS-	DUS-STR-0012	Performance Rod
DUS-OBDH-0023	The payload OBDH solution shall interface with the spacecraft OBC with a data bus capable of receiving data at no less than 2 (TBC) Mb/s	DUS-OBDH-0007, OBDH-0008, DUS-OBDH-0009	DUS-	DUS-STR-0012	Performance Rod
DUS-OBDH-0024	The payload OBDH solution shall interface with the instrument interferometer assembly with a bus capable of transmitting data at no less than 153 (TBC) Mb/s	DUS-OBDH-0012			Performance Rod
DUS-OBDH-0025	The payload OBDH solution shall interface with the instrument interferometer assembly with a bus capable of receiving data at no less than 611 (TBC) Mb/s	DUS-OBDH-0012			Performance Rod
DUS-OBDH-0026	The payload OBDH solution shall interface with the instrument detector assembly with a bus capable of receiving data at no less than 1 (TBC) Mb/s	DUS-OBDH-0002			Performance Rod
DUS-OBDH-0027	The payload OBDH solution shall interface with the instrument gimbal mirror assembly with a bus capable of transmitting data at no less than 4 (TBC) Mb/s	DUS-OBDH-0011			Performance Rod
DUS-OBDH-0028	The payload OBDH solution shall interface with the instrument active thermal actuators with a bus capable of transmitting data at no less than 1 (TBC) Mb/s	DUS-OBDH-0013			Performance Rod



A.2.4 EPS Requirements

Identifier	Description	Parents	Children	Type	Verification
DUS-EPS-0001	The payload EPS solution shall receive unregulated voltage from the spacecraft and condition it	HLR	DUS-OBDH-0010, DUS-EPS-0004, DUS-EPS-0005, DUS-EPS-0006, DUS-EPS-0007, DUS-EPS-0008, DUS-EPS-0009	Functional	Analysis, Test
DUS-EPS-0002	The payload EPS solution shall provide enough power to the active components for their correct operation	HLR	DUS-OBDH-0010, DUS-EPS-0009	Functional	Analysis, Test
DUS-EPS-0003	The payload EPS solution shall distribute the power to the active components of the instrument	HLR	DUS-OBDH-0010	Functional	Analysis, Test
DUS-EPS-0004	The payload EPS solution shall be able to dissipate the excess of electric power	HLR		Functional	Analysis, Test
DUS-EPS-0005	The payload EPS solution shall be able to switch on and off each power line (TBC)	HLR	DUS-OBDH-0010	Functional	Analysis, Test
DUS-EPS-0004	The payload EPS solution shall supply 1 (TBC) V regulated power to the payload components	1	DUS-EPS-0001	Performance	R&D
DUS-EPS-0005	The payload EPS solution shall supply 2.5 (TBC) V regulated power to the payload components	2.5	DUS-EPS-0001	Performance	R&D
DUS-EPS-0006	The payload EPS solution shall supply 3.3 (TBC) V regulated power to the payload components	3.3	DUS-EPS-0001	Performance	R&D
DUS-EPS-0007	The payload EPS solution shall supply 10 (TBC) V regulated power to the payload components	10	DUS-EPS-0001	Performance	R&D



Identifier	Description	Parents	Children	Type	Verification
DUS-EPS-0008	The payload EPS solution shall supply 12 (TBC) V regulated power to the payload components	DUS-EPS-0001		Performance	Rod
DUS-EPS-0009	The payload EPS solution shall receive 28 (TBC) V unregulated input voltage from the spacecraft	DUS-EPS-0001, DUS-EPS-0002	DUS-STR-0012	Interface	Analysis, Test
DUS-EPS-0010	The payload EPS solution shall receive, at least, 40.36 (TBC) W of peak power from the spacecraft at EOL	DUS-EPS-0002	DUS-STR-0012	Interface	Analysis, Test
DUS-EPS-0011	The payload EPS solution shall always operate between 218.15 (TBC) K and 398.15 (TBC) K	DUS-HLR-0005, DUS-HLR-0008	DUS-TCS-0001	Environmental Analysis	Test
DUS-EPS-0012	The payload EPS solution shall be exposed to a maximum Total Ionizing Dose (TID) of 100 (TBC) krad during its lifetime	DUS-HLR-0005, DUS-HLR-0008		Environmental Analysis	



A.2.5 TCS Requirements

Identifier	Description	Parents	Children	Type	Verification
DUS-TCS-0001	The payload TCS solution shall be able to keep the instrument temperature range between 278.15 (TBC) K and 308.15 (TBC) K	DUS-OPT-0009, OPT-0014, DUS-OPT-0020, DUS-OBDH-0020, EPS-0011	DUS-TCS-0002, DUS-TCS-0005, DUS-TCS-0006, DUS-TCS-0007, DUS-TCS-0008, DUS-STR-0012	Performance Analysis	Analysis, Test
DUS-TCS-0002	The payload structure shall thermally interface with the structure of the spacecraft	DUS-TCS-0001, DUS-TCS-0002	DUS-TCS-0003, DUS-TCS-0004, DUS-STR-0011	Interface	Analysis, Test
DUS-TCS-0003	The payload interface shall be conductively isolated from the spacecraft	DUS-TCS-0002		Functional	Analysis, Test
DUS-TCS-0004	The payload interface shall allow radiation heat exchange with the spacecraft	DUS-TCS-0002		Functional	Analysis, Test
DUS-TCS-0005	The payload TCS solution shall be able to emit radiation outward	DUS-TCS-0001		Functional	Analysis, Test
DUS-TCS-0006	The payload TCS solution shall include active thermal control	DUS-TCS-0001	DUS-OBDH-0013	Functional	Inspection
DUS-TCS-0007	The payload gimbal mirror assembly shall be conductive-connected to the outward emitter	DUS-TCS-0001	DUS-TCS-0009	Functional	Inspection
DUS-TCS-0008	The payload control board shall be conductive-connected to the outward emitter	DUS-TCS-0001	DUS-TCS-0009	Functional	Inspection
DUS-TCS-0009	The thermal connections between components shall be achieved by employing conductive heat	DUS-TCS-0007, DUS-TCS-0008	Design	Inspection	
DUS-TCS-0010	The payload calibration body shall be thermally isolated from the other components	DUS-OPT-0025		Functional	Analysis, Test



A.2.6 STR Requirements

Identifier	Description	Parents	Children	Type	Verification
DUS-STR-0001	The payload shall survive to the load environment expected in any phase of the mission after launch	DUS-HLR-0005, DUS-HLR-0008	DUS-STR-0005, DUS-STR-0014	Functional	Test
DUS-STR-0002	The payload structure shall mechanically interface with the structure of the spacecraft	HLR	DUS-STR-0011	Functional	Inspection
DUS-STR-0003	The payload structure shall protect all the subsystems from the radiation environment	DUS-HLR-0005, DUS-HLR-0008	DUS-STR-0014	Functional	Analysis, Test
DUS-STR-0004	The payload structure shall be capable of accommodating all the components and subsystems, including their harnesses	HLR	DUS-STR-0010, DUS-STR-0012, DUS-STR-0013, DUS-STR-0016	Functional	Inspection
DUS-STR-0005	The payload shall survive to the launch environment prescribed by the launch authorities	DUS-STR-0001	DUS-STR-0006, DUS-STR-0007, DUS-STR-0008, DUS-STR-0014	Functional	Test
DUS-STR-0006	The payload first primary lateral frequency shall be above 20 Hz	DUS-STR-0005		Performance	Test
DUS-STR-0007	The payload first primary axial frequency shall be above 35 Hz	DUS-STR-0005		Performance	Test
DUS-STR-0008	The payload secondary minimum resonant frequencies shall be above 45 Hz	DUS-STR-0005		Performance	Test
DUS-STR-0009	The maximum displacement seen by the OPTICS subsystem elements shall be kept in the order of micrometres during the mission lifetime	DUS-OPT-0002		Performance	Test
DUS-STR-0010	The payload primary structure shall hold the secondary and tertiary structures	DUS-STR-0004		Functional	Inspection



Identifier	Description	Parents	Children	Type	Verification
DUS-STR-0011	The payload primary structure shall act as thermo-mechanical interface with the space-craft	DUS-STR-0002, DUS-TCS-0002		Configuration Inspection, Test	
DUS-STR-0012	The payload primary structure shall hold the electronics plate	DUS-STR-0004, DUS-EPS-0009, DUS-EPS-0010, DUS-OBDH-0022, DUS-OBDH-0023, DUS-TCS-0001		Configuration Inspection	
DUS-STR-0013	The payload secondary structure shall hold the Cassegrain telescope	DUS-STR-0004		Functional	Inspection
DUS-STR-0014	The payload tertiary structure shall protect the instrument components from the external environment	DUS-STR-0001, DUS-STR-0003, DUS-STR-0005		Functional	Analysis
DUS-STR-0015	The payload tertiary structure shall keep the Total Ionizing Dose (TID) in the components under 100 (TBC) krad	DUS-STR-0014		Performance	Analysis
DUS-STR-0016	The payload tertiary structure shall include the elements and mechanisms to hold the instrument harness	DUS-STR-0004		Functional	Inspection